NASA CR-626

A REVIEW OF FLIGHT AND WIND TUNNEL MEASUREMENTS OF BOUNDARY LAYER PRESSURE FLUCTUATIONS AND INDUCED STRUCTURAL RESPONSE

By David Alan Bies

Prepared under Contract No. NAS 1-5120 by
BOLT BERANEK AND NEWMAN, INC.
Los Angeles, Calif.

for Langley Research Center

NATIONAL AERONAUTICS AND SPACE ADMINISTRATION

For sale by the Clearinghouse for Federal Scientific and Technical Information
Springfield, Virginia 22151 – Price $2.50

TABLE OF CONTENTS

A REVIEW OF FLIGHT AND WIND TUNNEL MEASUREMENTS OF BOUNDARY LAYER PRESSURE FLUCTUATIONS AND INDUCED STRUCTURAL RESPONSE

by David Alan Bies
Bolt Beranek and Newman Inc.

SUMMARY

A review is presented of available data on boundary layer pressure fluctuations and induced structural response, from flight and wind tunnel investigations. The wind tunnel data include flat plate pressure fluctuation spectra and space-time correlations, displacement and acceleration spectra of flat flexible panels, and sound power spectra radiated by flat flexible panels. The flight data include pressure fluctuation spectra and "equivalent acoustic spectra," the acoustic fields that would produce the same response as the aerodynamic fields.

In order to use the same normalization procedure with all the data, engineering curves have been derived for estimating boundary layer parameters. These curves extend the estimates to Mach numbers up to 4 and Reynolds numbers based on a characteristic length up to 2×10^9.

The pressure fluctuation data show considerable scatter, especially in the wind tunnel investigations. The experimental results suggest that the scatter may be due to highly localized flow perturbations. It is argued that these perturbations may not be significant in determining structural response. General recommendations are given to guide experimental studies. A simplified procedure for estimating boundary layer pressure spectra is given in an appendix.

INTRODUCTION

With the advent of high performance flight vehicles, aerodynamically-induced vibration has become of great significance to the vehicle designers. Aerodynamic

excitation may come about through various causes, such as flow over cavities or around steps, base pressure fluctuations, or loosely attached shock waves. One form of significance which has received much attention is that due to pressure fluctuations in the turbulent boundary layer over the vehicle skin. This source may be of particular significance to the supersonic transport designer.

A large literature exists that reports measurements of boundary layer pressure fluctuations over flat plates in wind tunnels and on the surfaces of various flight vehicles, evidencing a lively interest in such phenomena. Unfortunately, it is difficult to draw general conclusions from this literature because there is no uniformity of reporting the data. The interest which has prompted the many investigations has also prompted the writing of this report in which an attempt is made to intercompare published data and draw general conclusions.

In most cases of reported flight vehicle measurements, no information is given about the boundary layer. If one is to compare boundary layer pressure fluctuation measurements with each other or with wind tunnel measurements, some estimates of the boundary layer parameters must be provided. In addition many wind tunnel measurements are reported in such a way that intercomparison is rendered difficult, and here too some means for estimating missing information is required.

The path followed in this report follows from the stated objective and the problems listed above. Thus the first task is to construct a set of procedures and engineering curves by which boundary layer parameters can be estimated. This information is contained in the section labeled Boundary Layer Parameters. The literature and the procedures involved in generating the data given in this section are discussed in Appendix A.

A second problem arises in the consideration of the measurement of boundary layer pressure fluctuations due to the natural loss in sensitivity of a finite-size pressure transducer at high frequencies and short wavelength. This problem has been the subject of much discussion and

has been dealt with in various ways by various investigators. An effort has been made to give this matter consistent treatment in this report through work outlined in the section Microphone Size Correction.

In the section on Wind Tunnel Measurements, the results of pressure fluctuation measurements and correlation studies of the turbulent boundary layer over flat plates are discussed. Based on this material, a simplified procedure for estimating boundary layer pressure spectra is given in Appendix B. In addition a number of published papers on wind tunnel investigations of the response of panels to turbulent boundary layer excitation are reviewed, and the principal findings are summarized.

The results of a number of flight vehicle measurements of turbulent boundary layer pressure fluctuations and of response of structures to such excitation are given in the section on Flight Measurements. It is shown in this section that the available data form a fairly consistent and comprehensive picture of the phenomena.

The last section called Conclusions and Recommendations summarizes the principal findings of this report and makes some general recommendations for further work.

SYMBOLS

C_1	spatial part of the correlation function
C_2	time part of the correlation function
C_3, C_4	spatial part of the correlation function in longitudinal and traverse directions
c_f	local coefficient of skin friction
$\bar{c}_f$	local coefficient of skin friction in transformed coordinates (see ref. A7)
D	microphone diameter
F(f)	pressure spectral density
M	local Mach number

M_∞	free stream Mach number
q	free stream dynamic pressure
R	space-time correlation function
r	recovery factor
Re_s	Reynolds number based on distance from the wall to the sublayer (see ref. A7)
Re_x	Reynolds number based on distance x
Re_y	Reynolds number based on distance from wall
Re_δ	Reynolds number based on boundary layer thickness
Re_θ	Reynolds number based on momentum thickness
$\overline{Re}_{\overline{\theta}}$	Reynolds number based on momentum thickness in transformed coordinates (see ref. A7)
t	time
T	temperature
T_s	temperature in the sublayer (see ref. A7)
T_w	temperature at the wall
T_∞	free stream temperature
$T_{o\infty}$	free stream stagnation temperature
U	local flow velocity
U_c	convection velocity defined by means of the turbulent boundary layer correlation properties
U_∞	free stream flow velocity
x	coordinate in plane of wall in direction of flow, distance from inception of turbulence on a flat plate
y	coordinate normal to the wall into the stream

z	coordinate in plane of wall transverse to direction of flow
α	an exponent
γ	ratio of specific heats
δ	boundary layer thickness
δ^*	displacement thickness
η	displacement transverse to direction of flow
η_o	constant displacement transverse to direction of flow
θ	momentum thickness
μ	local gas viscosity
μ_∞	free stream gas viscosity
ξ	displacement parallel to direction of flow
ξ_o	constant displacement parallel to direction of flow
ρ	local gas density
ρ_∞	free stream gas density
τ	time delay
ψ	a function (equation A18)
ω	frequency in radians per second

BOUNDARY LAYER PARAMETERS

As mentioned in the introduction, it seldom happens that a complete description of the boundary layer is presented with measurements of the boundary layer pressure fluctuations. This shortcoming is especially true of flight measurements and is also quite often evident in

published wind tunnel measurements. To remedy the total or partial lack of such information, engineering curves have been developed and are given in figures 1 through 4. The information given in these curves is based on empirical data discussed in Appendix A and is valid strictly for unperturbed flow over a flat plate. We shall use the information contained in the figures to supply missing parameters in order to compare published and unpublished boundary layer pressure fluctuation data. In doing so, we shall attempt to represent the actual measurement configuration by an equivalent flat plate model.

The procedure which has been used in the preparation of this report is as follows. Typically, a report of flight measurements of boundary layer pressure fluctuations will give information about the location of the transducer, air speed, and altitude. From the information about the transducer location, an estimate of the characteristic length to the point of inception of turbulent flow on an equivalent flat plate is made. This characteristic length is quite often taken as the distance to some leading edge. With the altitude information and the characteristic length estimate just determined, an effective Reynolds number is computed from ARDC standard atmosphere tables (ref. 1). From the given air speed and the altitude information, a Mach number is computed, again by use of the ARDC standard atmosphere tables. The three bits of derived information -- characteristic length, Reynolds number, and Mach number -- are sufficient to determine the four boundary layer parameters -- boundary layer thickness using figure 1, displacement thickness using figure 2, momentum thickness using figure 3, and local skin friction coefficient using figure 4. Our normalization procedure makes use of the displacement thickness and the local skin friction coefficient.

MICROPHONE SIZE CORRECTION

Experimental and theoretical investigations have shown that the finite size of a pressure transducer limits its response in the upper frequency range. This happens

because frequency and spatial extent are related so that high frequency corresponds to small spatial extent. Thus, at some frequency determined by the ratio of microphone diameter to boundary layer displacement thickness D/δ^*, cancellation between positive and negative pressures begins to occur over the transducer surface.

This problem has been investigated by Corcos (ref. 2), Willmarth and Roos (ref. 3) and Chandiramani (ref. 4). Willmarth and Roos have shown theoretically and experimentally that the earlier work of Corcos overestimates the size correction for values of D/δ^* less than unity, but for values of unity or greater Corcos's estimates are correct. Corcos's estimates have been found to be in satisfactory agreement with the results of experiment for a value of D/δ^* much larger than unity, according to Gilchrist and Strawderman (ref. 5). Unfortunately, the latter authors have not specified the size of this parameter, but it may be estimated to be of the order of eight by reference to the work of one of their co-workers (ref. 6).

Chandiramani has independently estimated the microphone size effect and has obtained slightly different results from those of Willmarth and Roos. The expected reduction in pressure sensitivity of a transducer due to its finite size according to these authors is shown in figure 5. The curve for D/δ^* of the order of unity or greater is due to Corcos. The family of solid lines for D/δ^* of 0.1, 0.2 and 0.5 is due to Willmarth and Roos. The family of two dashed lines for D/δ^* of 0.33 and 0.66 is due to Chandiramani

In the presentation of data included in this report, microphone corrections according to Corcos, Willmarth and Roos have been included where sufficient information was given by the author. However, in some cases it is not clear that some such corrections have not already been made. In cases of doubt no corrections have been made. If the data has been corrected, this fact is indicated in the corresponding figure.

WIND TUNNEL MEASUREMENTS

Boundary Layer Pressure Fluctuations

Boundary layer pressure fluctuations have been measured by many investigators. Those whose work has been included in this review (refs. 7 through 19) are listed in Table I. For convenience the references have been listed roughly in order of increasing Mach number, and some of the parameters pertinent to particular investigations are also listed. The table serves as an index to the wind tunnel measurements presented in figures 6 through 19.

The investigators listed in Table I have reported their results in many different ways, so that it is difficult to determine a general concensus. Following procedures described earlier, we have attempted to determine reasonable estimates for quantities which are sometimes missing in published reports (such as the local coefficient of skin friction), and we have used such estimates to recast published work in the form shown in figures 6 through 19. The normalization presented in these figures or very similar normalizations have been used by a number of investigators, and in those cases little or no change has been made in the data as originally published.

The first thing that comes to mind as one scans the data shown in the figures is the question, "How do the various measurements compare?" Such a comparison is shown in figure 20. Below a Strouhal number of unity, there is quite a bit of agreement among most experimenters on an upper bound of the spectrum. Above a Strouhal number of unity, the upper bound of the spread is determined by the work of Kistler and Chen (ref. 17). The lower bound for all Strouhal numbers is determined by the work of Harrison (ref. 8). In the latter case it is not clear whether or not corrections for finite microphone size were included by Harrison, so that no corrections have been made in this report.

As an aid to the reader a line has been placed where most of the data seem to cluster. Where the line is discontinued, the data is about equally distributed over

TABLE I

MEASUREMENTS OF BOUNDARY LAYER PRESSURE FLUCTUATIONS

Investigator	Tunnel Size + Type	Mach No.	Reynolds No.	Mic. Diam. δ^*	Fig. No.
Jorgensen, Donald W. (ref. 7)	Continuous 18" x 15"	0.04 0.18	(x)5.9×10^5 2.4×10^6	6.7 11.4	6
Harrison, M. (ref. 8)	Continuous 15" x 20"	0.04 0.18	(x)1×10^6 4×10^6	1.2	7
Baroudi, Ludwig, + Ribner (ref. 9)	Continuous 8" x 12"	0.04 0.15		0.092	8
Bakewell, H. P. Jr., et al (ref. 6)	Continuous 3-1/2" diam.	0.1	(x)4×10^6	0.31	9
Wilmarth + Wooldridge (ref. 10)	Continuous 60" x 84"	0.2	(x)3.1×10^7 3.8×10^7	4.0	10
Bull, Wilby + Blackman (ref. 11)	Continuous 9" x 6"	0.3 0.5	(x)0.5×10^7 3×10^7	0.15 0.51	11
Murphy, J. S., et al (ref. 12)	Blowdown 12" x 12"	0.59	(θ)1.3×10^4	2.77	12
Serafini, J. S. (ref. 13)	Continuous 8" x 18"	0.6	(x)1×10^7 1.4×10^8	0.195 1.33	13
Maestrello, L. (refs. 14 and 15)	Continuous 7.3" x 3.5"	0.63 0.78		0.45	14
Williams, D. J. M. (ref. 16)	Continuous 6" x 2-1/2"	1.2 1.5		5 8	15
Kistler + Chen (ref. 17)	Continuous 18" x 20"	3.5	(θ)1.55×10^4	1.1	16
Murphy, J. S., et al (ref. 12)	Blowdown 12" x 12"	3.46	(θ)4.9×10^4	0.43	17
Westley, R. (ref. 18)	Blowdown 5" x 5"	2.91 3.96			18
Speaker + Ailman (ref. 19)	Blowdown 12" x 12"	0.42 3.45	(θ)1.6×10^4 5.3×10^4	0.17 1.3	19

(x) Reynolds number based on distance from inception of turbulence.

(θ) Reynolds number based on momentum thickness.

the indicated range. The large spread leads one to ask if a better normalizing scheme exists. For the consideration of this question the work of Speaker and Ailman is useful (ref. 19).

Speaker and Ailman report a large number of measurements of unperturbed flow over a flat plate for a large range of Mach numbers. In addition they provide a rather complete list of various boundary layer parameters. Their report shows quite a large variation in measured pressure fluctuations across the plate, for any one Mach number. It is clear that no choice of the given parameters would bring their data together for a single Mach number, since none of the parameters vary significantly across the plate. However, Speaker and Ailman do present a figure which summarizes the mean of their findings for each Mach number. These mean values are shown in figure 19.

Figure 19 shows the following interesting trend. Above a Strouhal number of two where all of the data curves roll off sharply, the trend is for the low and high Mach number measurements to lie furthest to the right, and the measurements close to Mach number unity furthest to the left. A review of the boundary layer parameters presented by Speaker and Ailman shows that the boundary layer thickness, displacement thickness, and momentum thickness show the same general behavior, being largest at lowest and highest Mach numbers and smallest near unity Mach number. Thus, normalization using either of the other boundary layer thicknesses in computing the Strouhal number would show the same general trend as shown by normalization based on displacement thickness.

One might wonder if some combination of parameters, perhaps involving a Reynolds number based on one of the thicknesses, might give better normalization. The author has not found any such dimensionless combination of parameters which could significantly coalesce the high-frequency rolloff portions of the spectra. It is clear that the behavior shown by the data of Speaker and Ailman follows from the choice of normalization parameter, displacement thickness, but it is not clear what other choice or combination of parameters should be made. Figure 20 unfortunately appears to represent the present state of the art for wind tunnel measurements.

Space-Time Pressure Correlations

Interest in the space-time surface-pressure correlation of the turbulent boundary layer stems primarily from the fact that a knowledge of the complete correlation is sufficient to calculate the response of a structure excited by the boundary layer. It has been pointed out (ref. 4) that the response of a structure excited by a turbulent boundary layer is unfortunately rather sensitive to the fine details of the space-time surface-pressure correlation. In addition to the primary interest in pressure correlations for investigating structural response, correlation measurements are of interest to provide insight into the basic mechanics of the turbulent boundary layer. For example, estimates of the convection velocities (refs. 10, 11, 13, 19, 20, 21) lifetimes (refs.10, 22) of the eddies which produce the random pressure fluctuations in the turbulent boundary layer have been deduced from correlation measurements.

Table II presents a summary of wind tunnel pressure correlation measurements. A review of these measurements indicates that, although the investigators have obtained quite detailed measurements of the correlation properties, there exists disagreement in the different measurements of some of the basic properties of the surface-pressure correlations. Efforts to relate these experimental discrepancies to differences in the flow conditions have been frustrated by the present lack of knowledge of the basic physics of the turbulent boundary layer.

Terminology. - Before discussing the wind tunnel measurements, it is convenient to define a coordinate system and review some terminology relevant to cross-correlations. Let us define an orthogonal coordinate system x, z in the plane of the wind tunnel wall. Let x be the coordinate in the direction of flow and z be the coordinate in the direction transverse to the flow. The complete space-time surface-pressure correlation $R(x, z, t; x + \xi, z + \eta, t + \tau)$ is a cross-correlation obtained by multiplying together two surface-pressure measurements and then time-averaging the resultant product.

TABLE II

SPACE-TIME CORRELATION MEASUREMENTS
OF BOUNDARY LAYER PRESSURE FLUCTUATIONS

INVESTIGATOR	Bull, Wilby and Blackman (ref. 11)	Speaker and Ailman (ref. 19)	Serafini (ref. 13)
MACH NUMBERS	0.3 and 0.5	0.59, 1.41, 3.45 and 3.48	0.6
δ^* (in.)	approx. 0.05 to 0.15	approx. 0.03 to 0.35	0.32
D/δ^*	approx. 0.15 to 0.51	approx. 0.16 to 2.6	0.38
MEASUREMENTS REPORTED			
1. Autocorrelations	x		x
2. Longitudinal correlations	x	x	x
3. Transverse correlations	x	x	x
4. Off-Axis correlations	x	x	x
5. Spatial correlation contours	x	x	
6. Convection velocity vs longitudinal sepration	x	x	x
7. Convection velocity vs frequency	x		
SPECIAL TYPES OF MEASUREMENTS	Correlations of narrow-band pressure fluctuation measurements	Correlations in perturbed supersonic flow Effects of assuming separable correlations	Correlations of low and high pass filtered pressure fluctuation measurements

TABLE II (cont.)

SPACE-TIME CORRELATION MEASUREMENTS
OF BOUNDARY LAYER PRESSURE FLUCTUATIONS

INVESTIGATOR	Maestrello (refs.14,15,22,23)	Willmarth and Wooldridge (ref. 10)
MACH NUMBER	0.52	approx. 0.18
δ^* (in.)	0.155	0.5
D/δ^*	0.4	0.33
MEASUREMENTS REPORTED		
1. Autocorrelations	x	x
2. Longitudinal correlations	x	x
3. Transverse correlations	x	x
4. Off-axis correlations		
5. Spatial correlation contours	x	x
6. Convection velocity vs longitudinal separation		x
7. Convection velocity vs frequency		x
SPECIAL TYPES OF MEASUREMENTS	Correlations of narrow-band pressure fluctuation measurements Eddy lifetime vs Mach number	Spatial decay of wave number components 3-D plot of longitudinal space-time correlation

One pressure measurement is taken at the point (x, z) on the surface at time t, and the other measurement is taken at a different point $(x + \xi, z + \eta)$ on the surface at a different time $T + \tau$.

In all the investigations summarized in Table II, except the perturbed flow study of Speaker and Ailman (ref. 19), it is assumed the surface-pressure field is spatially and temporally homogeneous, so that the correlation is a function only of the spatial differences ξ, η, and the temporal difference τ, and can be written as $R(\xi, \eta, \tau)$. The inhomogeneous cases considered in reference 19 give rise to correlations which are functions of the measurement positions as well as the separations. In actuality the correlations reported by the various investigators are special cases of the complete space-time surface-pressure correlation. We have used the following terminology in Table II and in the text: $R(0, 0, \tau)$ autocorrelation; $R(\xi, 0, 0)$ longitudinal correlation; $R(0, \eta, 0)$ transverse correlation; contours of constant $R(\xi, \eta, 0)$ - spatial correlation contours; $R(\xi_o, 0, \tau)$ longitudinal space-time correlation (ξ_o indicates a constant spatial separation); and $R(0, \eta_o, \tau)$ transverse space-time correlation.

Correlation results. - The cross correlation is the Fourier transform of the cross power spectral density. The autocorrelation is the transform of the power spectral density function. This relationship has been used by Speaker and Ailman (ref. 19) to determine the power spectral density of the turbulent boundary layer pressure fluctuations. The same relationship has been used by others (refs. 11 and 22) as a check on their correlation measuring equipment.

Measurements of the longitudinal and transverse correlations reported by the authors listed in Table II are presented in figures 21 and 22. With one exception (Maestrello) the subsonic data in figure 21 show that the correlation function drops to zero in the direction of flow within a space of the order of three to five times the displacement thickness, and stays negative. The correlation gradually approaches zero at some point beyond twenty times the displacement thickness of the boundary layer. The one supersonic measurement indicates the same general trend but the zero crossing occurs in a much shorter distance.

In plotting the data of Willmarth and Wooldridge (ref. 10) in figure 21 note has been taken of the fact that their space-time correlations show the presence of an acoustic disturbance traveling upstream. This disturbance had the effect of introducing positive correlation near zero time delay which only became significant for values of the transducer separation distance of the order of 5 to 7 times the displacement thickness. In replotting the data the hump in the correlation function due to the acoustic signal has been edited out in order to present the estimate of the longitudinal correlation shown in the figure.

The data of figure 12 show that the correlation laterally remains positive and gradually approaches zero at a distance greater than twenty times the boundary layer displacement thickness. Again the one piece of supersonic data indicates that the correlation approaches zero in a shorter distance than does the subsonic data. The trends indicated in figures 21 and 22 have been observed by other workers as well (for example, see refs. 6 and 24).

As shown in Table II, in addition to longitudinal and lateral spatial correlation, investigations have been carried out at various off-axis directions to the flow. Several authors have also presented contour plots of constant correlation $R(\xi, \eta, 0)$ (refs. 11, 19, 21). As might be expected from inspection of figures 21 and 22, such plots strongly show the differences between the various experimental results and do not look at all alike.

It is suggested that one might draw mean curves through the data given in figures 21 and 22 and use these to obtain estimates of contours of constant correlation. The off-axis spatial correlations indicate that such contours would take on a figure-eight configuration.

References 10, 11, 13, 19, and 22 listed in Table II all contain measurements of the longitudinal space-time correlation $R(\xi_o, 0, \tau)$, with a fixed longitudinal transducer separation ξ_o. References 11, 13, and 19 also contain measurements of the transverse space-time correlation $R(0, \eta_o, \tau)$ obtained for fixed transverse transducer

separation. In addition, reference 11 contains longitudinal and transverse space-time correlations of surface-pressure measurements which have been filtered in narrow bands and reference 10 contains longitudinal and transverse space-time correlations of surface-pressure measurements which have been filtered by high-pass and by low-pass filters.

Speaker and Ailman (ref. 19) considered the possibility of factoring complete space-time correlation into three functions, each of which depends only on one separation variable. For the flow conditions investigated, it was concluded that the correlation could be expressed as the product $C_1(\xi, \eta)\, C_2(\tau)$ of one function depending only on the spatial separation variables and another function depending only on the time delay. However, it was concluded that separation of the spatial correlation function $C_1(\xi,\eta)$ into two functions $C_3(\xi)$ and $C_4(\eta)$ resulted in considerable error, even for the case of unperturbed supersonic flow. In addition, it was concluded that, in the case of supersonic flows perturbed by steps or shocks, the spatial part $C_1(\xi,\eta)$ of the correlation behaved differently in different spatial regions of the flows, whereas the temporal part $C_3(\tau)$ of the correlation behaved similarly in the different spatial regions of the investigated flows.

Convection Velocities. - Figure 23 presents estimates of the broad band convection velocity as a function of longitudinal separation determined by various authors listed in Table II. [The convection velocity corresponding to the longitudinal separation ξ_o is usually calculated from measurements of the longitudinal space-time correlation $R(\xi_o, 0, \tau)$ by dividing the separation ξ_o by the time delay τ for which the correlation $R(\xi_o, 0, \tau)$ is a maximum. It has been argued (ref. 4) that a more acceptable, but more difficult, method of measuring the convection velocity would be to divide the separation ξ at which the longitudinal space-time correlation $R(\xi, 0, \tau_o)$ is a maximum by the fixed time delay τ_o.] The convection velocities shown

in the figure all start at approximately 0.5 U_∞ (one half the free stream velocity), increase quite rapidly with increasing longitudinal separation, and level off at a value of approximately 0.8 U_∞ at a longitudinal separation of approximately 10-30 δ^*. Since experimental measurements (refs. 10, 22) indicate that the high frequency eddies decay more rapidly than the low frequency eddies, the increase in convection velocity with increasing longitudinal separation is usually interpreted as evidence that the high frequency eddies travel slower than low frequency eddies.

Bull Wilby and Blackman (ref. 11), Bakewell (ref. 6) and Corcos (ref. 21) have investigated the convection velocity as a function of frequency (dispersion) obtained from narrow-band measurements of the longitudinal space-time correlation. These measurements are presented in figure 24, where the dimensionless convection velocity has been plotted as a function of dimensionless wavelength (reciprocal frequency). The measurements of Bull et al have been taken directly from the reference, but in order to include the work of Bakewell and Corcos, an estimate of the displacement thickness was required. In both cases fully turbulent flow in a pipe was investigated. We assumed that the displacement thickness was 1/16 of the pipe diameter.

The measurements shown in figure 24 indicate that the high frequency, short wavelength components travel more slowly than the low frequency long wavelength components. The measurements are consistent with the physical picture that the high frequency components are produced by small scale eddies, which are located close to the surface and therefore do not travel as fast as the low-frequency large-scale eddies, which project further out into the boundary layer.

The data in figure 24 may reasonably well be represented by a straight line with a slope of the order of 0.09.

Structural Response

Work on structural response to turbulent boundary layer excitation has been carried on by Lucio Maestrello of the Boeing Company (refs. 14, 15, 22, 23), J. F. Wilby et al of the University of Southampton (refs. 11, 25, 26) G. R. Ludwig of the University of Toronto (ref. 24), D. A. Bies of Bolt Beranek and Newman Inc. (ref. 27), and by Paul F. R. Weyers of California Institute of Technology (ref. 28). The first four investigators placed a test panel flush with the side wall of a wind tunnel for their investigation. The last investigator listed above investigated the response of a thin Mylar tube to turbulent flow through it. Information pertinent to these tests is given in Table III.

In all cases of response investigation except that of Bies, the displacement response was measured, and the resulting spectra were dominated by the fundamental modes of the panel or tube and the first few overtones. Workers at Southampton have identified the various panel modes and have compared measured frequency and amplitude with the predictions of theory outlined by them. The theory predicts fairly well the resonant frequencies observed but gives poor agreement with the measured amplitudes.

The workers at Southampton have used their theory to predict trends in response with variation of various parameters such as boundary layer displacement thickness and panel thickness. They have then sought to verify experimentally the dependence of panel response on these parameters, with mixed success.

In addition to investigating the response of panels to boundary layer excitation, the workers at Southampton have also investigated the response of their panels to a siren and an air jet. Their results indicate that the acoustic noise sources and the turbulent boundary layer are equally effective in producing displacement for a unit mean square pressure fluctuation. This matter is discussed further later in this section.

TABLE III

WIND TUNNEL STRUCTURAL RESPONSE MEASUREMENTS

INVESTIGATOR	PANEL DIMENSIONS		MODAL DENSITY RANGE	MACH NUMBER	DISPLACEMENT THICKNESS (inch)	QUANTITY MEASURED
	Size (inch)	Thickness (inch)				
Lucio Maestrello (refs. 14,15,22, 23)	aluminum 7 x 12	0.020 0.040 0.060 0.080	fundamental and first few overtones	0.34 to 0.64	0.155	radiated power, displacement
J. F. Wilby Bull, Wilby and Blackman Wilby and Richards (refs. 4,25,26)	steel 4 x 2 3.5 x 3.5 4 x 2.75	0.005 0.010 0.015	fundamental and first few overtones	0.3 0.5	0.053 to 0.176	displacement
G. R. Ludwig (ref. 24)	steel 11 x 11	0.0015 0.002 0.004 0.008	fundamental and first few overtones	0.05 to 0.17	0.054 0.43	radiated power, displacement
Paul F. R. Weyers (ref. 28)	mylar cylinder 1.0 dia.	0.005 0.001 0.0021	fundamental and first few overtones	0.11 to 0.28	--	radiated power
D. A. Bies (ref. 27)	steel 11.5 dia.	0.012 0.022	high modal density	1.4 3.5	0.068 0.306	acceleration

Maestrello and Ludwig have investigated both panel response and radiated sound power from panels of comparable size. As Table III shows, however, Ludwig has looked at very thin panels, whereas Maestrello's panels are an order of magnitude thicker. In both of these cases the panel response was dominated by the fundamental mode of the panel and its first few overtones. Ludwig concentrated his effort on the measurement of radiated sound power and reports only one measurement of panel displacement. Maestrello reports many measurements of both displacement and radiated sound power.

Typical of the spectra of the radiated sound power observed by Maestrello and also of Ludwig and Weyers is the set of curves shown in figure 25. In the figure is shown the sound power in one-third octave bands of noise radiated by a 0.080 inch thick panel into a reverberant room. The peaks in the spectra may be associated with the fundamental frequency of the panel and its first few overtones.

From the figure we notice that two things happen as the flow velocity increases: The general level rises, and the response extends to higher frequencies. The first observation is understandable in terms of increased pressure fluctuation levels with increased flow, since the form of the pressure normalization parameter implies that the low-frequency pressure spectrum increases proportionally to the cube of the flow velocity. The second observation may be understood on the following basis. If we define a hydrodynamic coincidence frequency as the frequency at which a flexural wave in the panel is equal to the mean convection speed of the turbulent boundary layer (taken as about 0.8 of the free stream velocity), we find that this frequency is directly proportional to the square of the flow velocity and inversely proportional to the panel thickness. The spectra shown in the figure begin their sharp upper frequency roll off near this coincidence frequency in each case. Thus, the strongly excited portion of the panel response spectrum lies between the fundamental frequency and the coincidence frequency.

Maestrello, Ludwig, and Weyers all report that the radiated sound power is proportional to the fifth power of the free stream velocity. This power law dependence has been observed in at least one flight measurement (ref. 29). This relationship is not precisely followed, however, since power law variations about the fifth power were also observed. In fact, Maestrello showed that, at high Mach numbers for all but his thickest panel, the power relationship abruptly decreased to the 2.5 power law. Data which illustrates these findings taken from Maestrello's work is shown in figure 26.

The dependence of radiated power or panel displacement response on panel thickness may be inferred from the data in figure 26. Maestrello, Ludwig, and Wilby found that the panel displacement is proportional to some inverse power of the panel thickness. The power ranges between 1.0 and 1.6. Maestrello summarizes these findings and compares them with the theoretical predictions of various workers whose predictions range between 1.0 and 3.0.

Figure 26 illustrates another fact discovered by these investigations. The radiated sound power follows the mean square amplitude of response of the panels when the low order modes dominate the response. This conclusion is borne out also by comparisons of displacement and radiated power spectra given by Ludwig and Maestrello. This conclusion is contrary to what would be expected if the radiation impedance of the panel had a significant large real part, since in this case the radiated power should follow the panel velocity rather than the displacement. It should be remembered that if the velocity remains constant with increasing frequency, the displacement should decrease in proportion to the frequency, so that the effect discussed here should be readily observable.

An effort was made to find relationships which would allow one to scale Maestrello's and Ludwig's work, but no simple scaling laws could be found. Ludwig gives relationships which seem to hold for his data, but they cannot be used to scale Maestrello's results. This difficulty may come about because Ludwig's panels may be controlled by membrane forces rather than panel stiffness forces. This point is not clear.

In summary we may say that the investigations of the first four investigators listed in Table III have shown the following:

(1) The displacement response of a lightly damped panel to turbulent boundary layer excitation is always dominated by the fundamental of the panel and its first few overtones.

(2) The frequency range most strongly excited extends up to the frequency of coincidence between flexural waves and the convected turbulent boundary layer. Above this frequency the displacement spectra fall off rapidly.

(3) In the frequency range of low modal density the radiated sound power is proportional to the mean panel displacement rather than panel velocity.

(4) In the frequency range of low modal density the radiated sound power is proportional to the fifth power of the free stream velocity over a range of low Mach numbers, but at high subsonic Mach numbers the power law decreases to about the 2.5 power.

(5) No theory apparently exists which gives good quantitative agreement between predicted and observed response, and no empirical relationships have been discovered by which one set of data may be scaled to that of another set of data.

As mentioned earlier and as pointed out in Table III, Bies has carried on quite a different investigation of panel response. In his experiment the panels investigated were highly damped, and the acceleration response (rather than displacement response) was measured. Consequently, the low order modes were deliberately suppressed. The frequency range of high modal density was investigated, where it was shown that fairly good agreement between theory and experiment exists. In actual flight measurements the dominant portions of the internally observed spectra

(for example, the vibration spectra from which curves of equivalent acoustic fields have been generated as in figures 36 through 41) are in the frequency range of high modal density for the skin panels. Thus, Bies claims that his results may be scaled to estimate response of full-scale supersonic transport panels.

In addition to investigating response of panels to unperturbed flow, Bies has also investigated the effect of mild perturbations such as an impinging shock and an expansion. He has also investigated the response of his panels to a reverberant acoustic field and has compared the response to such excitation to the response to a turbulent boundary layer. In addition, Bies's investigation has been carried out in the supersonic flow range, while all other investigations have been in the subsonic flow range.

The following conclusions are drawn from Bies's report:

(1) Fairly good quantitative agreement was obtained between theoretically predicted and measured panel response to turbulent boundary layer pressure fluctuations for the cases of unperturbed flow.

(2) To a fair approximation, one could associate a single transfer function with a panel, relating acceleration response to turbulent boundary layer pressure fluctuations under conditions of unperturbed or mildly perturbed flow.

(3) At Mach 3.5 boundary layer pressure fluctuations were of the order of 6 dB more effective in driving the 0.22" thick panel than comparable reverberant acoustic fields. This is in agreement with theory, which predicts the ratio to be 7 to 8 dB.

(4) At Mach 1.4 two regimes were observed. In the low-frequency range, a reverberant acoustic field was slightly more effective in driving the panels than were boundary layer pressure

fluctuations. In the high-frequency range, the boundary layer pressure fluctuations were as much as 7 or 8 dB more effective in driving the panel than the reverberant acoustic field. This observation is in qualitative agreement with the predictions of theory.

This last result appears also to be in qualitative agreement with the Southampton work which showed equivalence between acoustic and aerodynamic excitations. The Southampton investigation was in the low-frequency low-Mach number range, where Bies's work would indicate that such equivalence would exist.

FLIGHT MEASUREMENTS

Boundary Layer Pressure Fluctuation Measurements

Flight measurements of boundary layer pressure fluctuations have been assembled from various sources (refs. 29 through 41) and are presented in figures 27 through 42. In most cases the data come from published reports, while in the cases of Titan II, Titan III, and Saturn the data have been acquired by the author through contact with the people who made the measurements. Microphone size corrections have been made by the author wherever it was clear that the corrections were necessary.

In practically all cases of flight measurements considered here, no information about the boundary layer was available. In order to normalize the available data, the procedure outlined above was used. The altitude, air speed or Mach number, and a characteristic dimension were used to estimate a Reynolds number. From the estimated Reynolds number, characteristic dimension, and Mach number, estimates were made of displacement thickness and coefficient of skin friction. The normalizations used in most of the figures are thus necessarily approximate. However, the data contained in figures 27 and 30 are based on measured values of the boundary layer parameters.

The data in the figures have been placed in two groups, with measurements on airplanes in the first group and measurements on space vehicles in the second group. In general an effort was made to place the airplane microphones in regions of relatively smooth flow, but this was not possible for the space vehicle microphones. In fact, the space vehicle microphones were often in regions of highly perturbed flow (shocks or separated flow). Thus our figure grouping places the less perturbed flows first and the more perturbed flows last. Following this general line, the various measurements have been ordered in order of increasing Mach number within each group, assuming that flow will more likely be perturbed at higher Mach numbers than at lower Mach numbers.

The airplane flight data contained in figures 27 through 34 show the following trends: a general buildup in the low-frequency portion of the normalized spectrum with increase in Mach number, and a general asymptotic approach to the same values at high frequencies for all Mach numbers. The glider data contained in figure 27 form a lower bound for low Mach number and least perturbed flow. The glider data also define the asymptotic behavior of all data at high frequencies. The C-141 data of figure 30 form a kind of upper bound for relatively unperturbed flow but high subsonic Mach number at low frequencies. The data of figure 33 appear to be rather erratic for reasons unknown and perhaps should not be compared with the other data, since they were taken on a nose cone which does not simulate a flat plate very well. In summary, the airplane flight data appear to be fairly self-consistent and in line with wind tunnel measurements.

The spectrum levels observed on various space vehicles shown in figures 35 through 41 are generally quite high in the low portion of the spectrum but are in line with the idea that they might asymptotically approach the high-frequency spectrum levels of unperturbed flow of figure 27. The very high levels observed on the space vehicles are thought to be due to highly perturbed flow.

The data shown in figure 42 were taken on a Mercury test vehicle. The configuration was such that the flow was quite strongly perturbed. The very high levels in

the low-frequency range are thought to be due to the presence of a spoiler which strongly affected the subsonic and just sonic flow but was relatively ineffective at supersonic Mach numbers.

Structural Response

In figures 32 and 36 through 41 an additional bit of information has been included. In these figures we have inserted solid lines labeled "equivalent acoustic field." The lines are based on measurements of strain or acceleration on the skin or of acceleration on skin-mounted components under two conditions. The structure is excited by acoustic noise in the first condition and by turbulent boundary layer pressure fluctuations in the second. The lines represent the acoustic spectrum which would produce the same structural response as observed when excited by the boundary layer pressure fluctuations. Comparison of the equivalent acoustic pressures (represented by the line) with the measured boundary layer pressure fluctuations (shown as points) shows the relative efficiency of acoustic and aerodynamic exicitation.

For most of the measurements, the equivalent acoustic pressure spectra are close to the boundary layer spectra. From this we conclude that acoustic and aerodynamic pressure are approximately equally efficient in exciting structural response, for the configurations measured. However, the data shown in figures 37 and 38 are significant exceptions to this conclusion. In these two cases acoustic and aerodynamic exictation appear to be equally effective over the low-frequency portion of the spectrum, but above a Strouhal number of about 0.2, the acoustic excitation becomes less effective, as indicated by the higher equivalent acoustic levels required to achieve the same response as produced aerodynamically. This general behavior is in line with Bies's observations on panel response in a wind tunnel, discussed above. The order of magnitude difference in efficiency from the flight data is also in agreement with Bies's results.

CONCLUSIONS AND RECOMMENDATIONS

The principal conclusions of this report are as follows:

(1) Fourteen published wind tunnel measurements of boundary layer pressure fluctuations show spectra that vary widely one from another. However, over a limited frequency range, $0.05<\omega\delta^*/U_\infty<5.0$, sufficient experimental data agree to define a characteristic spectrum about which many of the measurements cluster.

(2) Flight measurements of boundary layer pressure spectra in unperturbed flows are in general agreement with each other and with the characteristic spectrum of the wind tunnel measurements.

(3) Flight measurements of perturbed flow generally show a buildup of the low frequency portion of the spectrum. The spectrum asymptotically approaches the unperturbed flow spectrum at high frequencies.

(4) There is general agreement that the mean convection velocity determined by space-time correlation measurements of the turbulent boundary layer increases with spatial separation between observation points and that the asymptotic value for large separation distances is about 0.8 of the free stream velocity.

(5) The narrow band convection velocity is approximately proportional to $(\omega\delta^*/U_\infty)^{-.09}$ for subsonic flow.

(6) Longitudinal and lateral spatial correlation are in general agreement though they differ widely in detail. As a consequence there is a general lack of agreement between various investigators on the shape of the contours of constant correlation in the turbulent boundary

layer, although the measurements have all been made in approximately the same Mach number range.

(7) Measurements of structural response of panels excited by boundary layer turbulence in wind tunnels have shown that the displacement response is dominated by the first few modes of the panel. At low flow velocities the displacement response is proportional approximately to the fifth power of the flow velocity, but at high flow velocities the dependence decreases to the 2.5 power. No general theory or empirical relations exists which enable the scaling of one set of panel displacement response measurements (first few modes) to another set of measurements.

(8) Sound power radiated by aerodynamically excited panels is proportional to the mean square displacement of the panel and thus follows the power law relationships to flow velocity described in item 6.

(9) In the frequency range of high modal density, one set of acceleration response measurements shows reasonable agreement with the predictions of theory. At low frequencies acoustic and aerodynamic excitations are approximately equally effective in exciting panel response. At high frequencies aerodynamic excitation may be as much as 8 dB more effective than acoustic noise in exciting panel response. The frequency of crossover between these two ranges decreases with increasing Mach number, but the general conditions which determine this crossover frequency quantitatively remain to be determined.

(10) Measurements of the structural response of flight vehicles show a relative response to acoustic and aerodynamic excitations in qualitative agreement with the wind tunnel measurements described in item 9.

(11) Although there have been many measurements of surface pressure fluctuations, very few measurements include sufficient aerodynamic data to permit comparisons with other data, or to extrapolate the data to other conditions. In order to generate the aerodynamic data, a system of engineering curves has been developed from published measurements of local skin friction and boundary layer profiles to enable the estimation of boundary layer parameters for Mach numbers up to 4 and Reynolds numbers based on a chacteristic length up to 2×10^9. Use of this system of curves has enabled the uniform presentation of flight and wind tunnel surface pressure measurements for intercomparison in this report.

In addition to the specific conclusions drawn from the body of material reviewed in this report, some general conclusions and recommendations may be drawn. A great many wind tunnel measurements of turbulent boundary layer pressure fluctuation have been reviewed. In spite of apparent care taken by the various investigators, their spectrum and correlation results show wide variation when compared with each other, although each investigator generally presents data that are quite self consistent. One exception exists, however, where the investigators made a great many measurements over an extended region in the test section of their tunnel (ref. 19). Their results showed rather wide scatter, but their results are well within the scatter of all of the measurements discussed in this report. One wonders whether other experimenters have looked over extended regions of their test sections and found similar nonuniformity of measured results.

The flight measurements reviewed in this report seem generally to be quite self consistent, perhaps more consistent than are wind tunnel measurements. One wonders whether the presence of opposite walls in the wind tunnel may introduce subtle local perturbations of the boundary layer that are only detectable as changes in the structure of the pressure fluctuations. Such subtle perturbations may strongly affect local measurements of pressure fluctuations

or the correlation properties of the pressure field without being representative of the overall boundary layer.

Wind tunnels have been used for studying panel response. It is quite likely that if local perturbations to the boundary layer do exist as suggested above, that the overall response of test panels will not be seriously affected, since the panel may be thought of as integrating the forces that it sees. It thus may act to smooth or average the pressure fluctuation field in the same way as flight hardware might do. If this is indeed the case, it would appear that measurements of the detailed space-time properties of the pressure field could not provide information that can readily be related to structural response. This line of argument leads to the recommendation that wind tunnel investigations should emphasize response measurements and deemphasize pressure measurements.

However, most of the response experiments performed to date have been concerned with displacement response of relatively small panels. If the linear dimensions of these experiments are scaled to sizes of interest to the designers of high performance aircraft, the scaled frequency ranges fall well below the frequency ranges of interest. For the purpose of the designer, the models investigated should simulate real structures and should cover the frequency range of interest. If such programs are undertaken, then particular care should be taken to properly scale such pertinent parameters as the hydrodynamic coincidence frequency and the boundary layer thickness. Such measurements should be performed in conjunction with suitable flight measurements in order to verify the scaling relationships utilized in designing the model experiment.

The data on flight measurements (ref. 39) and wind tunnel measurements of structure response (ref. 27) indicate that the use of one-to-one correspondence between aerodynamic and acoustic excitation can be very misleading. Also the use of inflight pressure data can be misleading if the pressure transducer is located near a region of strongly perturbed flow confined to a very local region about the transducer. To avoid these problems, it is recommended that "equivalent acoustic fields" such as presented in

this report be used for estimating the response of flight hardware and designing ground acoustic tests to simulate the flight environment.

REFERENCES

1. Anon: The ARDC Model Atmosphere, Air Force Surveys in Geophysics No. 115, Air Force Cambridge Research Center TR-59-267 (August 1959).

2. Corcos, G. M.: Resolutions of Pressure in Turbulence, J. Acoust. Soc. Am., Vol. 35, No. 2, pp. 192-199, February 1963.

3. Willmarth, W. W.; and Roos, F. W.: Resolution and Structure of the Wall Pressure Field Beneath a Turbulent Boundary Layer, J. Fluid Mech., Vol. 22, Part 1, pp. 81-94, 1965. Fig. 8.

4. Chandiramani, K. L.: Interpretation of Wall Pressure Measurements Under a Turbulent Boundary Layer, Bolt Beranek and Newman Inc. Report No. 1310, August 1965.

5. Gilchrist, R. B.; and Strawderman, W. A.: Experimental Hydrophone-Size Correction Factor for Boundary-Layer Pressure Fluctuations, J. Acoust. Soc. Am., Vol. 38, No. 2, pp. 298-302, August 1965.

6. Bakewell, H. P., Jr.; et al: Wall Pressure Correlation in Turbulent Pipe Flow, U. S. Navy Sound Laboratory Report No. 559 (AD 283 683), 20 August 1962.

7. Jorgensen, Donald W.: Measurements of Fluctuating Pressures on a Wall Adjacent to a Turbulent Boundary Layer, U. S. Navy J. of Underwater Acoustics, Vol. 13, No. 2, pp. 329-336, April 1963.

8. Harrison, M.: Pressure Fluctuations on the Wall Adjacent to a Turbulent Boundary Layer, Department of the Navy, David Taylor Model Basin Hydromechanics Laboratory, Research and Development Report No. 1260, December 1958.

9. Baroudi, M. Y.; and Ludwig, G. R.; and Ribner, H. S.: An Experimental Investigation of Turbulence - Excited Panel Vibration and Noise (Boundary-Layer Noise), NATO Report No. 465, Advisory Group for Aeronautical Research and Development, April 1963.

10. Willmarth, W. W.; and Wooldridge, C. E.: Measurements of the Fluctuating Pressure at the Wall Beneath a Thick Boundary Layer, University of Michigan Department of Aeronautical Engineering Technical Report No. 02920-1-T, April 1962.

11. Bull, M. K.; Wilby, J. F.; and Blackman, D. R.: Wall Pressure Fluctuations in Boundary Layer Flow and Response of Simple Structures to Random Pressure Fields, University of Southampton, Department of Aeronautics and Astronautics Report No. 243, July 1963.

12. Murphy, J. S.; et al: Wind Tunnel Investigation of Turbulent Boundary Layer Noise as Related to Design Criteria for High Performance Vehicles, NASA TND-2247, April 1964.

13. Serafini, J. S.: Wall-Pressure Fluctuations and Pressure Velocity Correlations in a Turbulent Boundary Layer, NASA TR R-165, December 1963.

14. Maestrello, L.: Measurement of Noise Radiated by Boundary Layer Excited Panels, J. of Sound and Vibr., Vol. 2, No. 2, pp. 100-115, 1965.

15. Maestrello, L.: Response of Panels to Boundary Layer Turbulence, Boeing Company, Document No. D6-9944, Vol. 1, February 1964.

16. Williams, D. J. M.: Measurements of the Surface Pressure Fluctuations in a Turbulent Boundary Layer in Air at Supersonic Speeds, University of Southampton, AASU Report No. 162, Department of Aeronautics and Astronautics, December 1960.

17. Kistler, A. L.; and Chen, W. S.: The Fluctuating Pressure Field in a Supersonic Turbulent Boundary Layer, Jet Propulsion Laboratory Technical Report, No. 32-277, August 1962.

18. Westley, R.: Aerodynamic Sound and Pressure Fluctuations in a Supersonic Blowdown Wind Tunnel, National Research Council of Canada, Aeronautical Report No. LR-274, January 1960.

19. Speaker, W. V.; and Ailman, C. M.: Spectra and Space-Time Correlations of the Fluctuating Pressures at a Wall Beneath a Supersonic Turbulent Boundary Layer Perturbed by Steps and Shock Waves, Douglas Report SM-49806, November 1965.

20. Corcos, G. M.: Pressure Fluctuations in Shear Flows, University of California, Institute of Engineering Research Report, Series 183, No. 2, 1962.

21. Corcos, G. M.: The Structure of the Turbulent Pressure Field In Boundary Layer Flows, University of California, Institute of Engineering Research Report, Series 183, No. 4, 1963.

22. Maestrello, L.: Measurement and Analysis of the Response Field of Turbulent Boundary Layer Excited Panels, J. of Sound and Vibr., Vol. 2, No. 3, p. 270, July 1965.

23. Maestrello, L.: Measurement of Panel Response to Turbulent Boundary-Layer Excitation, AIAA Journal, Vol. 3, No. 2, pp. 359-361, March 1965.

24. Ludwig, G. R.: An Experimental Investigation of the Sound Generated by Thin Steel Panels Excited by Turbulent Flow (Boundary Layer Noise), University of Toronto, Institute of Aerophysics, UTIA Report No. 87, November 1962.

25. Richards, E. J.; and Wilby, J. F.: Panel Response and Its Relation to the Type of Excitation, Paper W5, Presented at the 67th Meeting of the Acoust. Soc. of Am., 6-9 May 1964, New York.

26. Wilby, J. F.: Random Excitation of a Simple Panel, Some Experimental Results, University of Southampton, Department of Aeronautics and Astronautics, Report No. 231, January 1963.

27. Bies, D. A.: A Wind Tunnel Investigation of Panel Response to Boundary Layer Pressure Fluctuations at Mach 1.4 and Mach 3.5, Bolt Beranek and Newman Inc., Report No. 1264, October 1965.

28. Weyers, P. F. R.: Vibration and Near-Field Sound of Thin-Walled Cylinders Caused by Internal Turbulent Flow, NASA Technical Note D-430, June 1960.

29. McLeod, N. J.; and Jordan, G. H.: Preliminary Flight Survey of Fuselage and Boundary-Layer Sound-Pressure Levels, National Advisory Committee for Aeronautics, RM H58B11, 13 May 1958.

30. Hodgson, T. H.: Pressure Fluctuations in Shear Flow Turbulence, College of Aeronautics, Cranfield University of England, CoA Note No. 129, May 1962.

31. Mull, Harold R.; and Algranti, J. S.: Flight Measurements of Wall-Pressure Fluctuations and Boundary-Layer Turbulence, Lewis Research Center, Ohio, NASA Technical Note D-280, October 1960.

32. Gibson, J. S.: Boundary Layer Noise Measurements on a Large Turbofan Aircraft, Paper I 10, 70th Meeting of the Acoust. Soc. of Am., November 1965.

33. Leech, F. J.; and Sackschewsky, V. E.: Boundary Layer Noise Measurements of the F-102 Aircraft, Air Force Systems Command, Wright-Patterson Air Force Base, Ohio, Technical Document Report No. MRL-TDR-62-71, August 1962.

34. Webb, D. R. B.; and Keeler, A. R.; and Allen, B. R.: Surface Pressures and Structural Strains Resulting from Fluctuations in the Turbulent Boundary Layer of a Fairey Delta 2 Aircraft, UDC No. 532-526.4: 629, 13.012.5:533,6.0482, c.p. No. 638, May 1962.

35. McLeod, N. J.: Flight-Determined Aerodynamic-Noise Environment of an Airplane Nose Cone up to a Mach No. of 2, Flight Research Center, Edwards California, NASA Technical Note No. D-1160 (N62 10644), March 1962.

36. Maestrello, L.: Boundary Layer Pressure Fluctuations on the 707 Prototype Airplane, Presented to the 64th Meeting of the Acoust. Soc. Am., 7-10 November 1962, Seattle, Washington.

37. Hilton, D. A.: In-Flight Aerodynamic Noise Measurements on a Scout Launch Vehicle, NASA TN D-1818, July 1963.

38. Unpublished Data Reduced from Bolt Beranek and Newman Inc. Data Tapes, Titan II Mark IV Decoy Vibration Environmental Study, BBN Report No. 1096, 11 August 1964.

39. Acoustical Vibration Data from Titan III Flight, BBN Report Nos. 1252, 1256, and 1261, 1965.

40. Unpublished Data obtained from Marshall Space Flight Center, Huntsville, Alabama, November 1965.

41. Mayes, W. H.; and Hilton, D. A.; and Hardesty, C. A.: In-Flight Noise Measurements for Three Project Mercury Vehicles, Langley Research Center, Virginia NASA Technical Note D-997 (N62 10083), January 1962.

A1. Schlichting, H.: Boundary Layer Theory, Pergamon Press, 1955, pp. 432-433.

A2. Moore, D. R.; and Harkness, J.: Experimental Investigation of the Compressible Turbulent Boundary Layer at Very High Reynolds Numbers, AIAA J3 No. 4, pp. 631-638 (April 1965).

A3. Jackson, M. W.; and Czarnecki, K. R.; and Monta, W. J.: Turbulent Skin Friction at High Reynolds Numbers and Low Supersonic Velocities, NASA TN D-2687, 1965.

A4. Matting, F. W.; and Chapman, D. R.; and Nyholm, J. R.; and Thomas, A. G.: Turbulent Skin Friction at High Mach Numbers and Reynolds Numbers in Air and Helium, NASA TR R-82, 1961.

A5. Murphy, J. S., and Bies, D. A., and Speaker, W. V., and Franken, P. A.: Wind Tunnel Investigation of Turbulent Boundary Layer Noise as Related to Design Criteria for High Performance Vehicles, NASA TN D-2247, 1964.

A6. Speaker, W. V.; Ailman, C. M.: Spectra and Space-Time Correlations of the Fluctuating Pressures at a Wall Beneath a Supersonic Turbulent Boundary Layer Perturbed by Steps and Shock Waves, Douglas Report SM-49806, November 1965.

A7. Coles, D. E.: The Turbulent Boundary Layer in a Compressible Fluid, Rand Corporation Report R-403-PR, 1962, also Phys. Fluids, 7, No. 9, pp. 1403-1423.

A8. Schlichting, H.: op. cit., p. 283.

A9. Anon: Handbook of Chemistry and Physics, 33rd Edition, Chemical Rubber Publishing Co.

A10. Schlichting, H.: op. cit., p. 443.

A11. Roshko, A.: Private Communication.

APPENDIX A

INVESTIGATION OF BOUNDARY LAYER PARAMETERS AT HIGH REYNOLDS NUMBERS AND MACH NUMBERS

At subsonic Mach numbers and low Reynolds numbers, certain well defined relations exist between the boundary layer parameters. These relations are essentially independent of the Mach number, and are defined by the characteristic length and the Reynolds number. For example, Schlichting (ref. A1) gives the following relations for the boundary layer thickness

$$\frac{\delta}{x} = 0.37\ Re_x^{-1/5} \quad , \tag{A1}$$

the displacement thickness

$$\delta^* = \frac{\delta}{8} \quad , \tag{A2}$$

and the momentum thickness

$$\theta = \frac{7}{72}\ \delta \quad . \tag{A3}$$

These relations follow when the boundary layer profile follows the well known seventh power law. At high Reynolds numbers and Mach numbers, the experimental evidence reviewed here indicates that the relationships given above must be considerably modified.

Boundary Layer Thicknesses

In figures A1, A2, and A3 we have plotted data from several sources (refs. A2-A7) to determine the behavior of the

boundary layer thickness, the boundary layer shape parameter, and the ratio of boundary layer thickness to momentum thickness. The form of the presentations is the result of empirical experimentation with the data to determine Mach number and Reynolds number dependence. In each figure we have indicated our choice of an empirical equation which seems both to fit the data best and to take on a limiting form at low Mach numbers and Reynolds numbers consistent with equations A1, A2, and A3.

Some remarks about the data shown in the figures are in order. In many cases a good deal of additional work was required to obtain values of such parameters as displacement thickness from the original published data. In a few cases judicious guesses had to be made to fill in partially complete information. In drawing the empirical curves of best fit, a knowledge of the reliability of the data shown was kept in mind. In any case the final results, the empirical equations, are based on the best information available to us and have been derived using sound engineering principles. The empirical system of equations given in the figures A1, A2, and A3 were used to determine the following set of equations.

$$\frac{\delta}{x} = 0.37\ Re_x^{-1/5} \left[1 + \left(\frac{Re_x}{6.9 \times 10^7} \right)^2 \right]^{1/10} \tag{A4}$$

$$\frac{\delta^*}{x} = \frac{[1.3 + 0.43M^2][\delta/x]}{10.4 + 0.5M^2\ [1 + 2x10^{-8}\ Re_x]^{1/3}} \tag{A5}$$

$$\frac{\theta}{x} = \frac{[\delta/x]}{10.4 + 0.5M^2\ [1 + 2x10^{-8}\ Re_x]^{1/3}} \tag{A6}$$

Figures 1, 2, and 3 of the text were prepared using these formulas.

Local Coefficient of Skin Friction

A voluminous literature exists describing the local coefficient of skin friction. The measurement of the quantity seems to contain a number of pitfalls, so that the calculation of the local skin friction coefficient from empirically based equations appears to lie in a somewhat controversial field. We have chosen to follow the lead of Coles (ref. A7) and have attempted to extend his formulation to high Reynolds numbers.

In figure A4 we have plotted the local coefficient of skin friction against Reynolds number based on momentum thickness, where both parameters are expressed in transformed coordinates based on a reference sublayer temperature (ref. A7). The references from which the data were taken are given in the figure. The solid line represents Coles' empirical approximation to all of the data available to him at the time of publication of his work, September 1962. The dotted line represents our extension to Coles' work based on the plotted points. The plotted points shown in figure A4 show more scatter and are generally somewhat below Coles' solid line and our dotted extension. The scatter of our data, which is greater than that of Coles' reduced data, is thought to be due to the approximations that we have made in representing the boundary layer. We have used the comparison between our plotted data points and Coles' line where they overlap to determine the adequacy of our approximations. This comparison has also been used to determine the placement of our dotted extension.

Procedure for Computing $\bar{c}_f$

The following procedure was used to enter the data in figure A4. It is based on an interpretation of Coles' work, and it contains a number of approximations to simplify the necessary computation. Coles shows that all available data on measured local skin friction for a turbulent boundary layer may be plotted on a single line if the appropriate parameters are referenced to local conditions at a mean position in the boundary layer. He finds that the local Reynolds number based on the distance from the wall to the mean position should have the value

$$Re_s = 8500. \qquad \text{(A7)}$$

This value will be used to compute the mean position temperature relative to the free stream static temperature.

The following relations will be assumed to hold for air where the ratio of specific heats $\gamma = 7/5$.

$$\frac{T}{T_\infty} = \frac{1 + 0.2M_\infty^2 r}{1 + 0.2M^2 r}, \quad r = 0.89 \tag{A8}$$

$$\frac{U}{U_\infty} = \frac{M}{M_\infty}\left(\frac{T}{T_\infty}\right)^{1/2} \tag{A9}$$

$$\frac{\rho}{\rho_\infty} = \frac{T_\infty}{T} \tag{A10}$$

$$\frac{\mu}{\mu_\infty} = \left(\frac{T}{T_\infty}\right)^{\alpha}, \quad \alpha = 0.905 \tag{A11}$$

$$\frac{y}{\delta} = \left(\frac{U}{U_\infty}\right)^7 \tag{A12}$$

Equation A8 follows from equation 15.7 of reference A8 and holds for air. It is assumed that the recovery factor r is in general different from unity and equal to 0.89. Equations A9 and A10 follow from the assumption of a perfect gas. Equation A11 holds fairly well for air over the temperature range from 70°K to 350°K, according to reference A9. Equation A12 seems to fit velocity profile data available to us well enough for our purpose (ref. A6, A10).

We proceed as follows by forming the relation

$$\frac{Re_y}{Re_\delta} = \frac{U}{U_\infty}\frac{\rho}{\rho_\infty}\frac{\mu_\infty}{\mu}\frac{y}{\delta} \tag{A13}$$

Use of equations A9 through A12 enables the transformation of equation A13 to read

$$\frac{Re_y}{Re_\delta} = \left(\frac{T_\infty}{T}\right)^{1+\alpha}\left[\frac{M}{M_\infty}\left(\frac{T}{T_\infty}\right)^{1/2}\right]^8 \tag{A14}$$

We introduce our expression for the boundary layer thickness, equation A4 and write

$$Re_\delta = Re_x\frac{\delta}{x} = 0.37\ Re_x^{4/5}\left[1+\left(\frac{Re_x}{6.9\times 10^7}\right)^2\right]^{1/10} \tag{A15}$$

From equation A8 we obtain

$$\frac{M}{M_\infty} = \sqrt{\frac{5}{rM^2}\left(\frac{T_\infty}{T}-1\right)+\left(\frac{T_\infty}{T}\right)} \tag{A16}$$

Use of equation A16 allows us to write equation A14 as

$$Re_y = Re_\delta\left(\frac{T_\infty}{T}\right)^{1+\alpha}\left[\frac{5}{rM^2}\left(1-\frac{T}{T_\infty}\right)+1\right]^4 \tag{A17}$$

We set the boundary layer Reynolds number given above equal to Coles' value given by equation A7. The corresponding temperature becomes the mean sublayer temperature T_s. Thus, equation A17 becomes

$$12.31 = Re_x^{1/5} \left(\frac{T_\infty}{T_s}\right)^{\frac{1+\alpha}{4}} \left[\frac{5.62}{M_\infty^2}\left(1 - \frac{T_s}{T_\infty}\right) + 1\right] \psi \ ,$$

$$\psi = \left[1 + \left(\frac{Re_x}{6.9 \times 10^7}\right)^2\right]^{1/40} \qquad \text{(A18)}$$

Equation A18 defines the quantity T_s/T_∞ in terms of the free stream Mach number and the Reynolds number based on characteristic length. This approximate equation was used to compute the value of the temperature ratio which was then used to compute the transformed local skin friction coefficient and Reynolds number. For the latter purpose the following equations were used

$$\bar{c}_f = c_f \left(\frac{T_s}{T_\infty}\right)^{\alpha} \left(1 + 0.2rM_\infty^2\right)^{1-\alpha} \qquad \text{(A19)}$$

$$\overline{Re}_{\bar{\theta}} = \left(\frac{\theta}{\delta}\right) Re_x \left(\frac{T_\infty}{T_s}\right)^{\alpha} \qquad \text{(A20)}$$

Procedure for Computing c_f

The following procedure was used to calculate the curves for local skin friction coefficient shown in figure 4 of the text. The method makes use of the solid curve with its dotted extension shown in the figure A4 and is based on an

interpretation of Coles' work due to Roshko (ref.A11). The steps involved in the computation are as follows:

1. Assume values of Reynolds number Re_x and Mach number M. Determine θ/x using figure 3 of the text and compute Re_θ.

2. Assume a value of k and compute $\overline{Re}_{\overline{\theta}} = k\, Re_\theta$. (One may start with a value of unity for k.)

3. Determine a value of $\overline{c}_f$ from Coles' curve in figure A4.

4. Compute

$$\frac{T_s}{T_w} = 1 + 17.2\left(\frac{0.022M_\infty^2}{1 + 0.178M_\infty^2}\right)\sqrt{\frac{\overline{c}_f}{2}} - 305\left(\frac{0.2M_\infty^2}{1 + 0.178M_\infty^2}\right)\frac{\overline{c}_f}{2}$$

(The above equation follows from Coles' work.)

5. Compute

$$k = \frac{\mu_\infty}{\mu_s} = \left(\frac{T_{o\infty}}{T_w}\,\frac{T_w}{T_s}\,\frac{1}{1 + 0.2M_\infty^2}\right)^{\alpha}$$

6. Compare k of step 5 with k of step 1.
   a) if they are the same, proceed to step 7
   b) if they are different, use the k of step 5 or a new choice of k and repeat steps 2 through 5.

7. Compute the ratio

$$\frac{T_{o\infty}}{T_w} = \frac{1 + 0.2M_\infty^2}{1 + 0.2rM_\infty^2}$$

8. Compute

$$c_f = \overline{c}_f\,\frac{T_{o\infty}}{T_w}\left(1 + 0.2M_\infty^2\right)^{-1}\left(\frac{T_w}{T_s}\right)^{\alpha}$$

APPENDIX B

PROCEDURE FOR ESTIMATING BOUNDARY LAYER PRESSURE SPECTRA

The following simplified procedure may be used for estimating boundary layer pressure spectra for Mach numbers up to 4 and Reynolds numbers based on characteristic length from 10^7 to 10^8. It will be found to be of particular use for new vehicle configurations, when a minimum amount of aerodynamic information may be available.

Given:

M_∞ Free stream Mach number

q Free stream dynamic pressure, in lbs/sq ft

U_∞ Free stream flow velocity, in ft/sec

x Distance from inception of turbulence (assume approximately 10 ft or distance from leading edge, whichever is greater)

1) Calculate the overall fluctuating pressure level

$$FPL_{overall} = 20 \log_{10} q + 84 \text{ dB} \qquad \text{(B1)}$$

The standard reference sound pressure of 2×10^{-4} dyn/sq cm has been used.*

---

* Equation (B1) is based on the integration of the normalized spectrum of Fig. 20 of the text. The value of the integral, in conjunction with a mean value for the local coefficient of skin friction in the range up to Mach 2, then gives the ratio of overall pressure fluctuation level to free stream dynamic pressure as 0.0054. This value has been used in the equation. It gives a value for overall sound pressure level which may be three decibels too high for Mach numbers greater than two.

2) Calculate the displacement thickness

$$\delta^* = \begin{cases} 0.0016\ x\ , & 0 < M_\infty < 2 \\ 0.004\ x\ , & 2 < M_\infty < 4 \end{cases} \qquad \text{(B2)}$$

3) Calculate the characteristic frequency

$$f_o = 0.1 \frac{U_\infty}{\delta^*} \qquad \text{(B3)}$$

4) Utilize the value of f_o and Fig. B1 to obtain the estimated boundary layer pressure spectrum. The fluctuating pressure level in 1-Hz bands is obtained by adding the quantity ($FPL_{overall}$ - 10 log $_{10}$ f_o) to the vertical scale of Fig. B1.

   The spectrum shape of Fig. B1 pertains to unperturbed flows. Strong perturbations tend to increase the portion of the spectrum below f_o. These increases are typically 10-20 dB at 10^{-1} f_o.

The engineering procedure presented here is valid for a range of Reynolds numbers and Mach numbers which essentially cover the range of interest for present-day booster systems and supersonic aircraft. The effects of changing the aerodynamic parameters may be evaluated from the figures in the main body of this report.

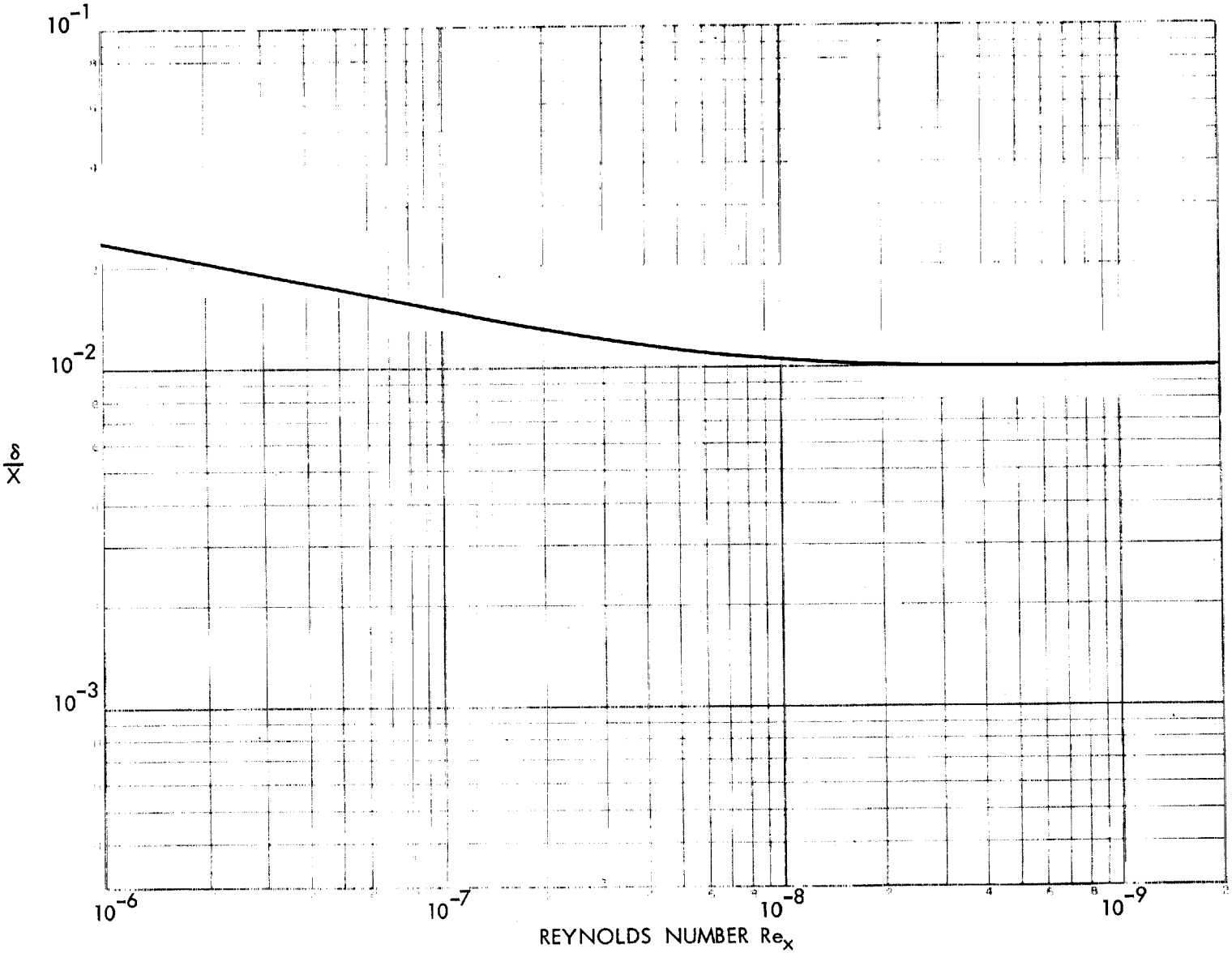

FIGURE 1. EMPIRICAL EQUATIONS FOR BOUNDARY LAYER PARAMETERS
NORMALIZED BOUNDARY LAYER THICKNESS δ/X

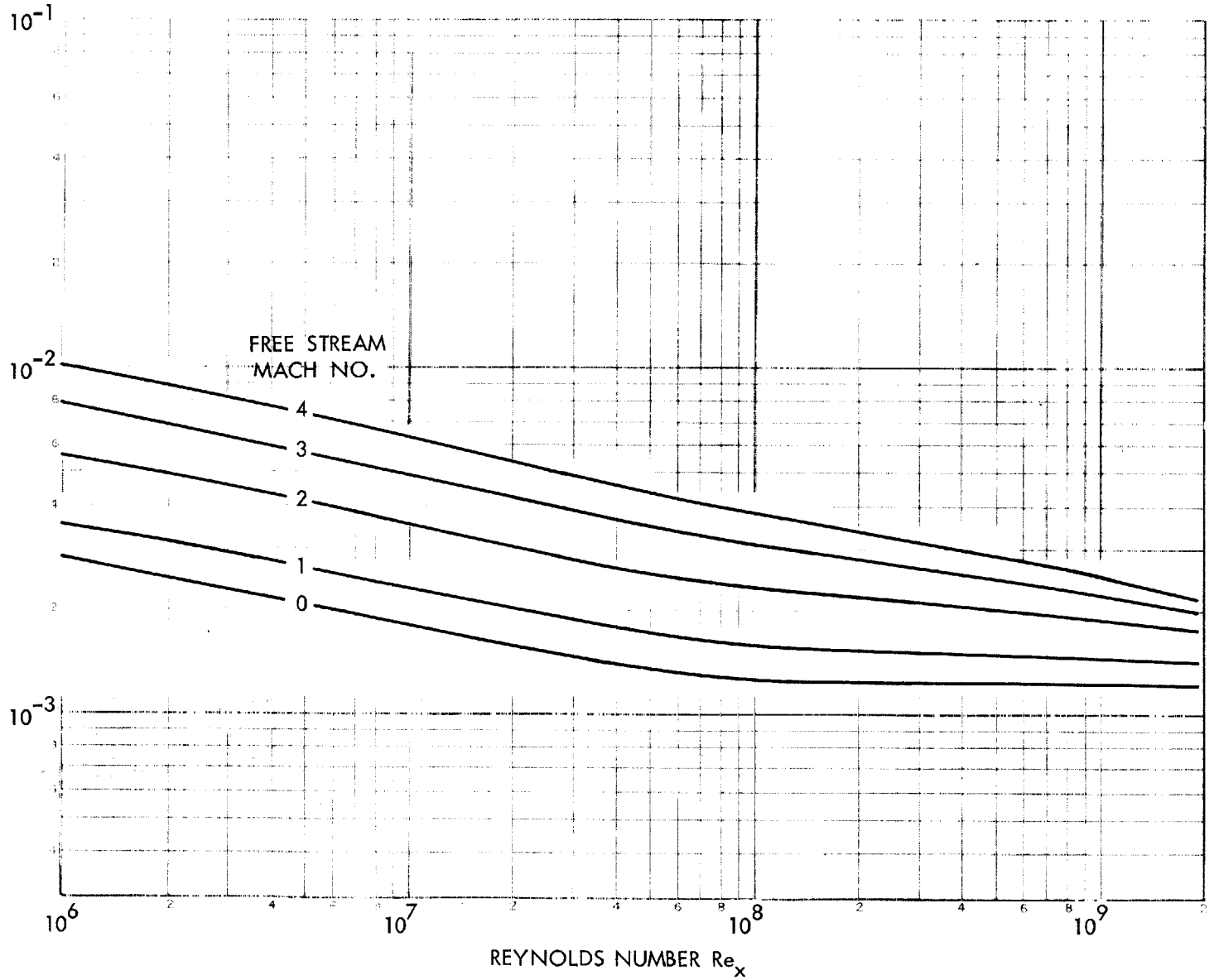

FIGURE 2. EMPIRICAL EQUATIONS FOR BOUNDARY LAYER PARAMETERS
NORMALIZED BOUNDARY LAYER DISPLACEMENT THICKNESS δ^*/X

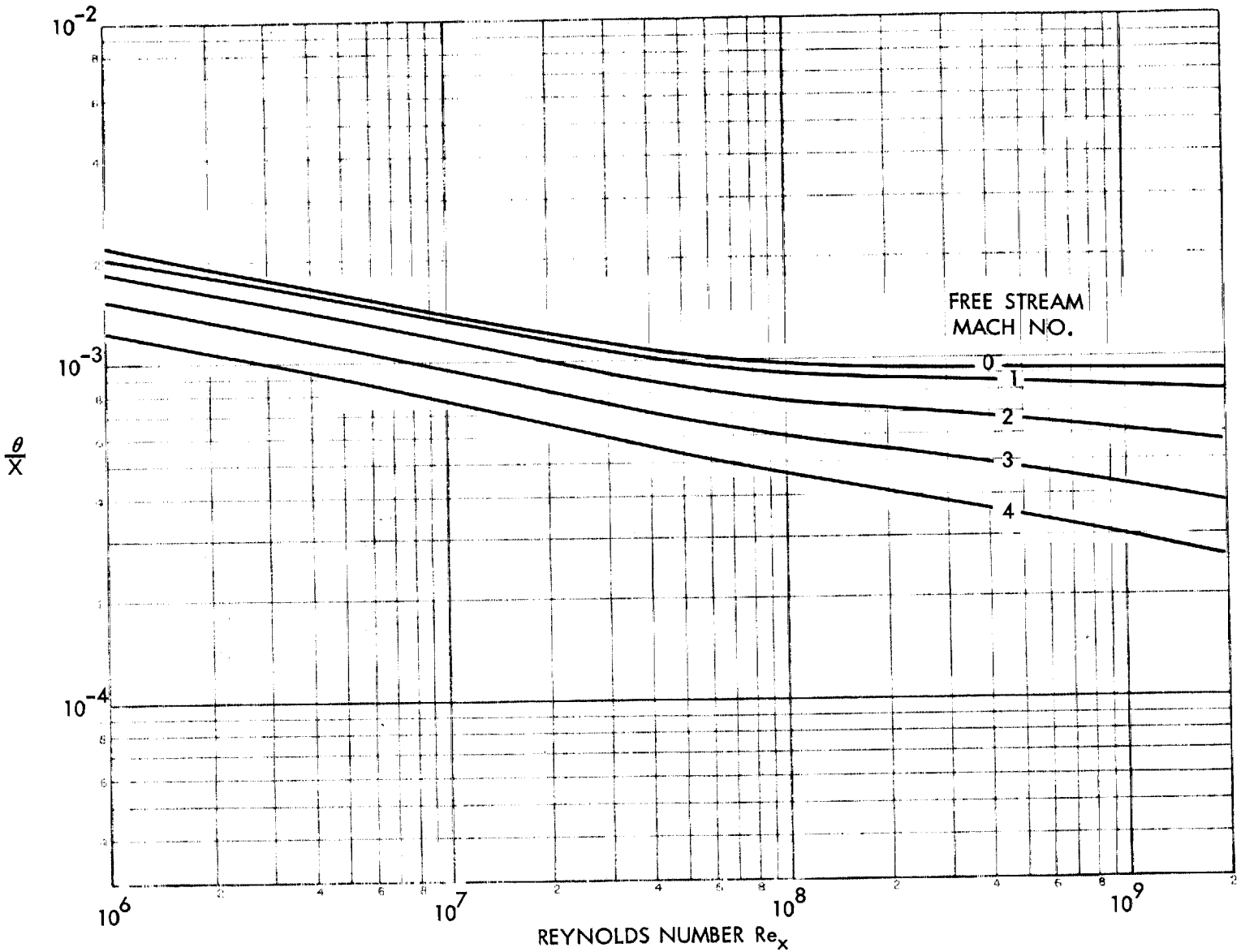

FIGURE 3. EMPIRICAL EQUATIONS FOR BOUNDARY LAYER PARAMETERS
NORMALIZED MOMENTUM THICKNESS

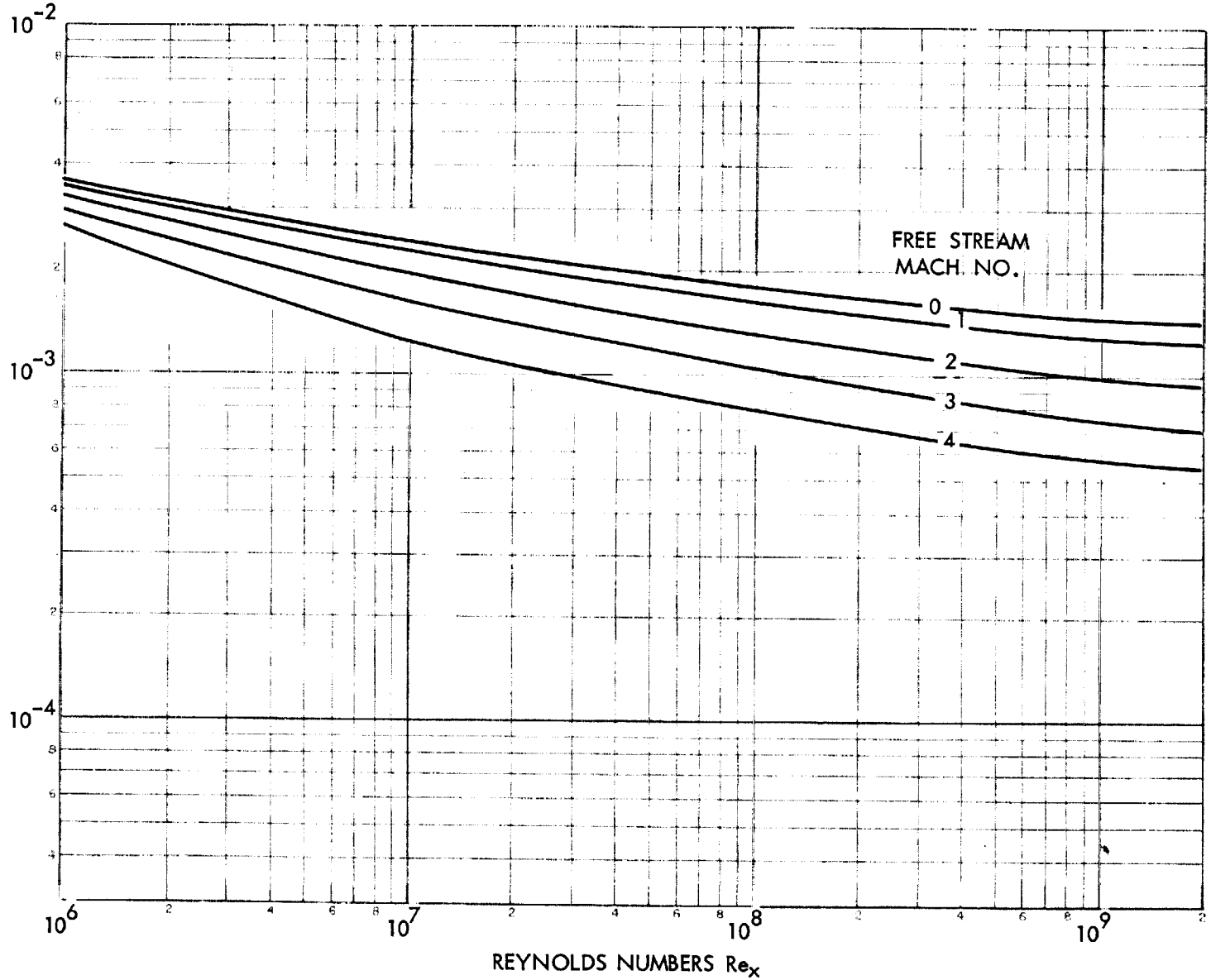

FIGURE 4. EMPIRICAL EQUATIONS FOR BOUNDARY LAYER PARAMETERS
COEFFICIENT OF LOCAL SKIN FRICTION C_f

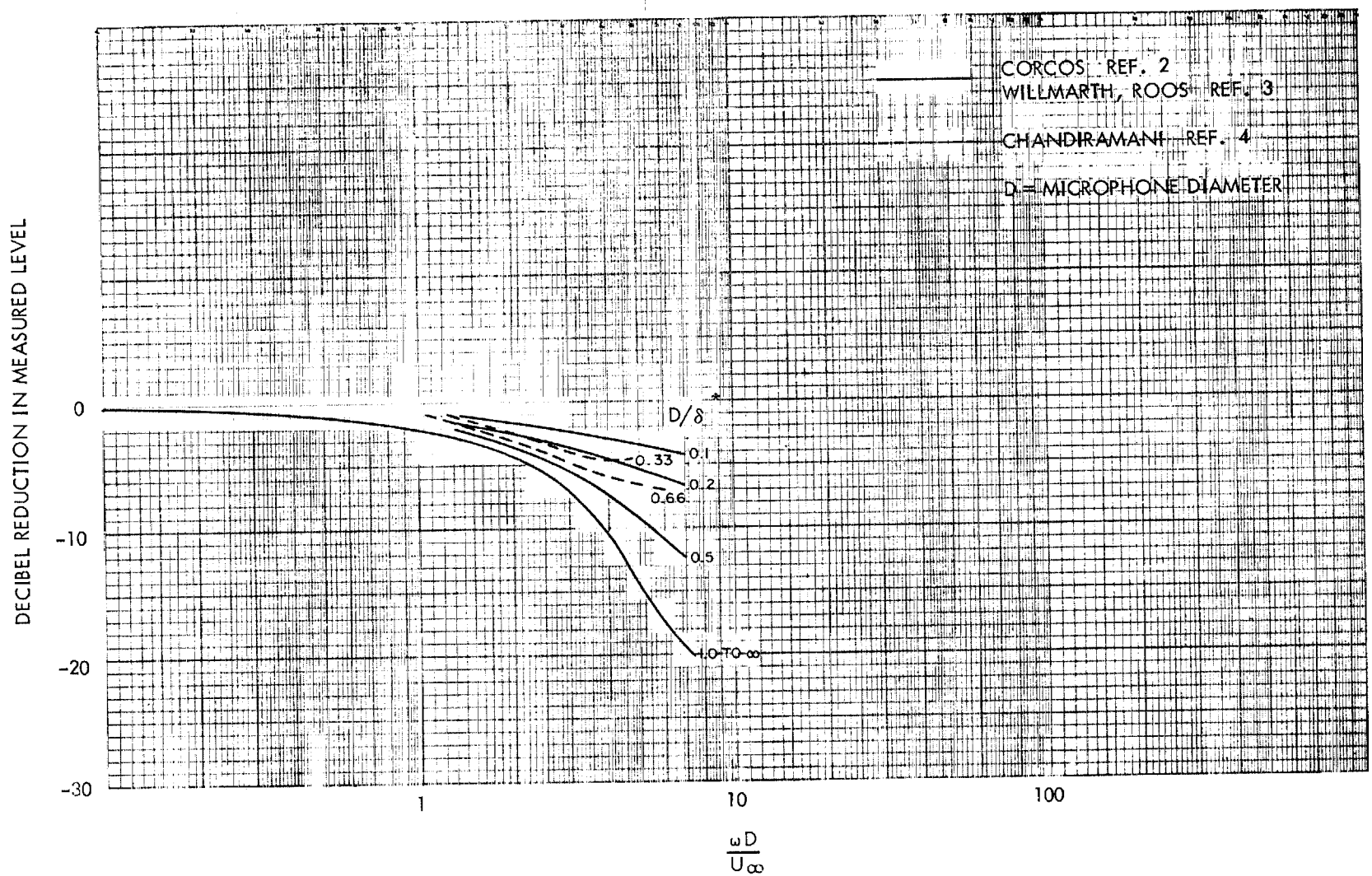

FIGURE 5. FREQUENCY RESPONSE OF A TRANSDUCER TO BOUNDARY LAYER PRESSURE FLUCTUATIONS

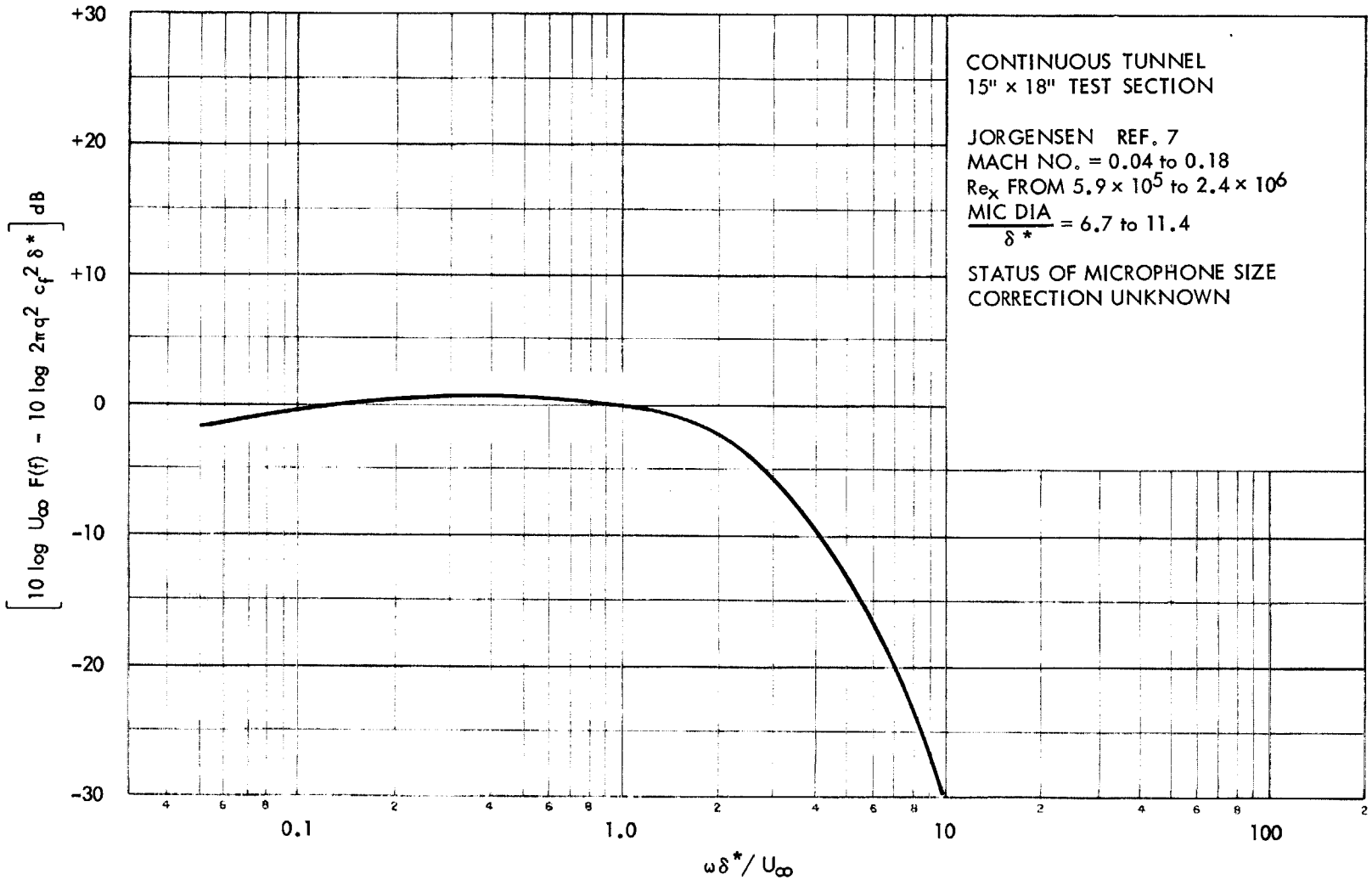

FIGURE 6. TUNNEL MEASUREMENTS OF BOUNDARY LAYER PRESSURE FLUCTUATIONS

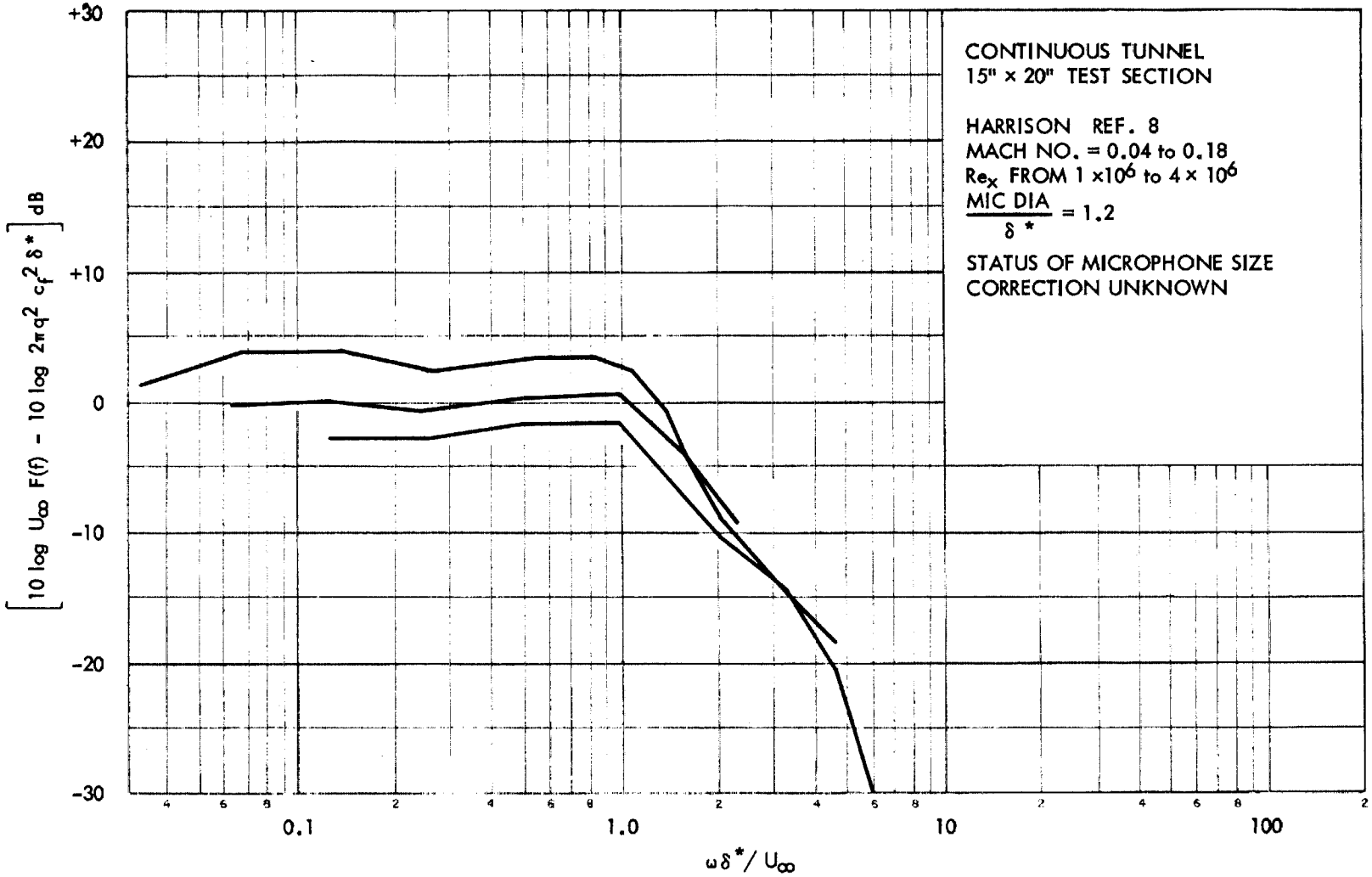

FIGURE 7. TUNNEL MEASUREMENTS OF BOUNDARY LAYER PRESSURE FLUCTUATIONS

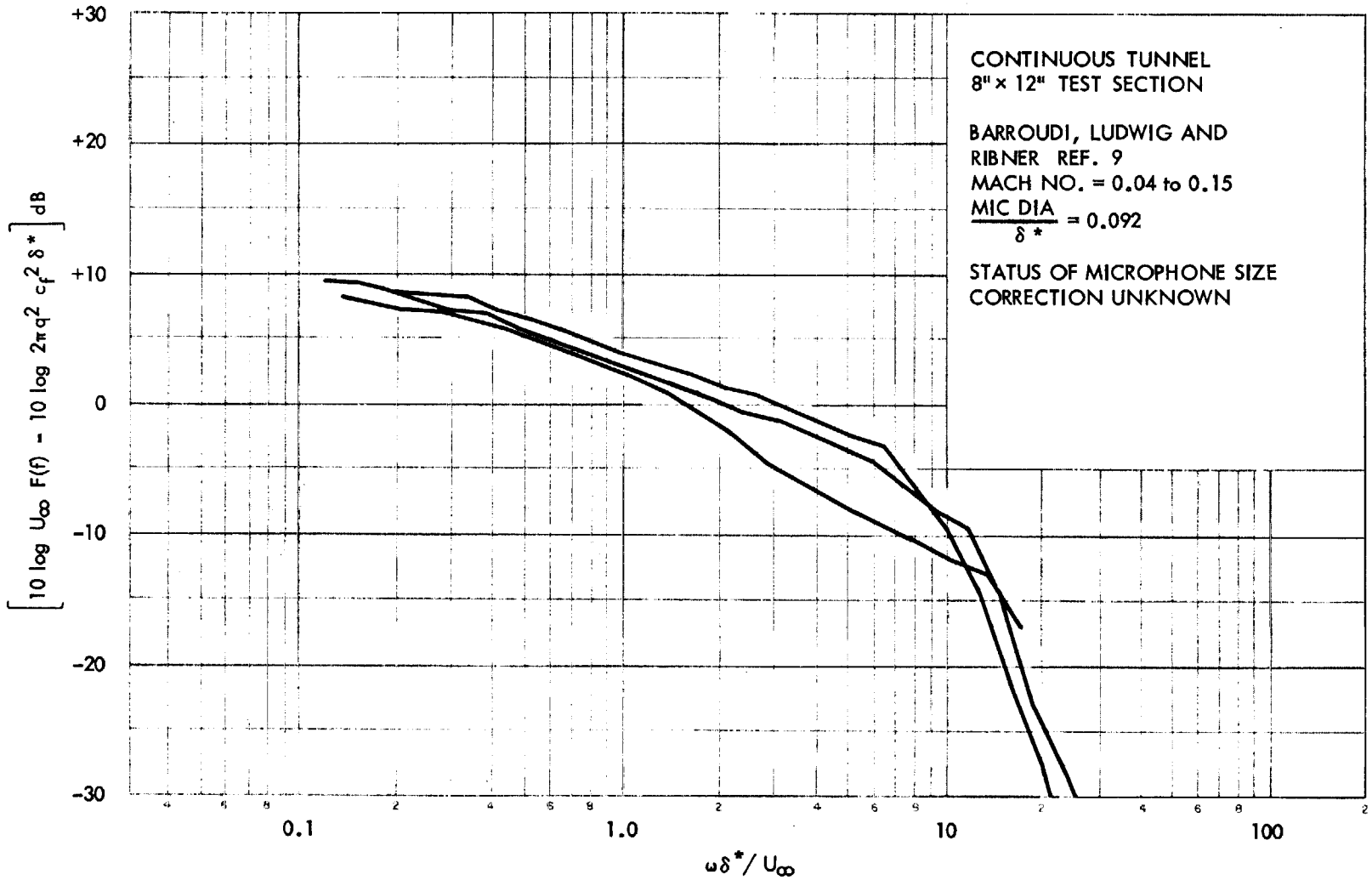

FIGURE 8. TUNNEL MEASUREMENTS OF BOUNDARY LAYER PRESSURE FLUCTUATIONS

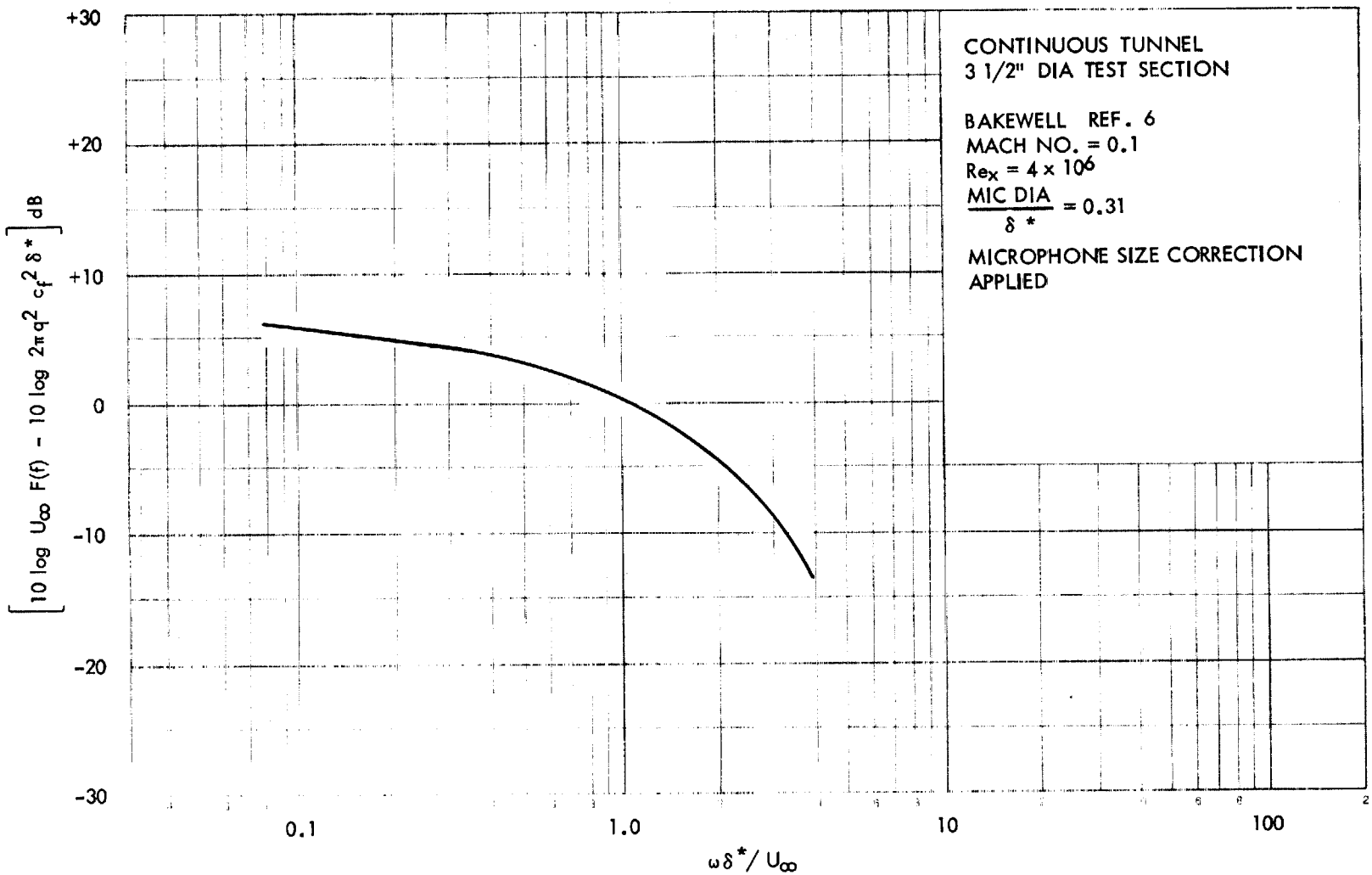

FIGURE 9. TUNNEL MEASUREMENTS OF BOUNDARY LAYER PRESSURE FLUCTUATIONS

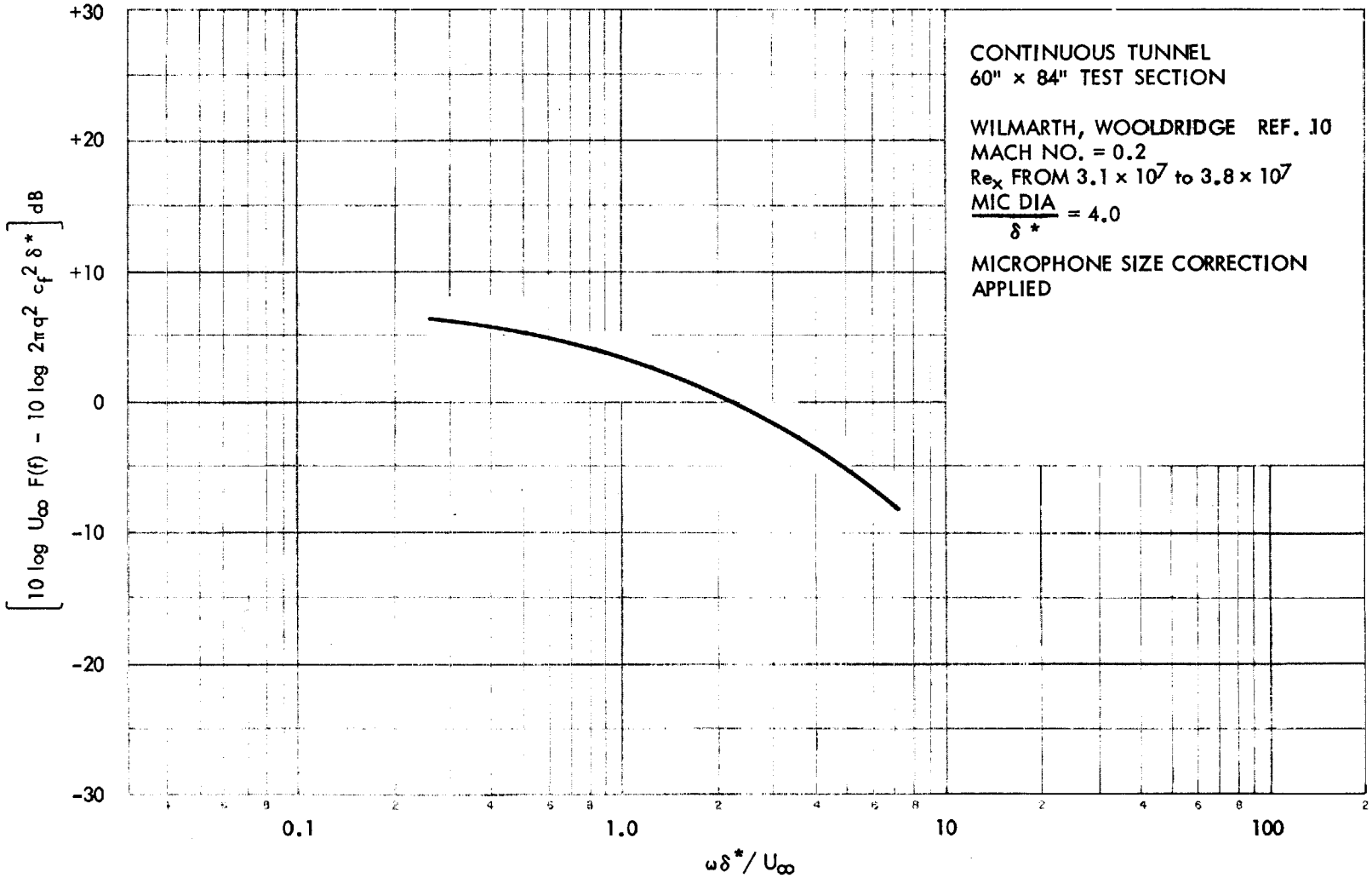

FIGURE 10. TUNNEL MEASUREMENTS OF BOUNDARY LAYER PRESSURE FLUCTUATIONS

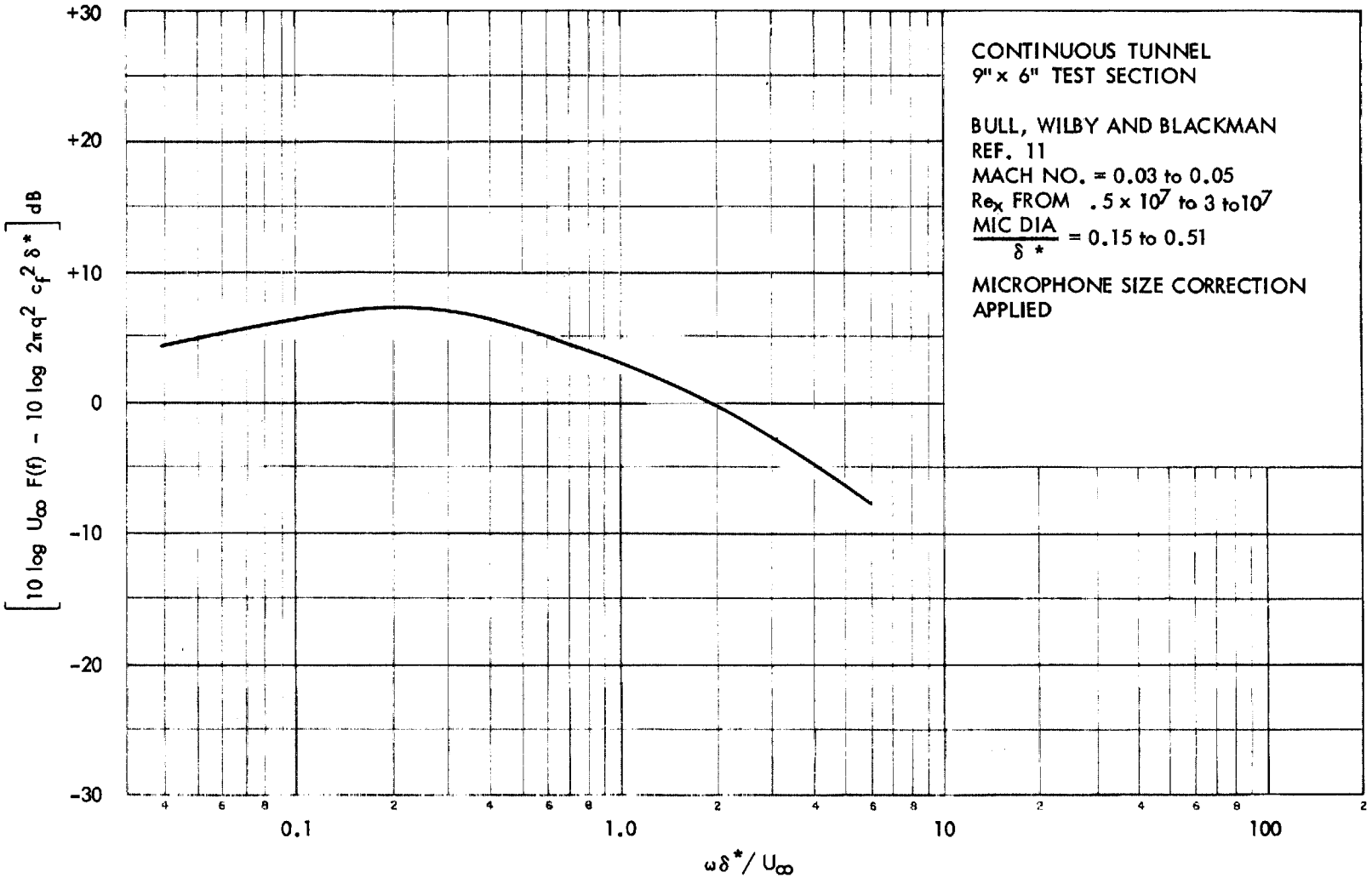

FIGURE 11. TUNNEL MEASUREMENTS OF BOUNDARY LAYER PRESSURE FLUCTUATIONS

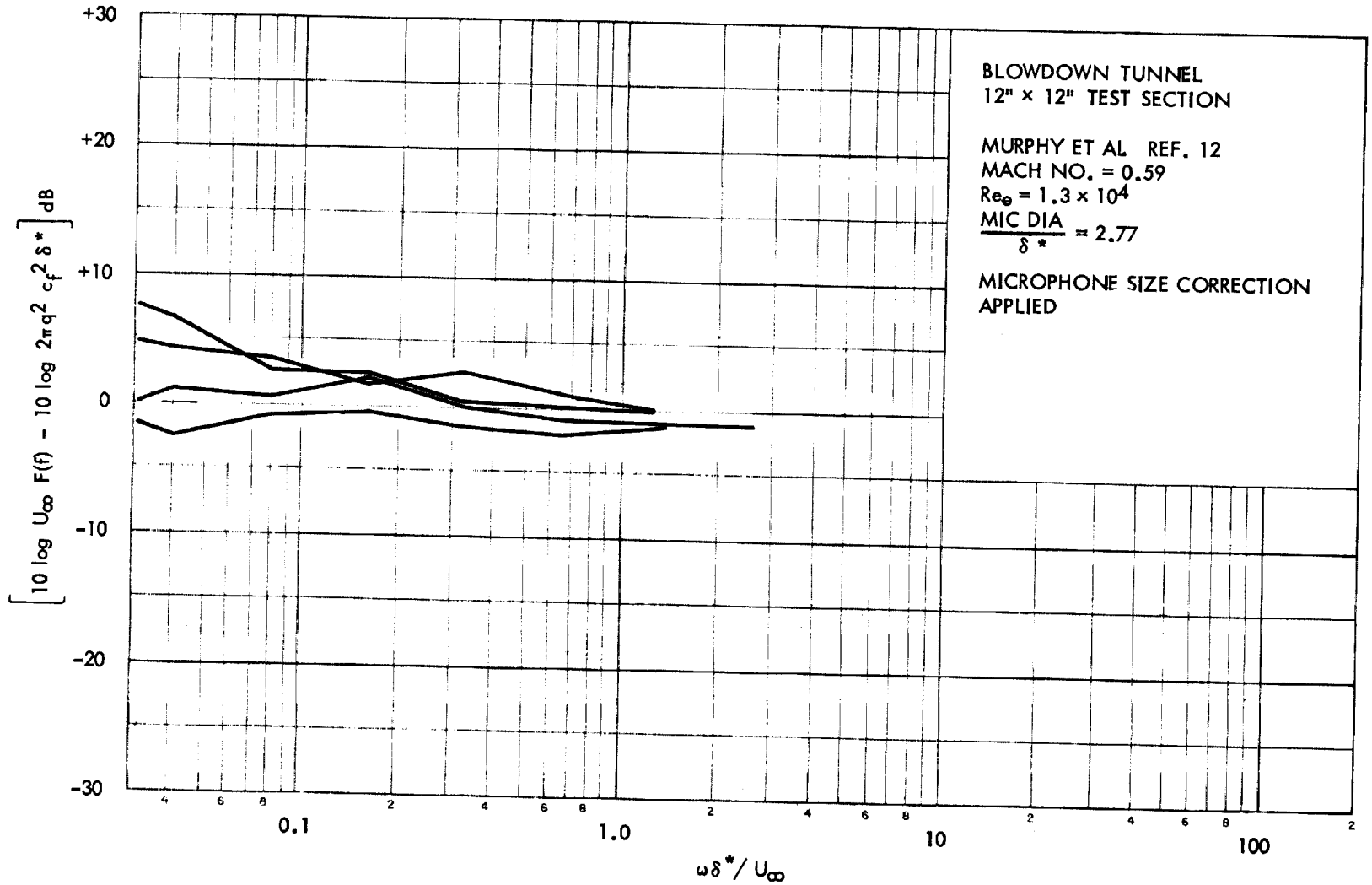

FIGURE 12. TUNNEL MEASUREMENTS OF BOUNDARY LAYER PRESSURE FLUCTUATION

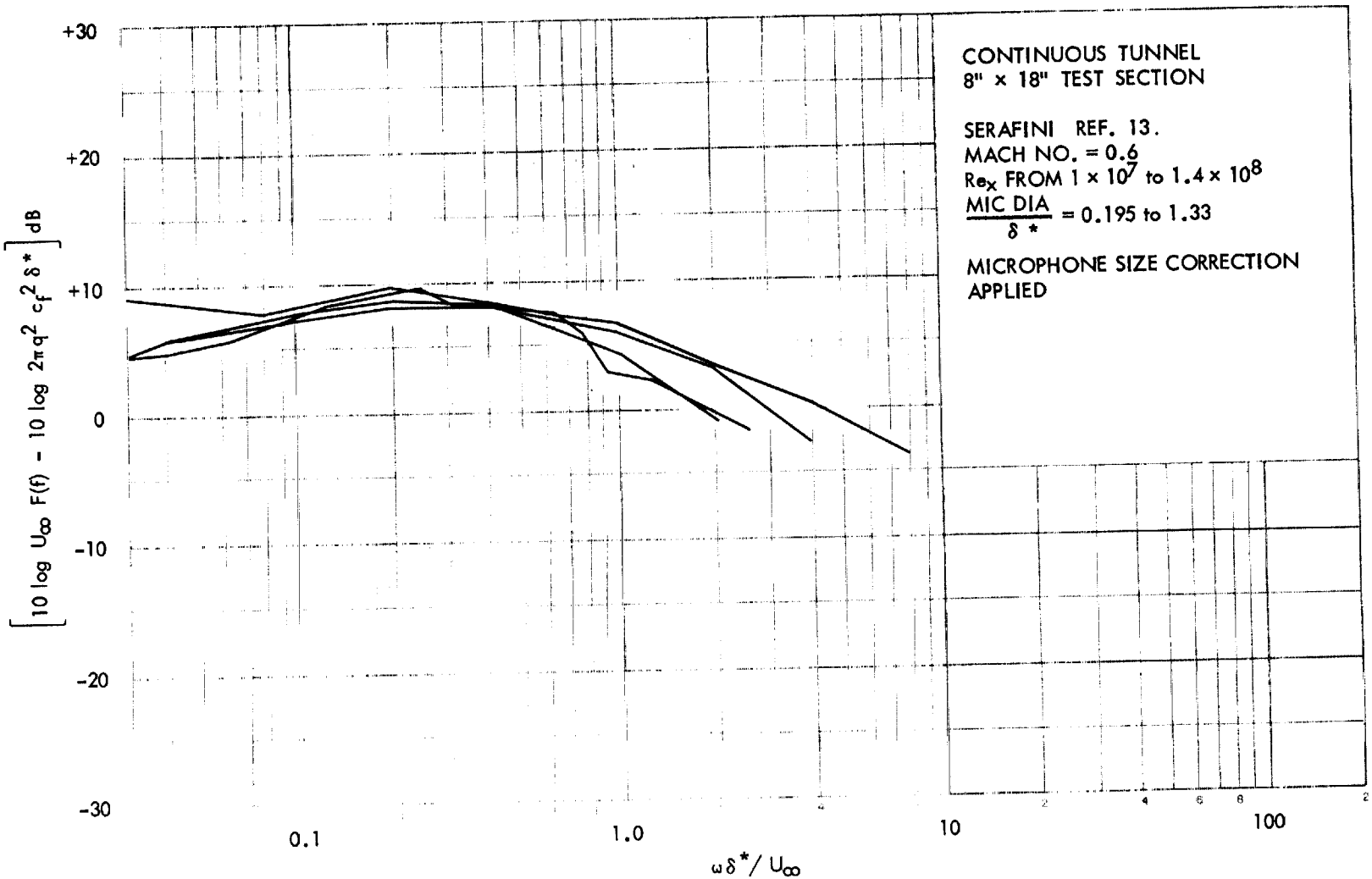

FIGURE 13. TUNNEL MEASUREMENTS OF BOUNDARY LAYER PRESSURE FLUCTUATIONS

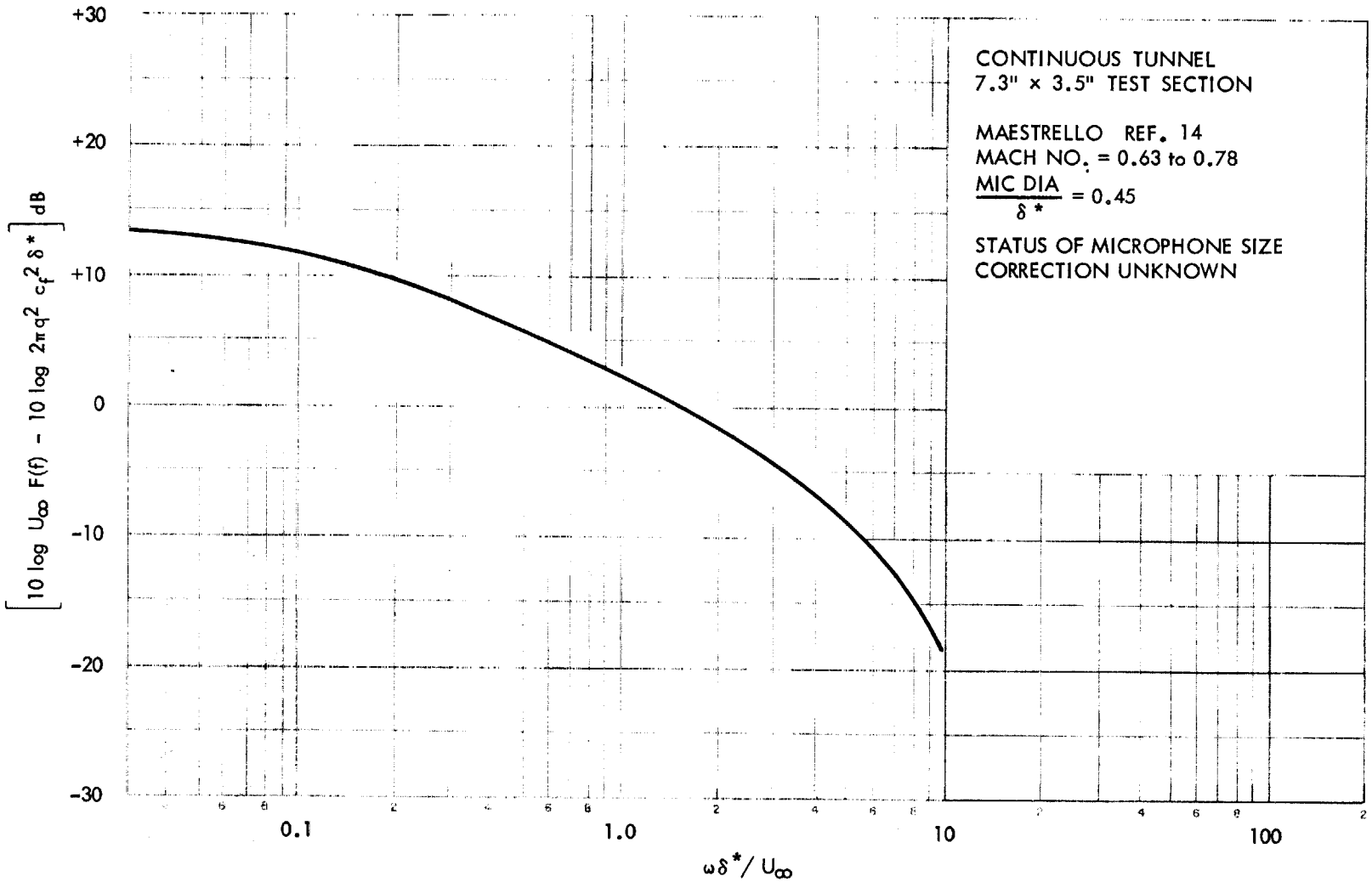

FIGURE 14. TUNNEL MEASUREMENTS OF BOUNDARY LAYER PRESSURE FLUCTUATION

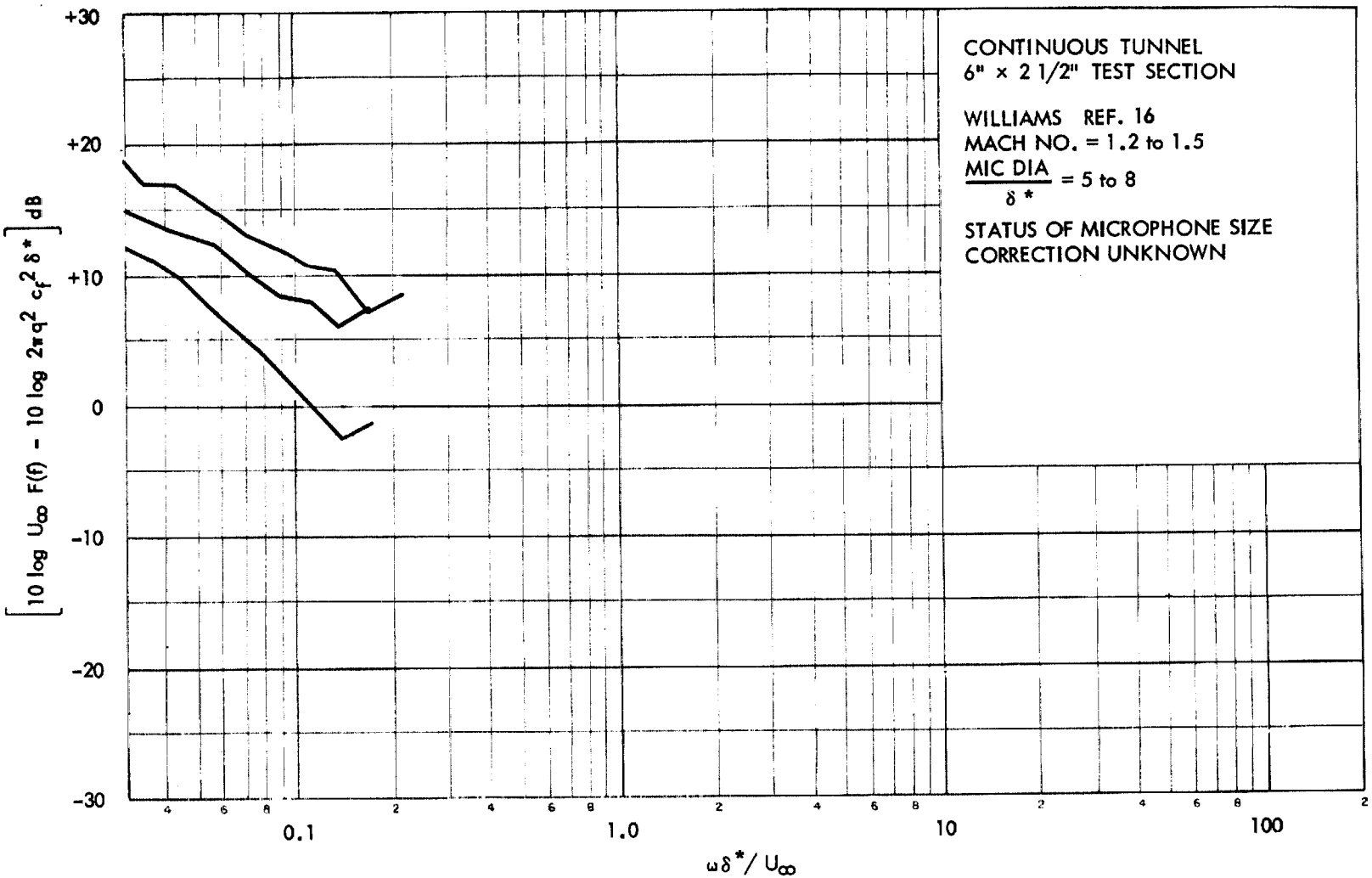

FIGURE 15. TUNNEL MEASUREMENTS OF BOUNDARY LAYER PRESSURE FLUCTUATIONS

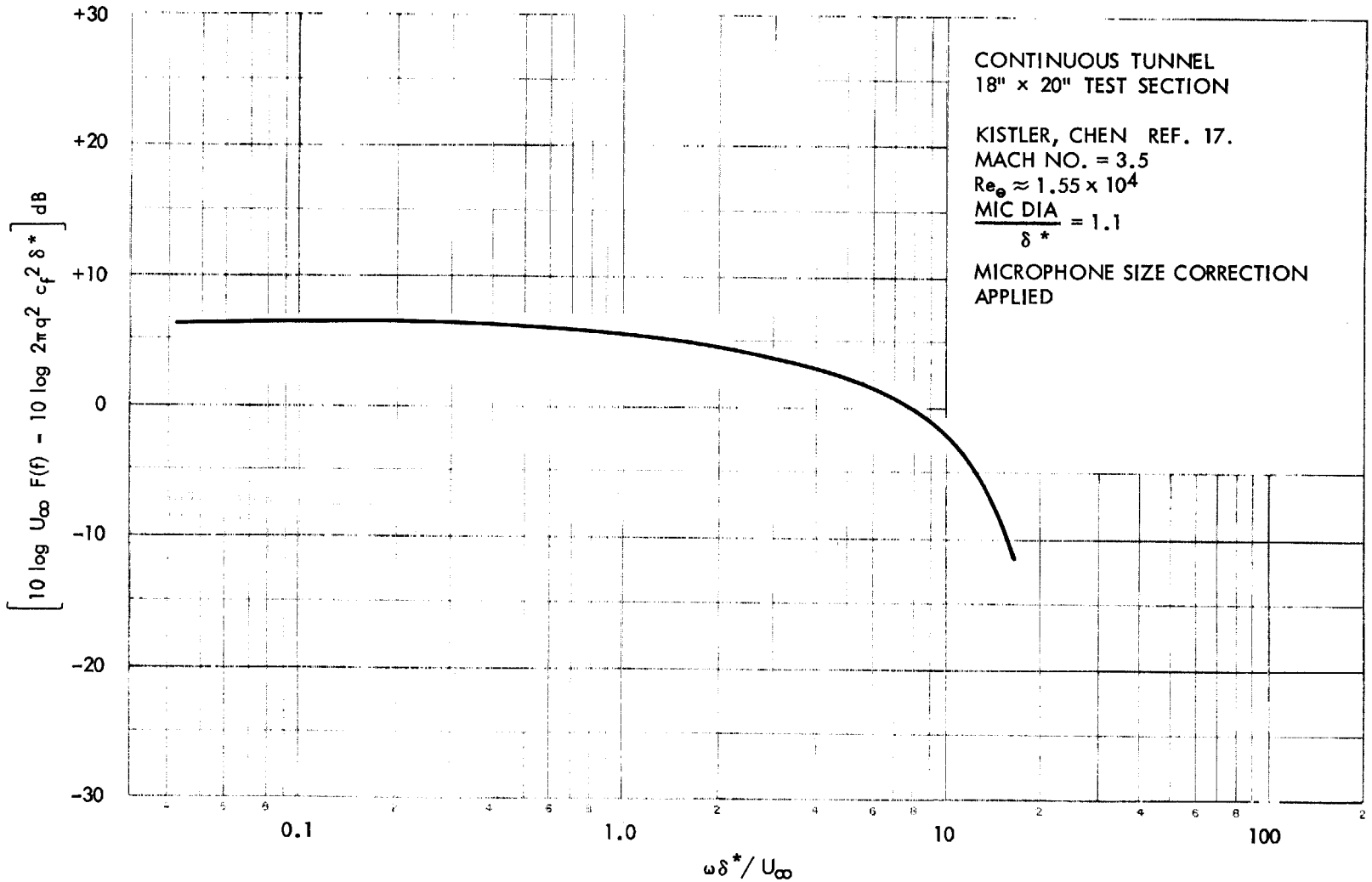

FIGURE 16. TUNNEL MEASUREMENTS OF BOUNDARY LAYER PRESSURE FLUCTUATIONS

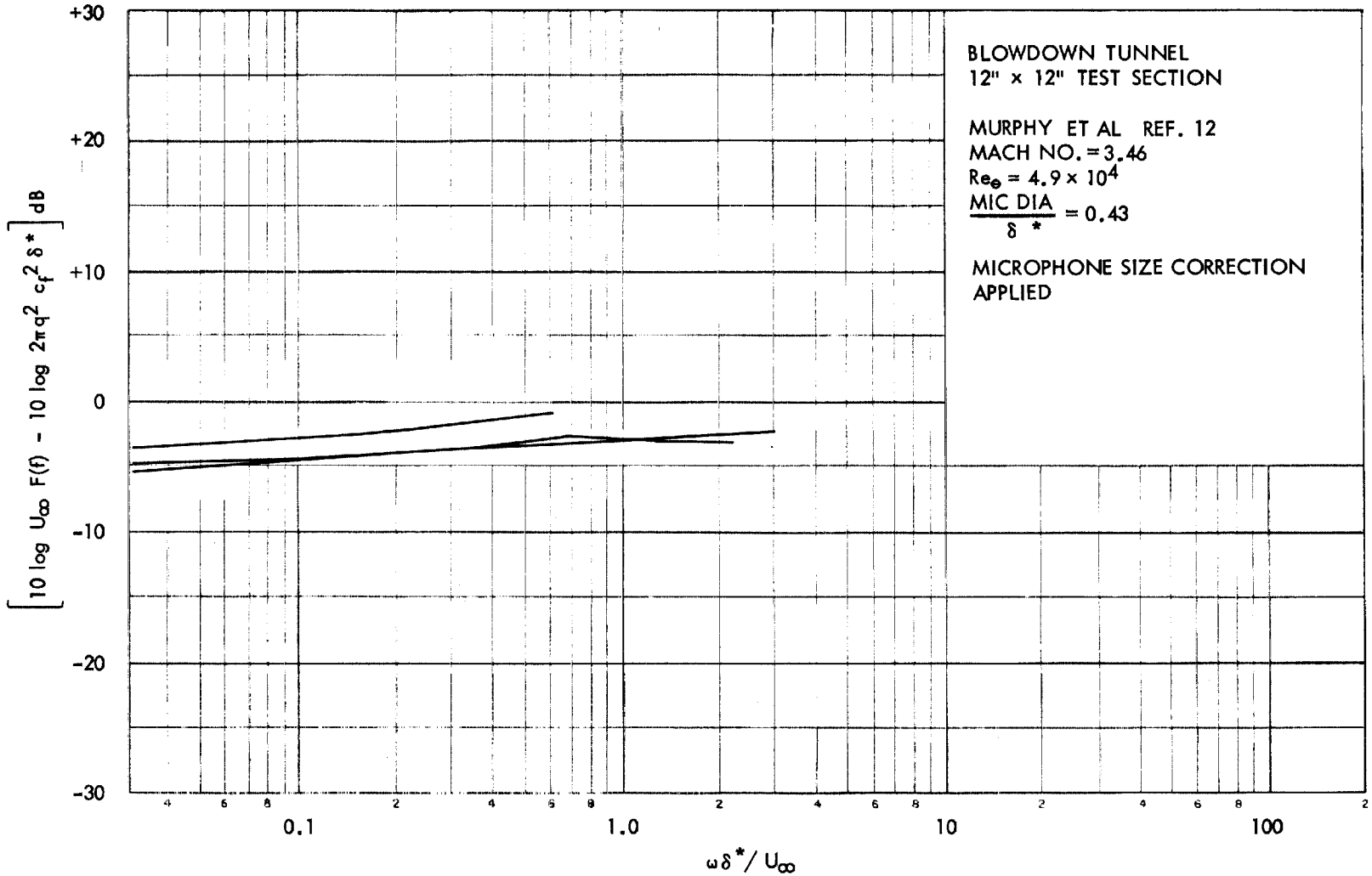

FIGURE 17. TUNNEL MEASUREMENTS OF BOUNDARY LAYER PRESSURE FLUCTUATIONS

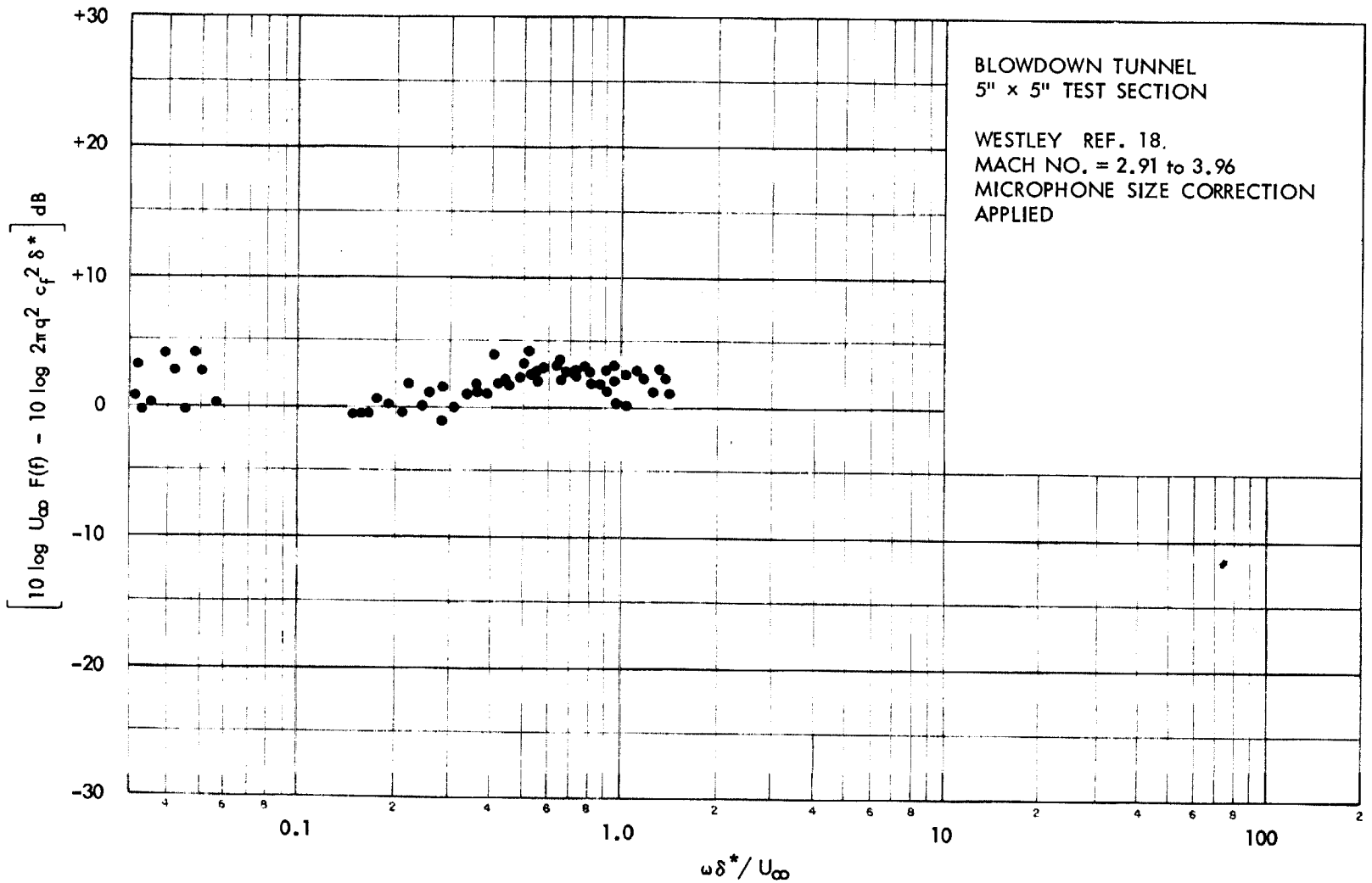

FIGURE 18. TUNNEL MEASUREMENTS OF BOUNDARY LAYER PRESSURE FLUCTUATIONS

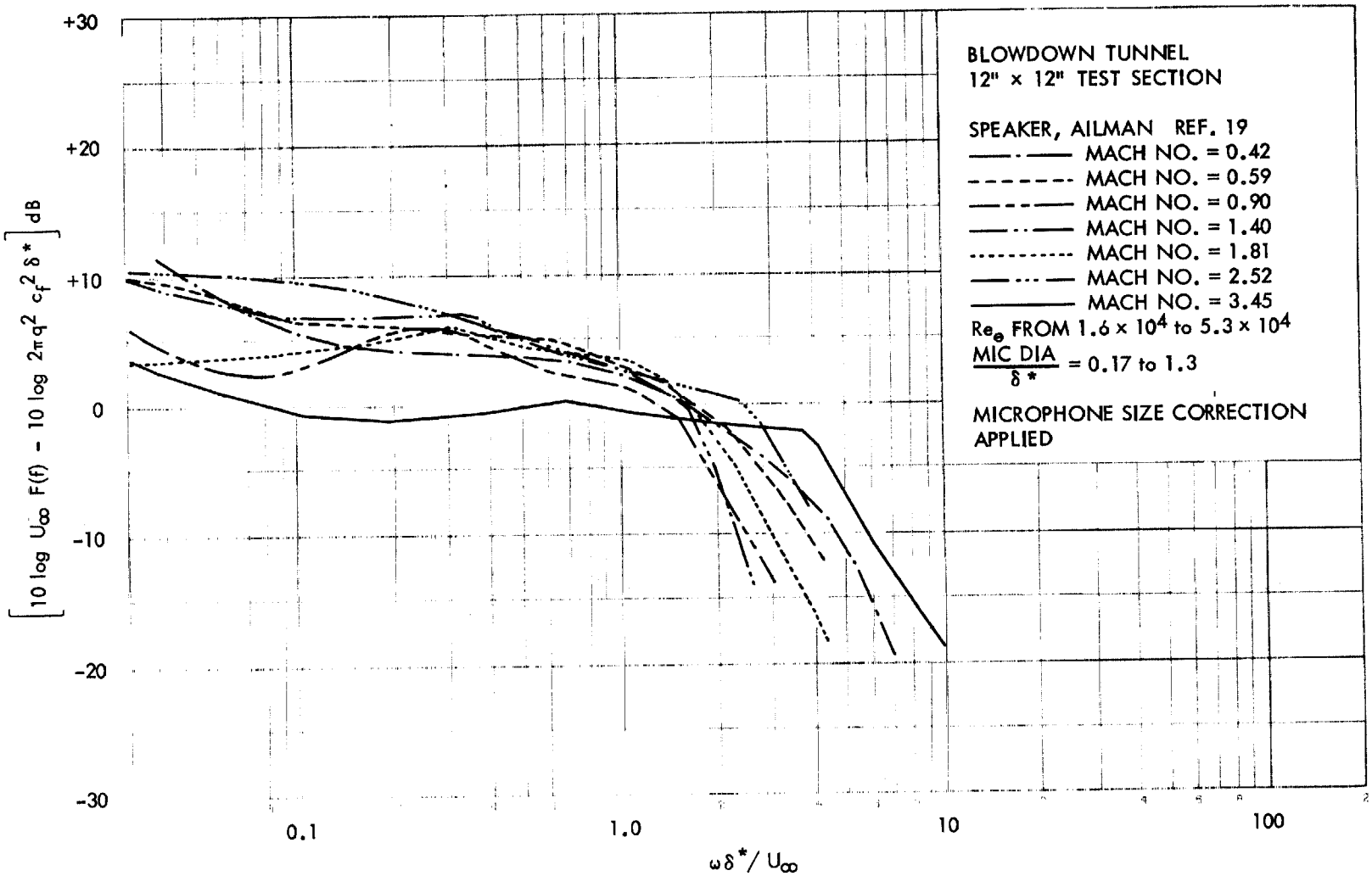

FIGURE 19. TUNNEL MEASUREMENTS OF BOUNDARY LAYER PRESSURE FLUCTUATIONS

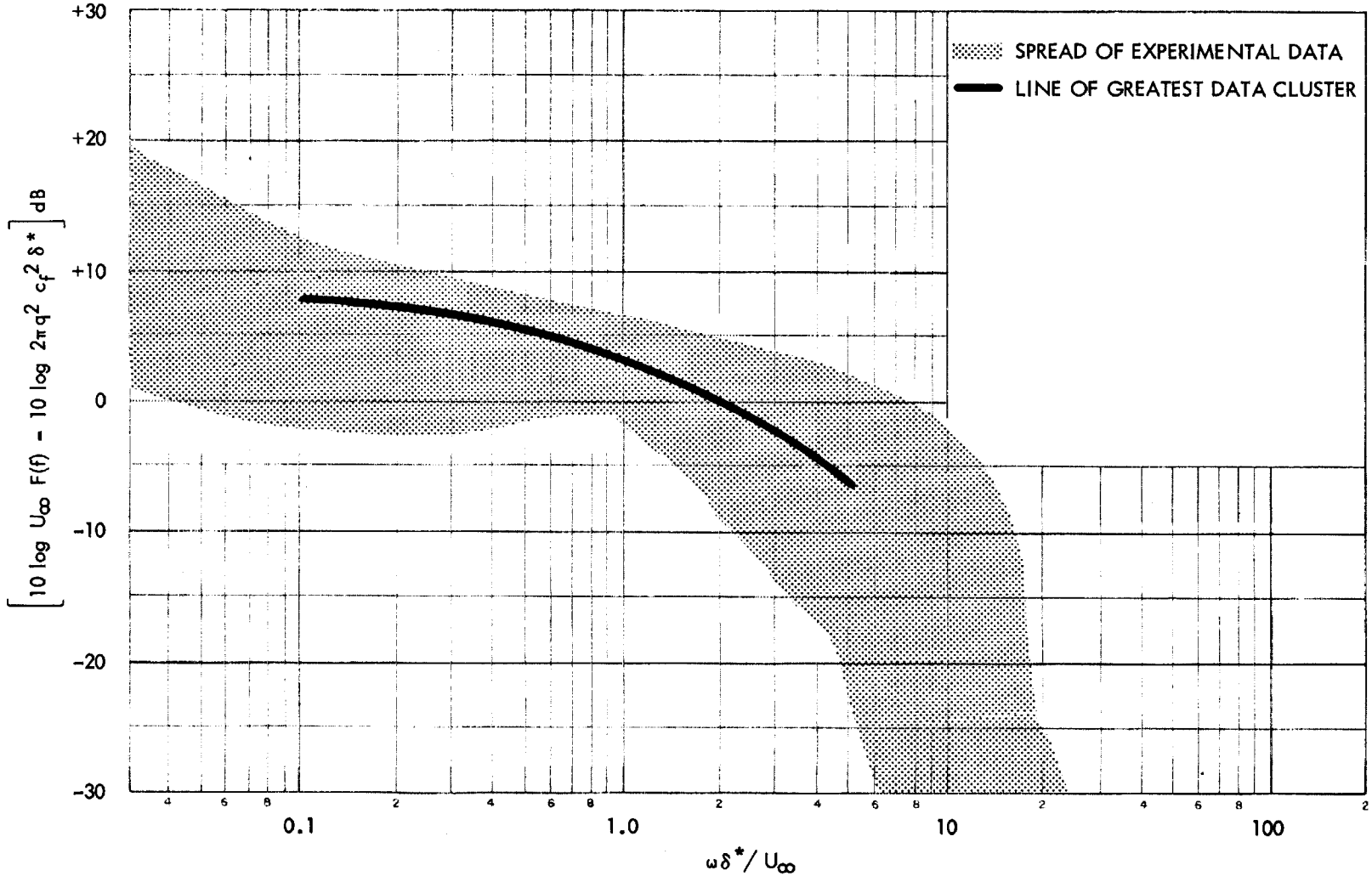

FIGURE 20. TUNNEL MEASUREMENTS OF BOUNDARY LAYER PRESSURE FLUCTUATIONS

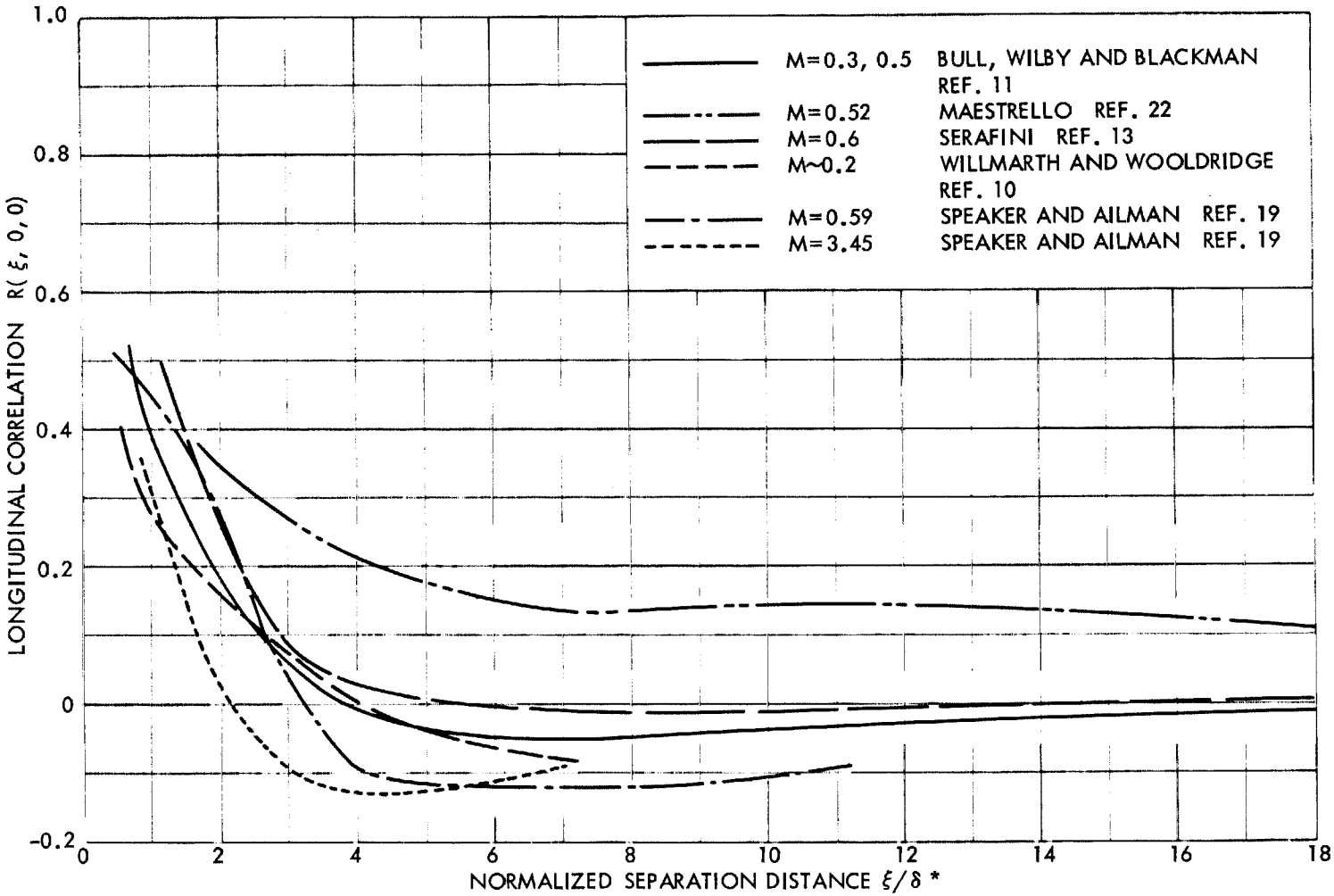

FIGURE 21. LONGITUDINAL SPACE CORRELATION OF THE BOUNDARY LAYER PRESSURE FLUCTUATIONS

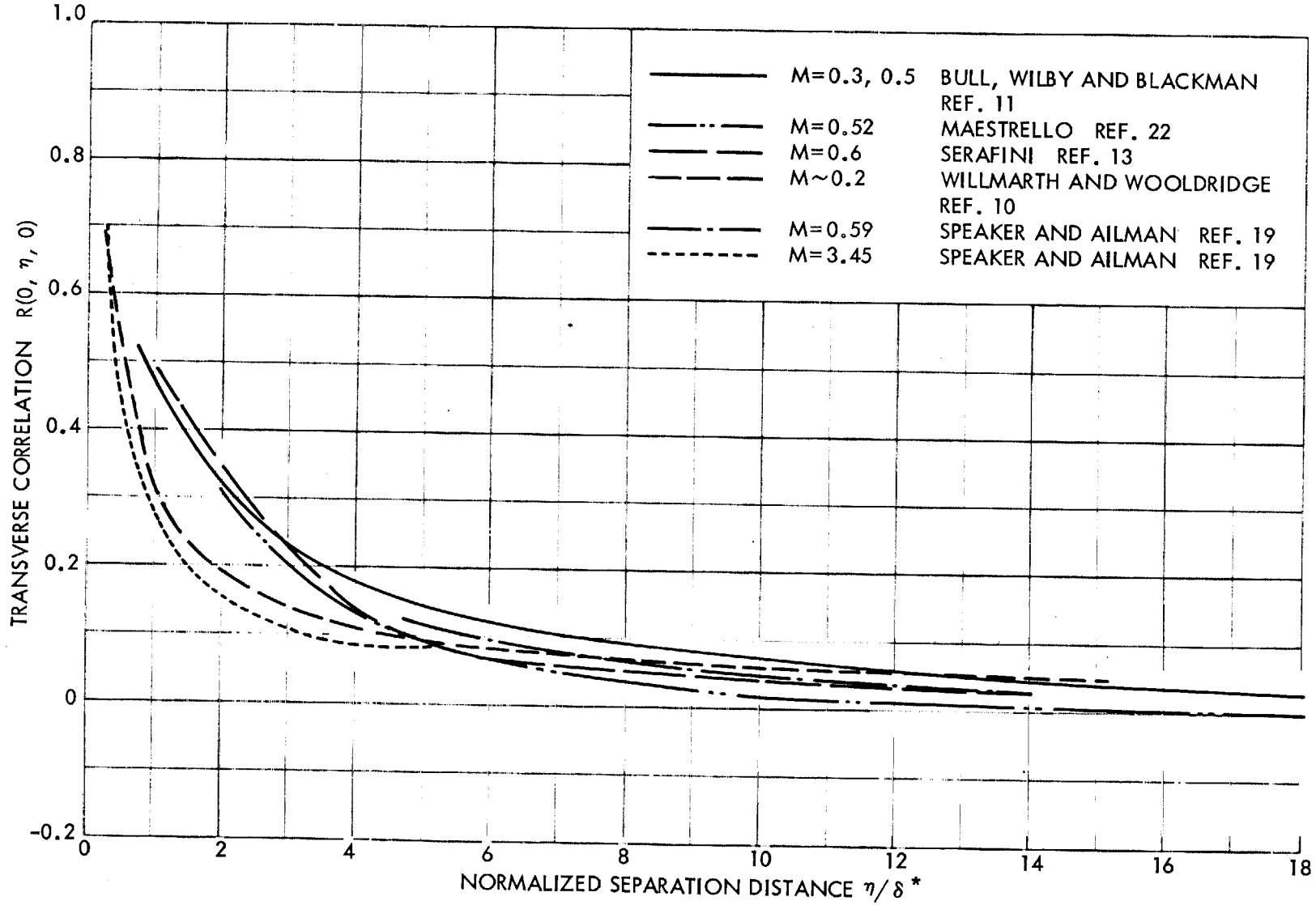

FIGURE 22. TRANSVERSE SPACE CORRELATION OF THE BOUNDARY LAYER PRESSURE FLUCTUATIONS

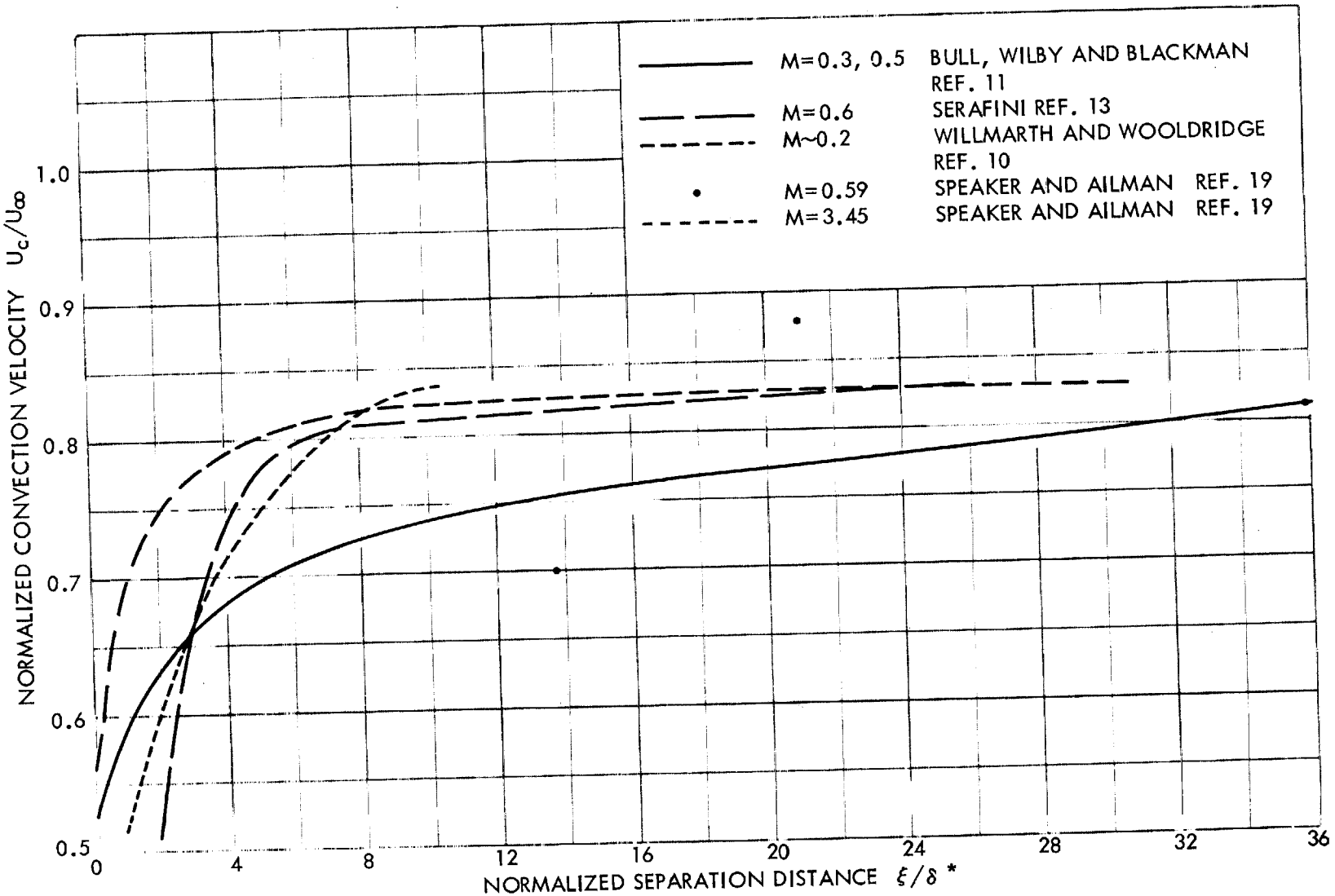

FIGURE 23. VARIATION OF BROAD BAND CONVECTION VELOCITY WITH SPATIAL SEPARATION

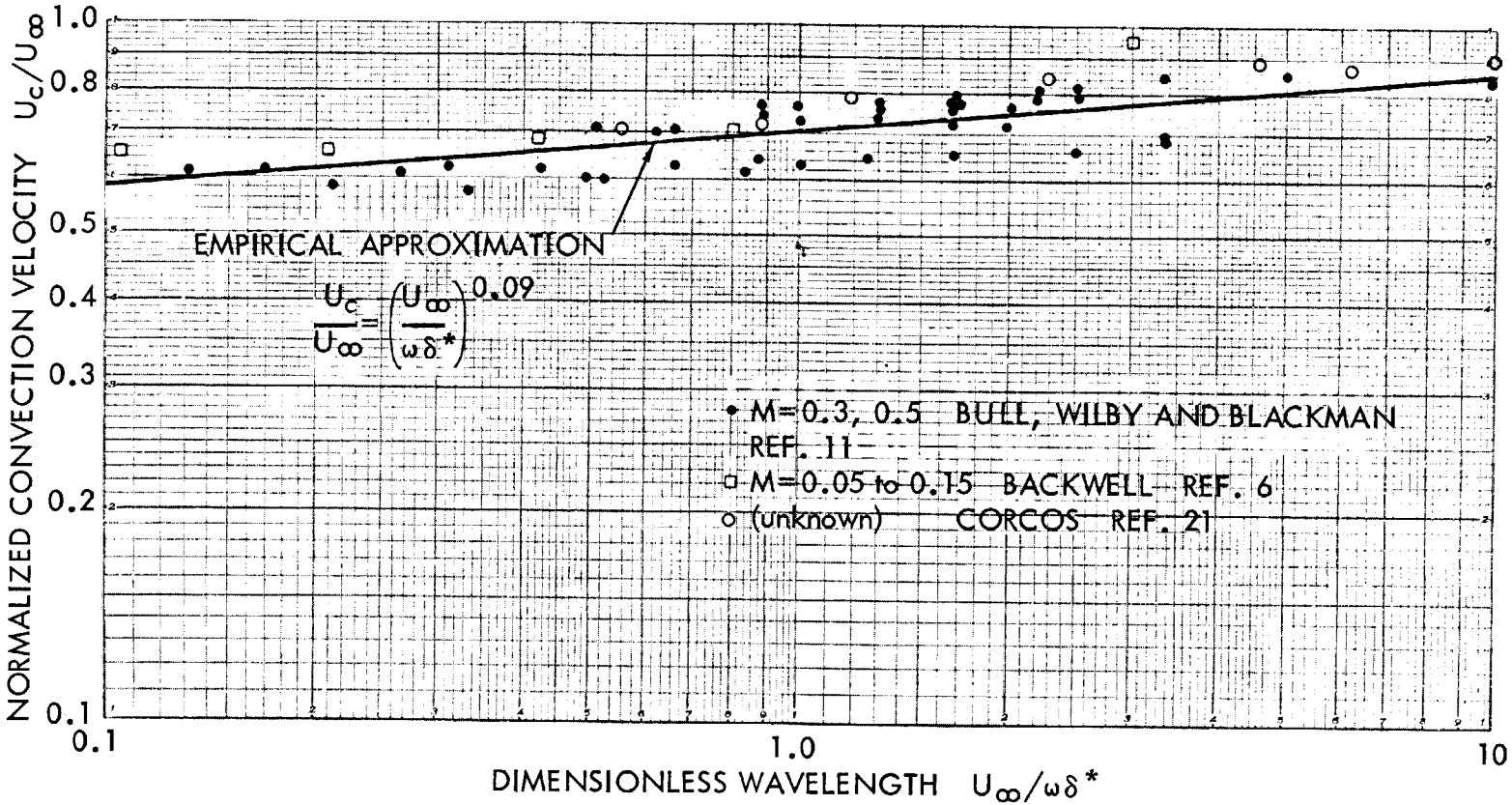

FIGURE 24. TURBULENT BOUNDARY LAYER CONVECTION VELOCITY DERIVED FROM NARROW BAND LONGITUDINAL SPACE-TIME CORRELATION MEASUREMENTS

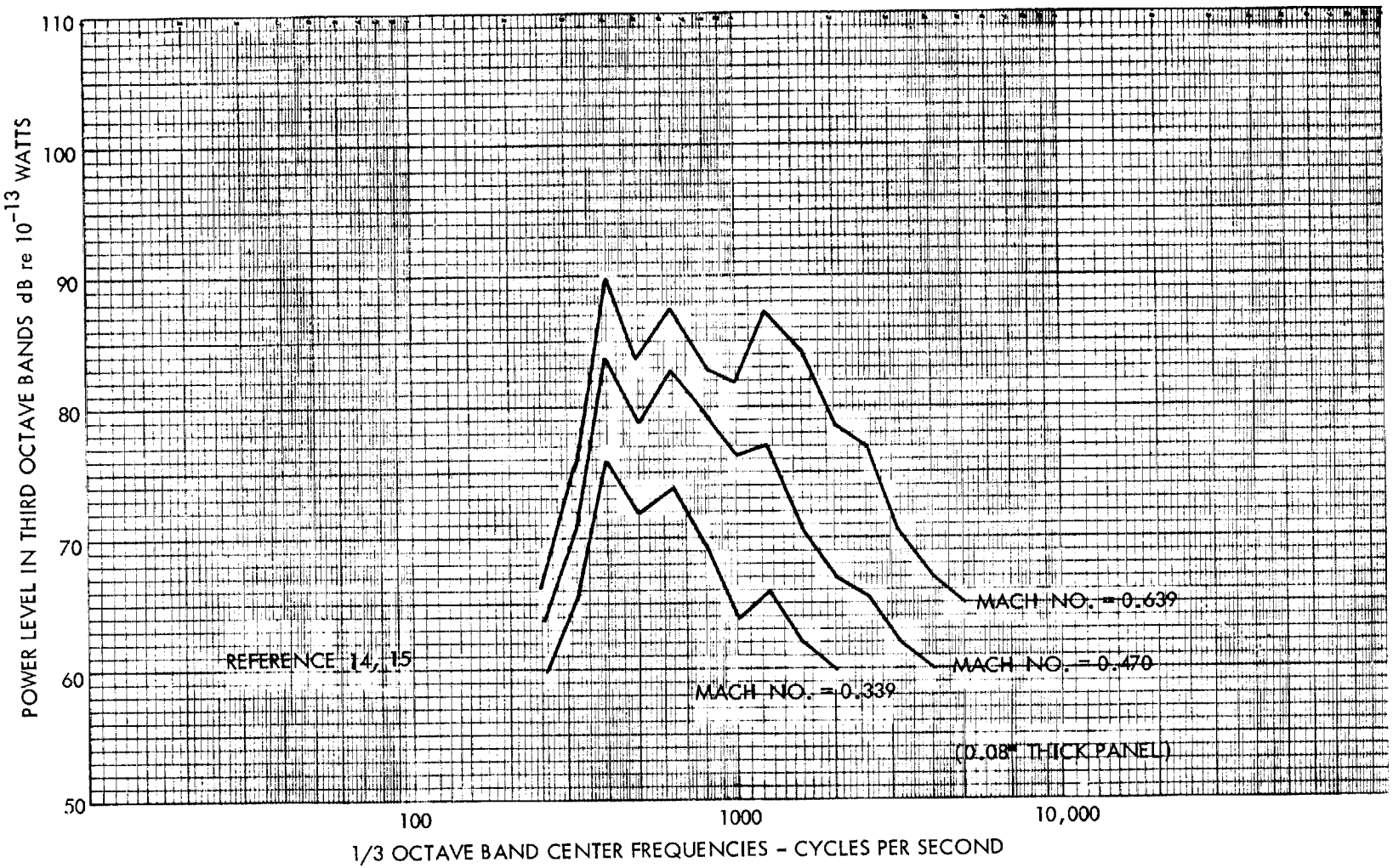

FIGURE 25. TYPICAL RADIATED POWER SPECTRUM OF A THIN METAL PANEL EXCITED BY BOUNDARY LAYER PRESSURE FLUCTUATIONS

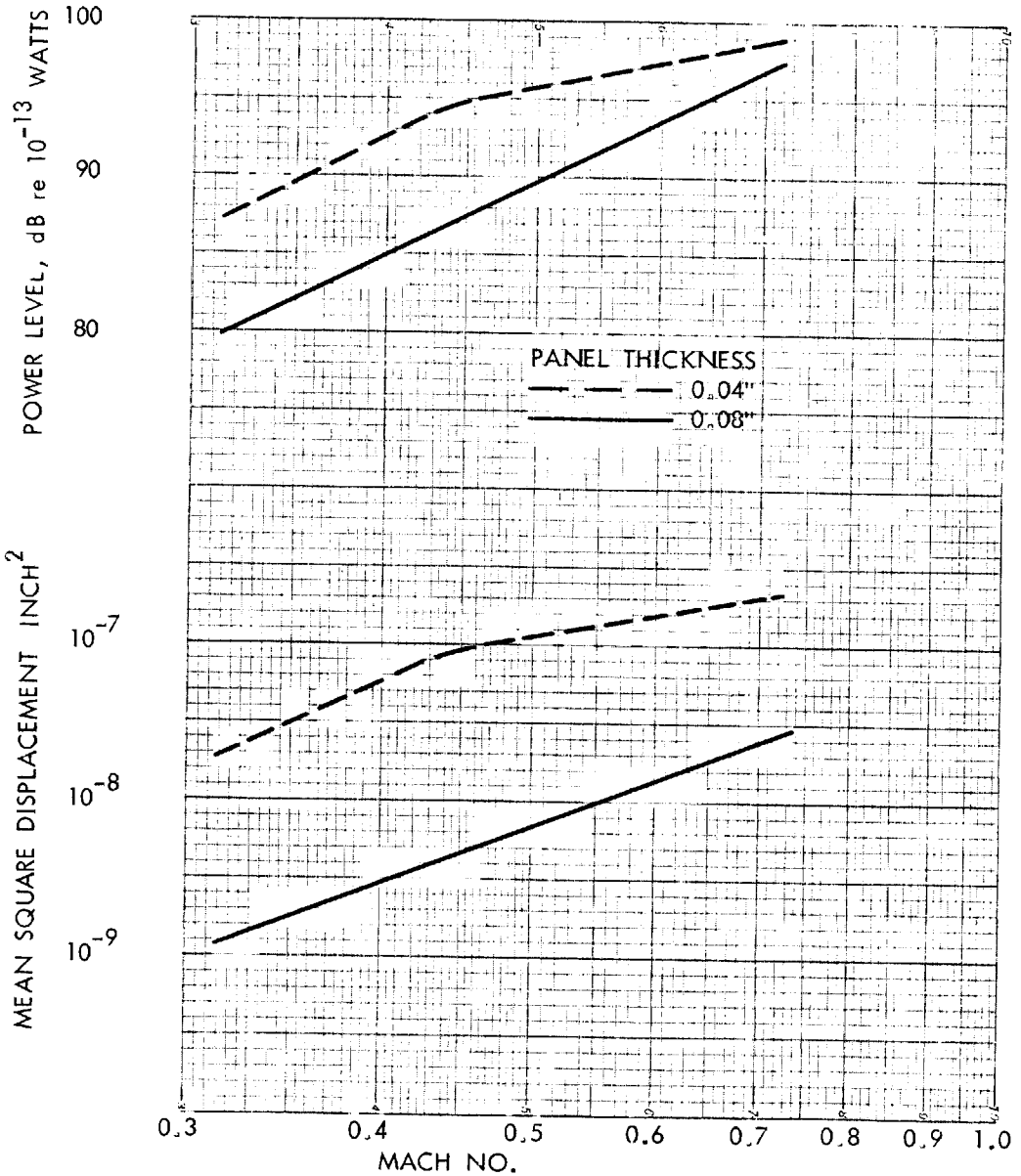

FIGURE 26. RADIATED POWER AND AMPLITUDE RESPONSE OF THIN METAL PANELS EXCITED BY BOUNDARY LAYER PRESSURE FLUCTUATIONS

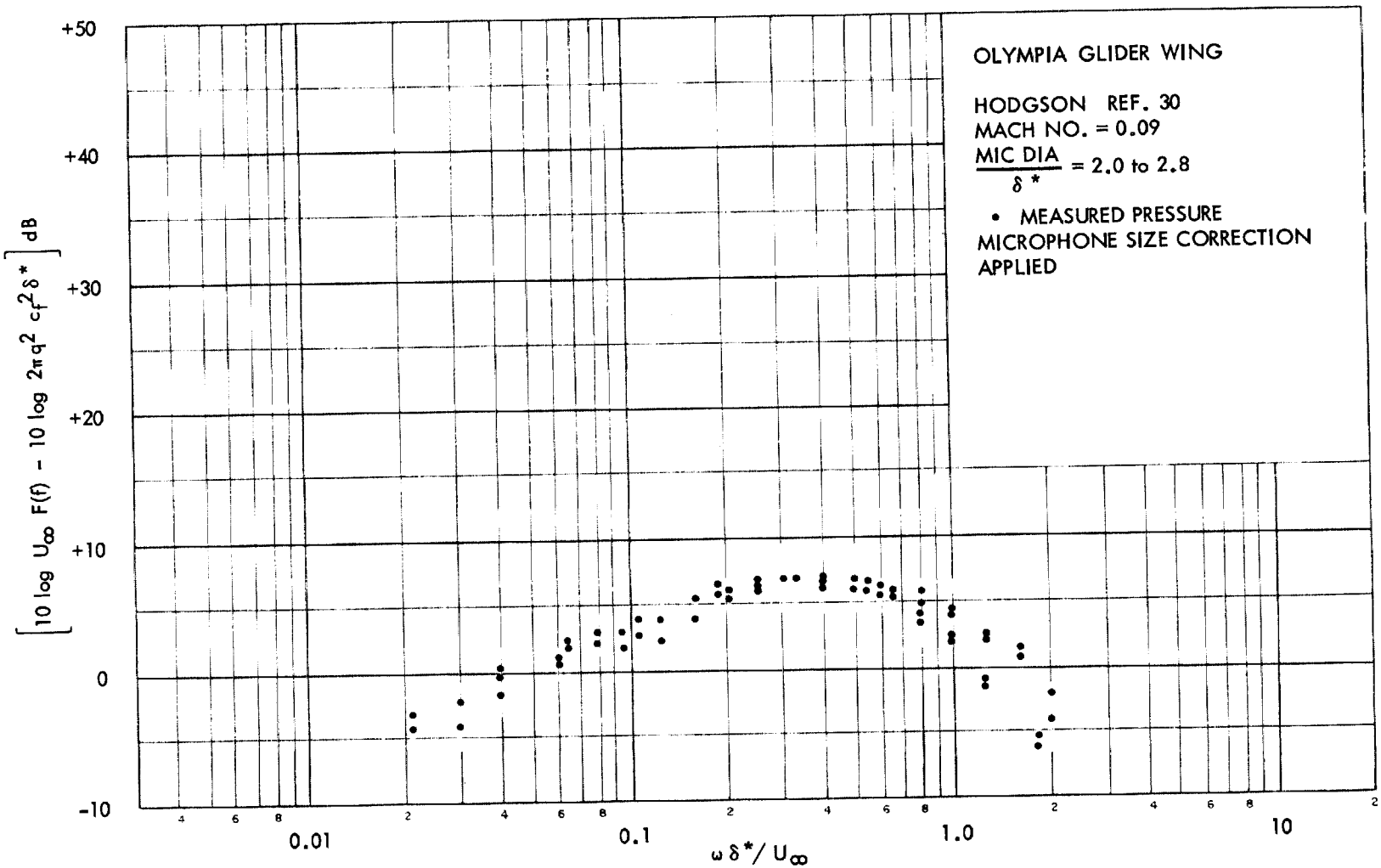

FIGURE 27. FLIGHT MEASUREMENTS OF BOUNDARY LAYER PRESSURE FLUCTUATIONS

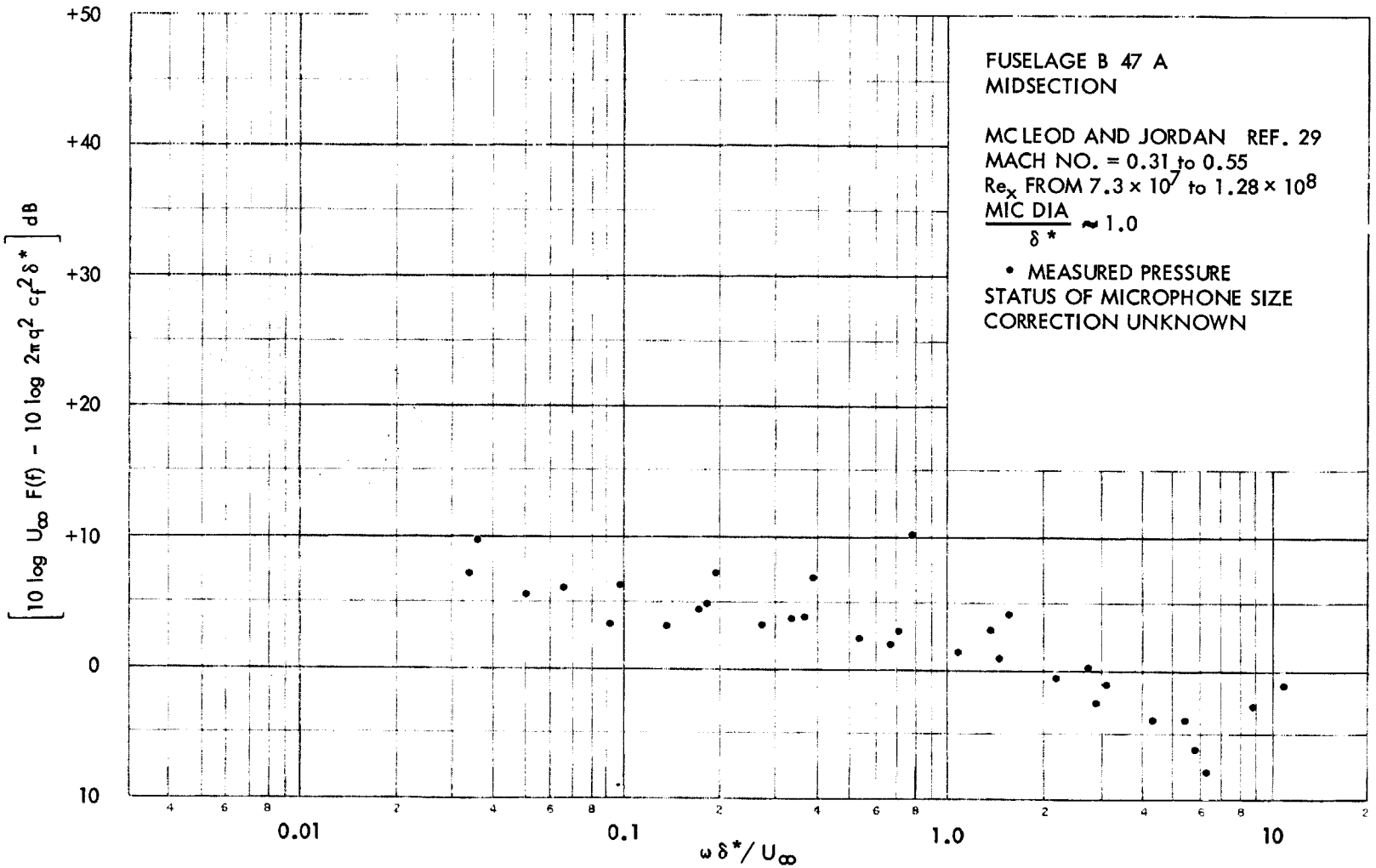

FIGURE 28. FLIGHT MEASUREMENTS OF BOUNDARY LAYER PRESSURE FLUCTUATIONS

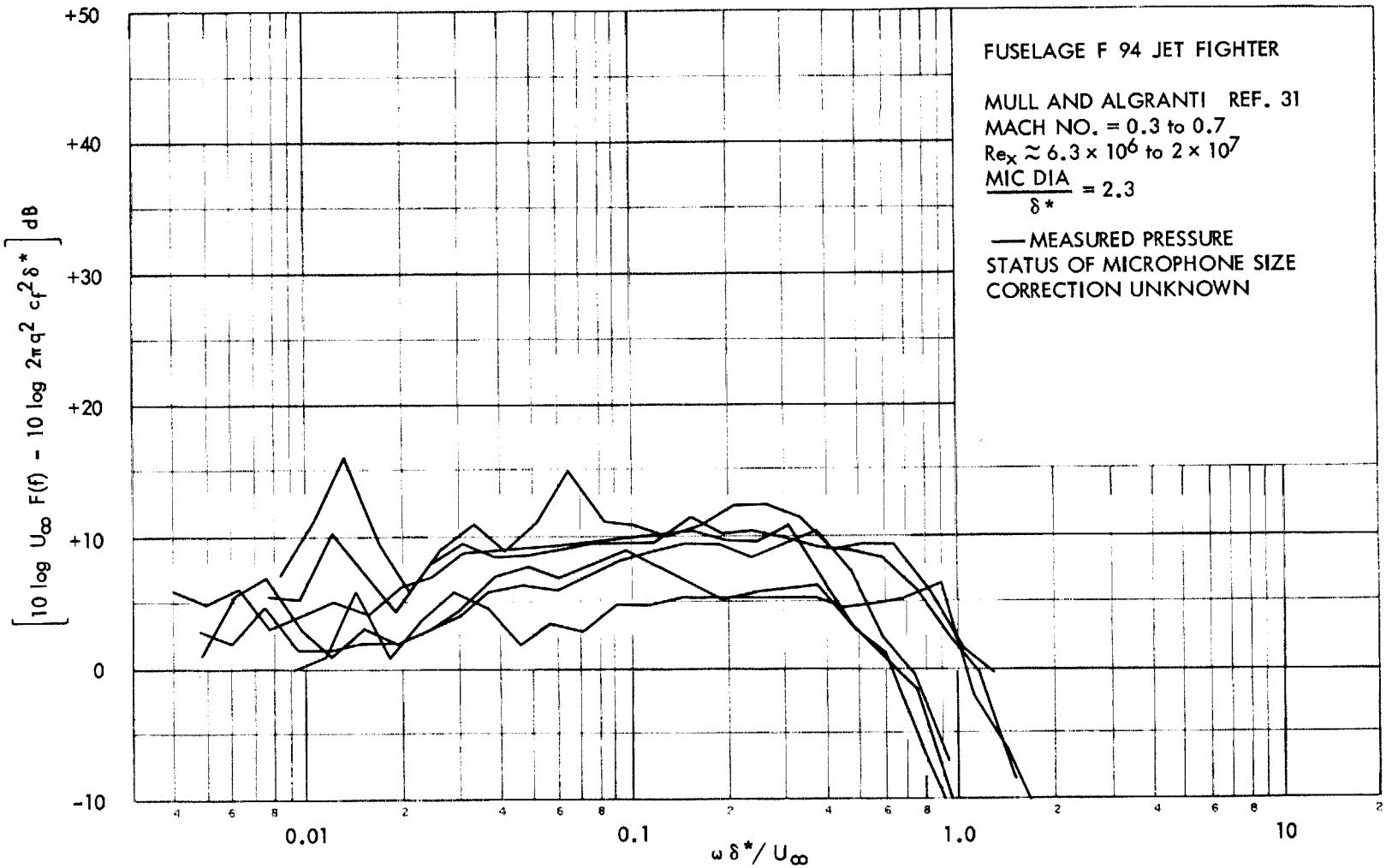

FIGURE 29. FLIGHT MEASUREMENTS OF BOUNDARY LAYER PRESSURE FLUCTUATIONS

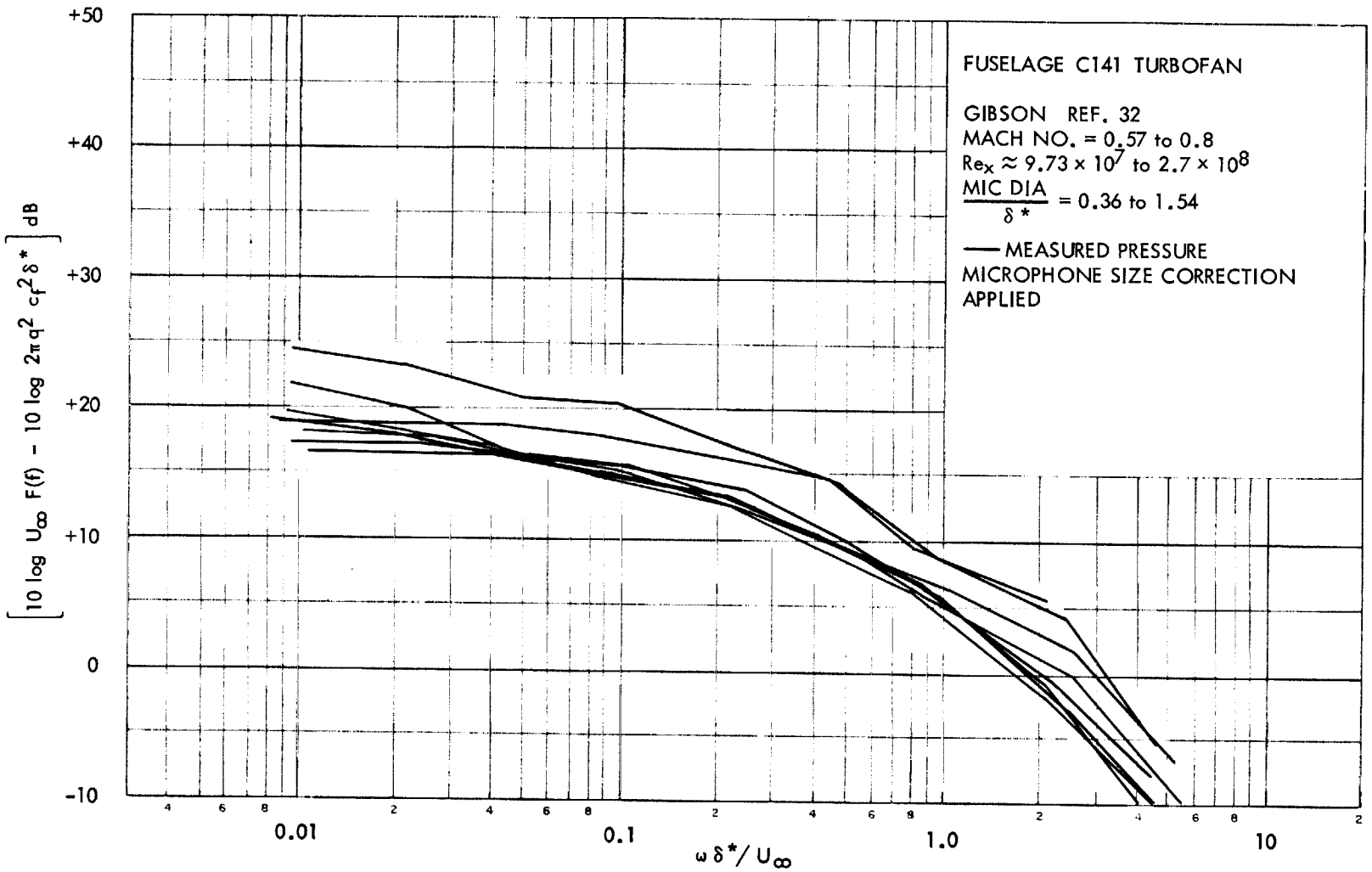

FIGURE 30. FLIGHT MEASUREMENTS OF BOUNDARY LAYER PRESSURE FLUCTUATIONS

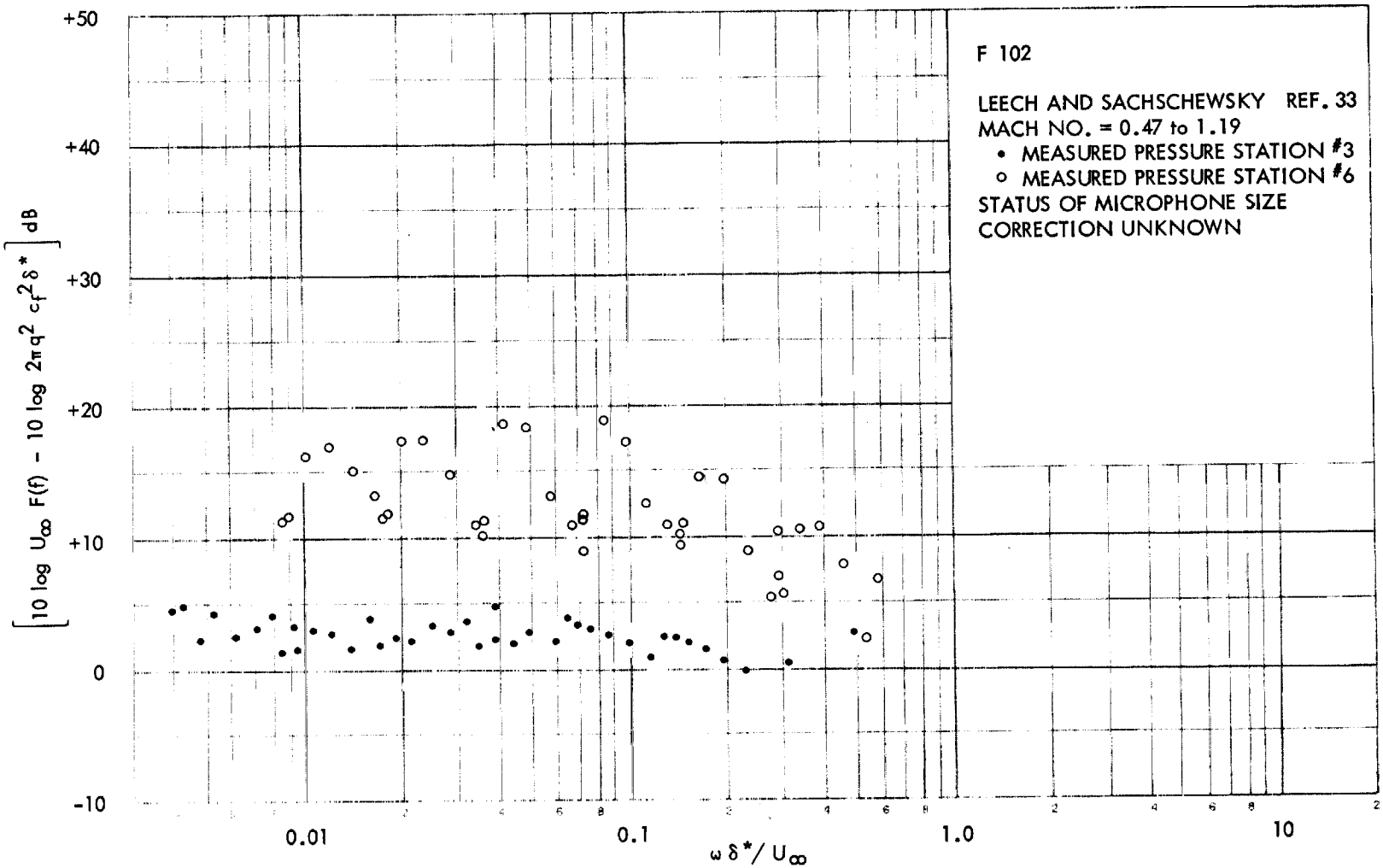

FIGURE 31. FLIGHT MEASUREMENTS OF BOUNDARY LAYER PRESSURE FLUCTUATIONS

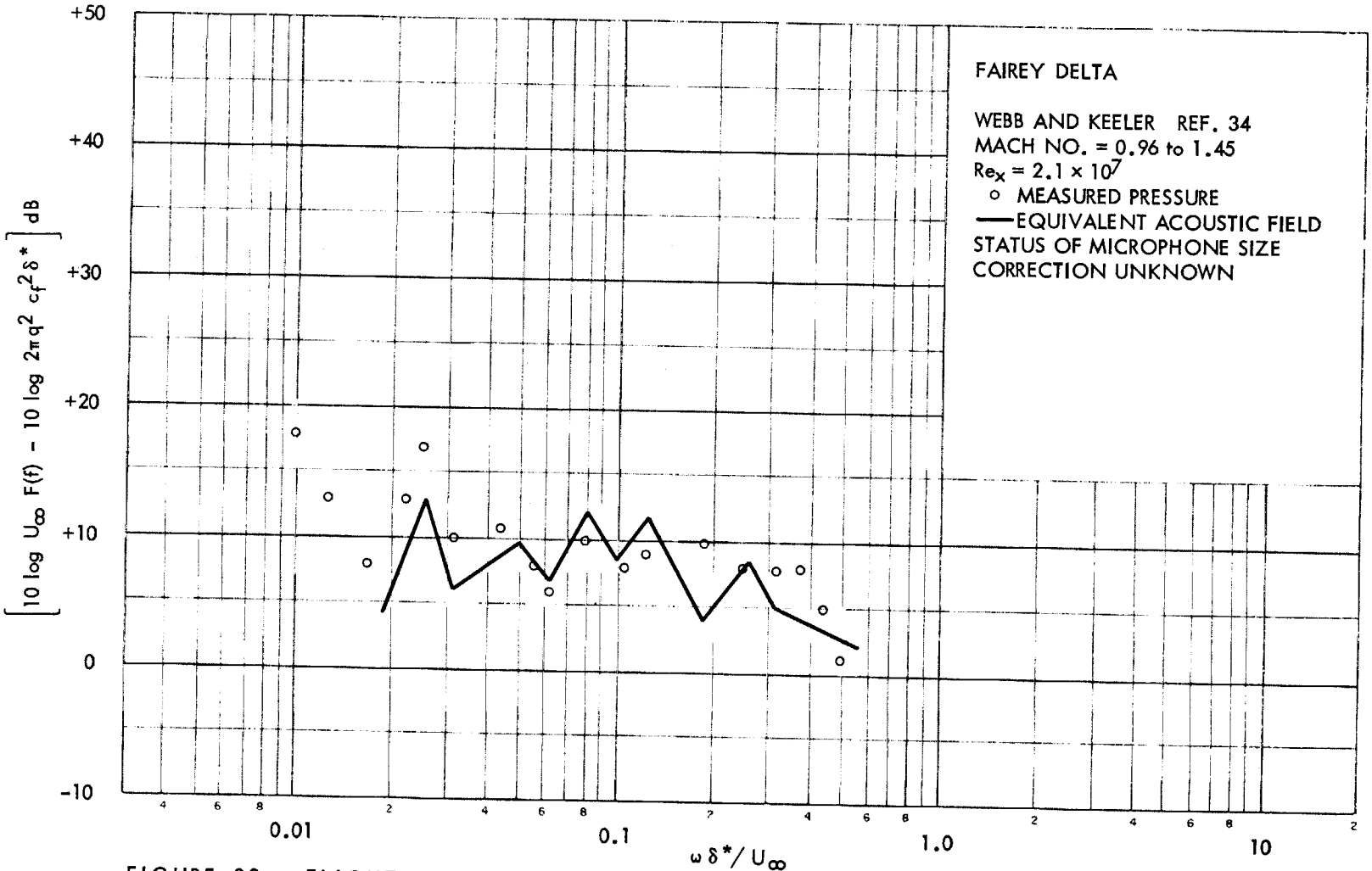

FIGURE 32. FLIGHT MEASUREMENTS OF BOUNDARY LAYER PRESSURE FLUCTUATIONS AND AN EQUIVALENT ACOUSTIC FIELD BASED ON MEASURED STRUCTURAL RESPONSE (see test)

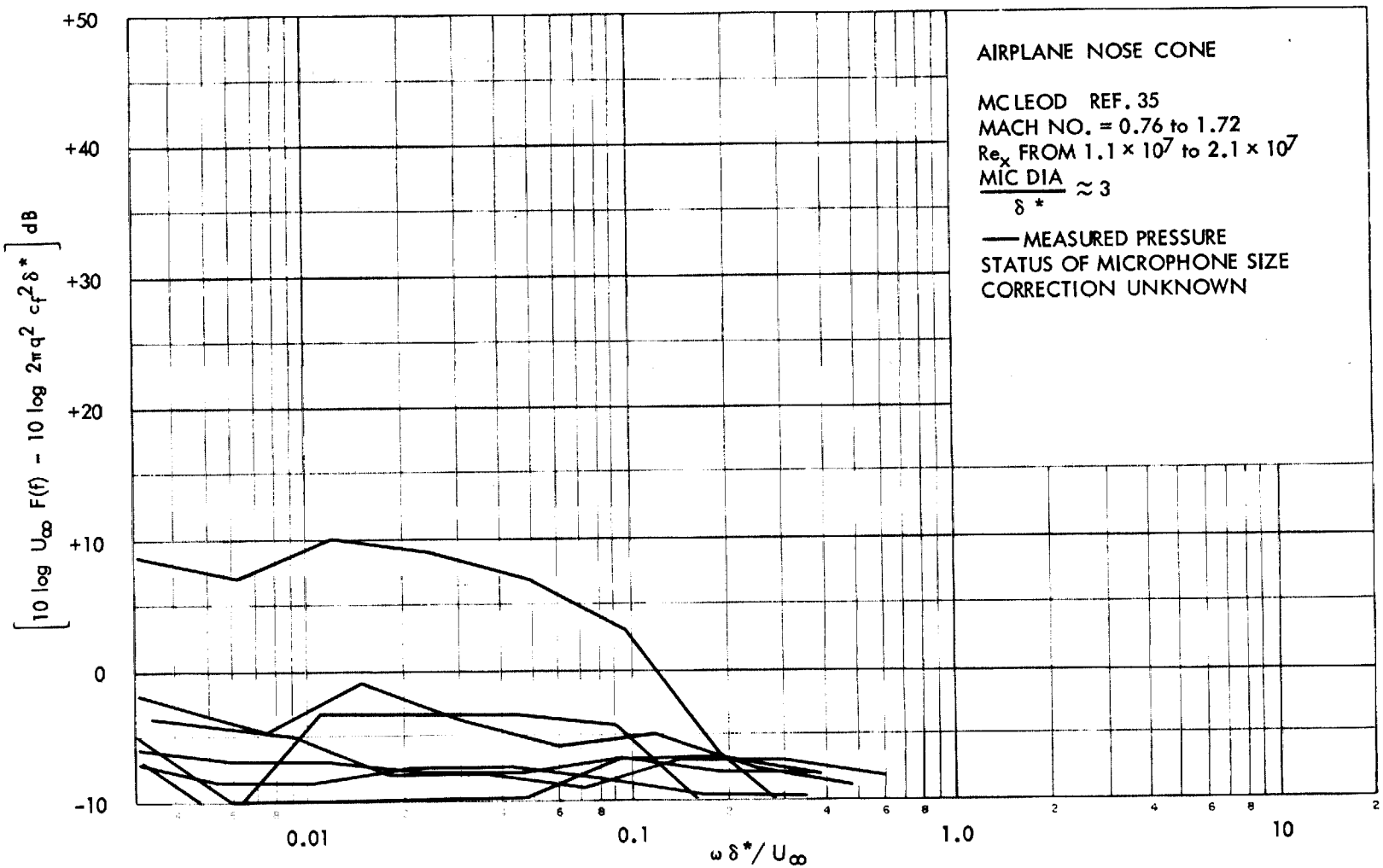

FIGURE 33. FLIGHT MEASUREMENTS OF BOUNDARY LAYER PRESSURE FLUCTUATIONS

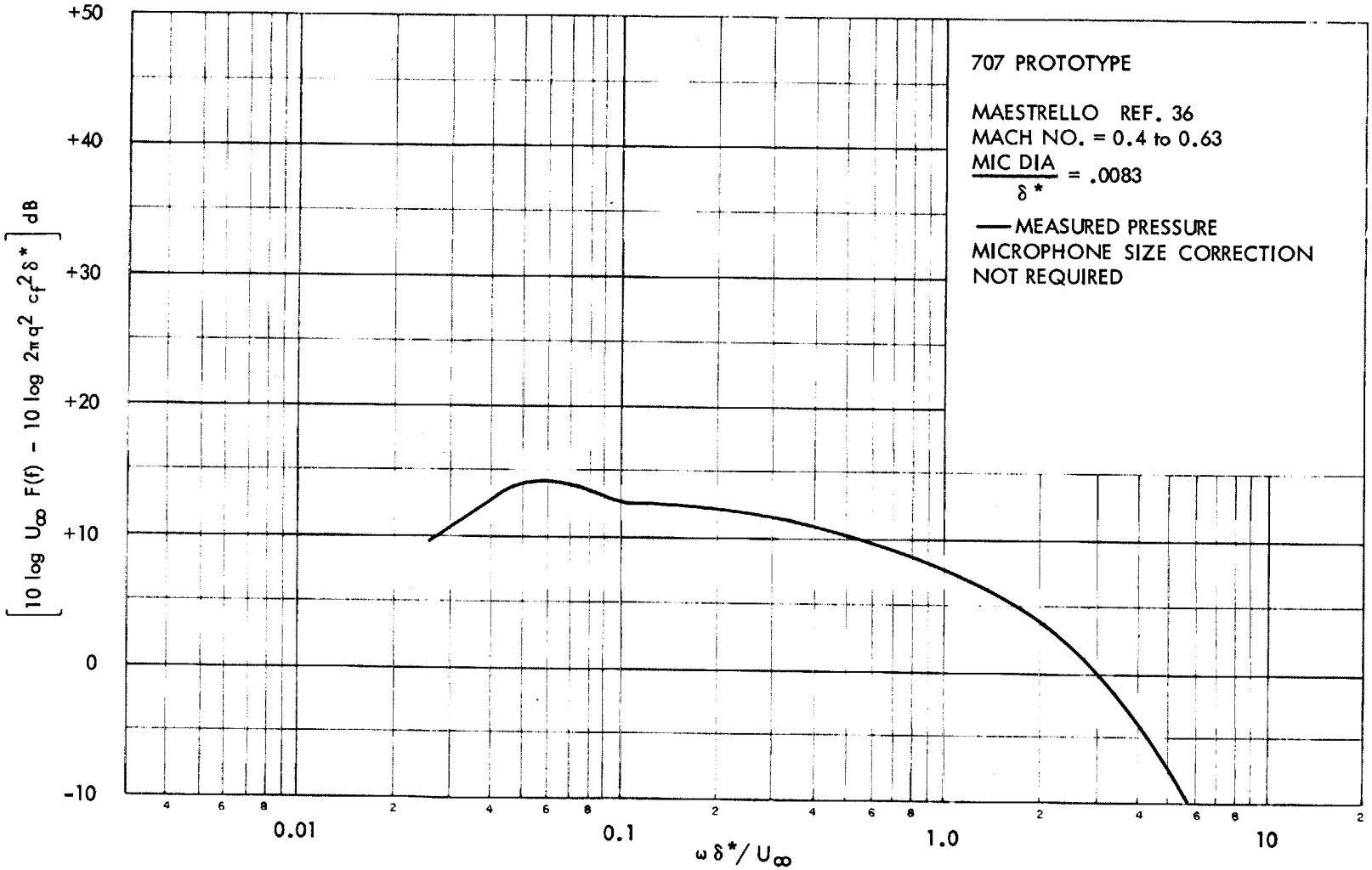

FIGURE 34. FLIGHT BOUNDARY LAYER PRESSURE FLUCTUATION MEASUREMENTS

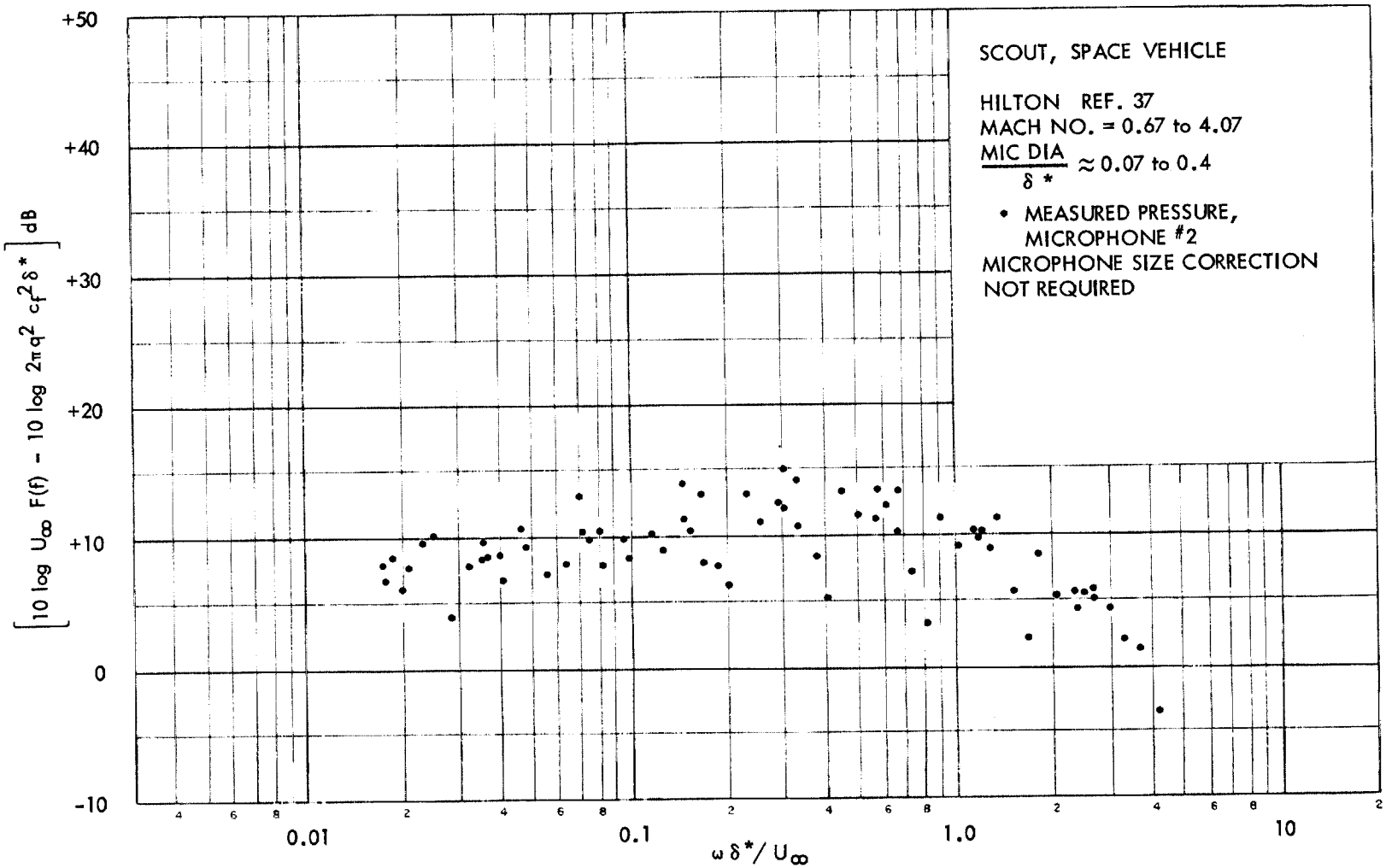

FIGURE 35. FLIGHT MEASUREMENTS OF BOUNDARY LAYER PRESSURE FLUCTUATIONS AND AN EQUIVALENT ACOUSTIC FIELD BASED ON MEASURED STRUCTURAL RESPONSE (see text)

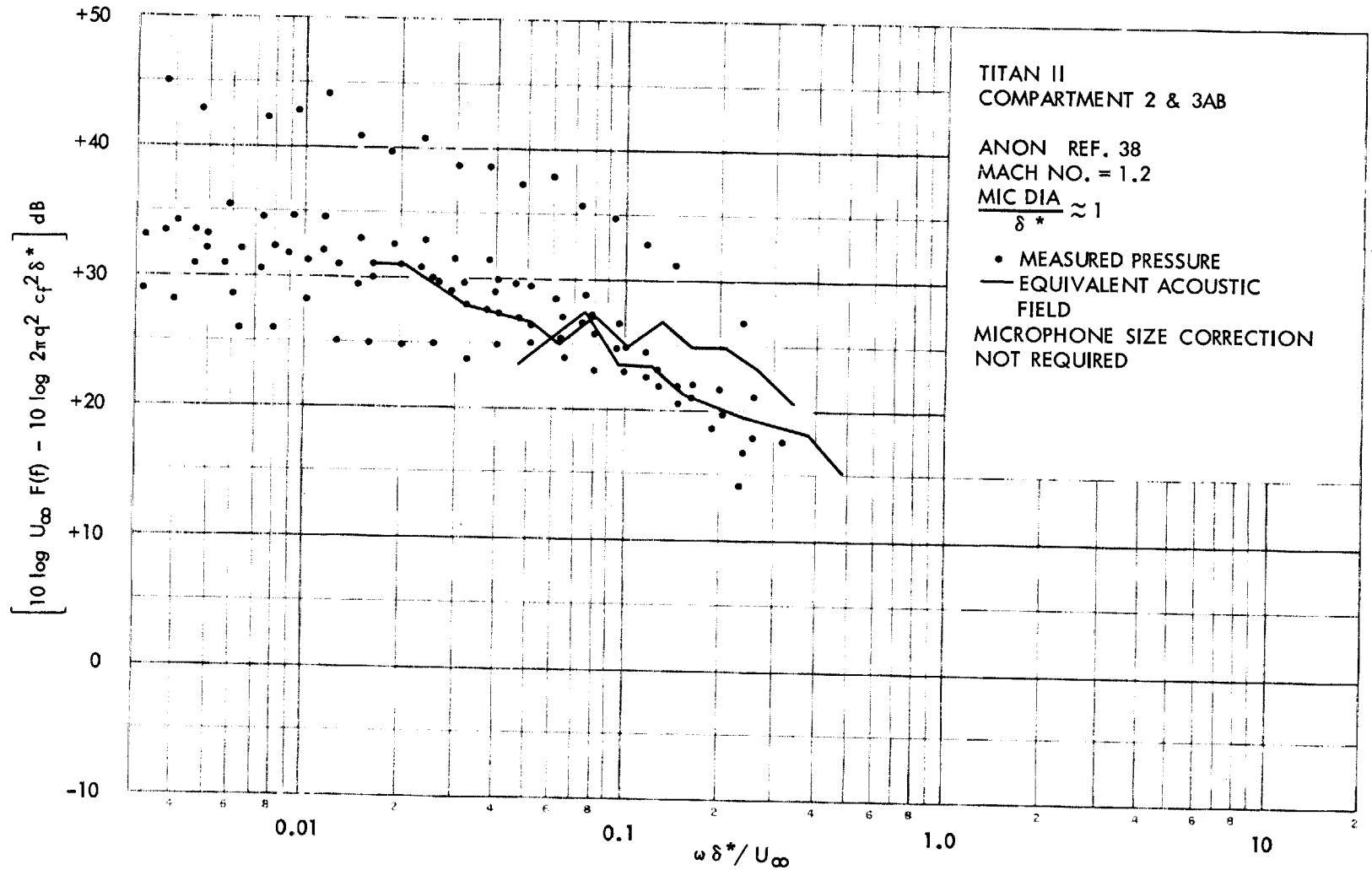

FIGURE 36. FLIGHT MEASUREMENTS OF BOUNDARY LAYER PRESSURE FLUCTUATIONS AND AN EQUIVALENT ACOUSTIC FIELD BASED ON MEASURED STRUCTURAL RESPONSE
(see test)

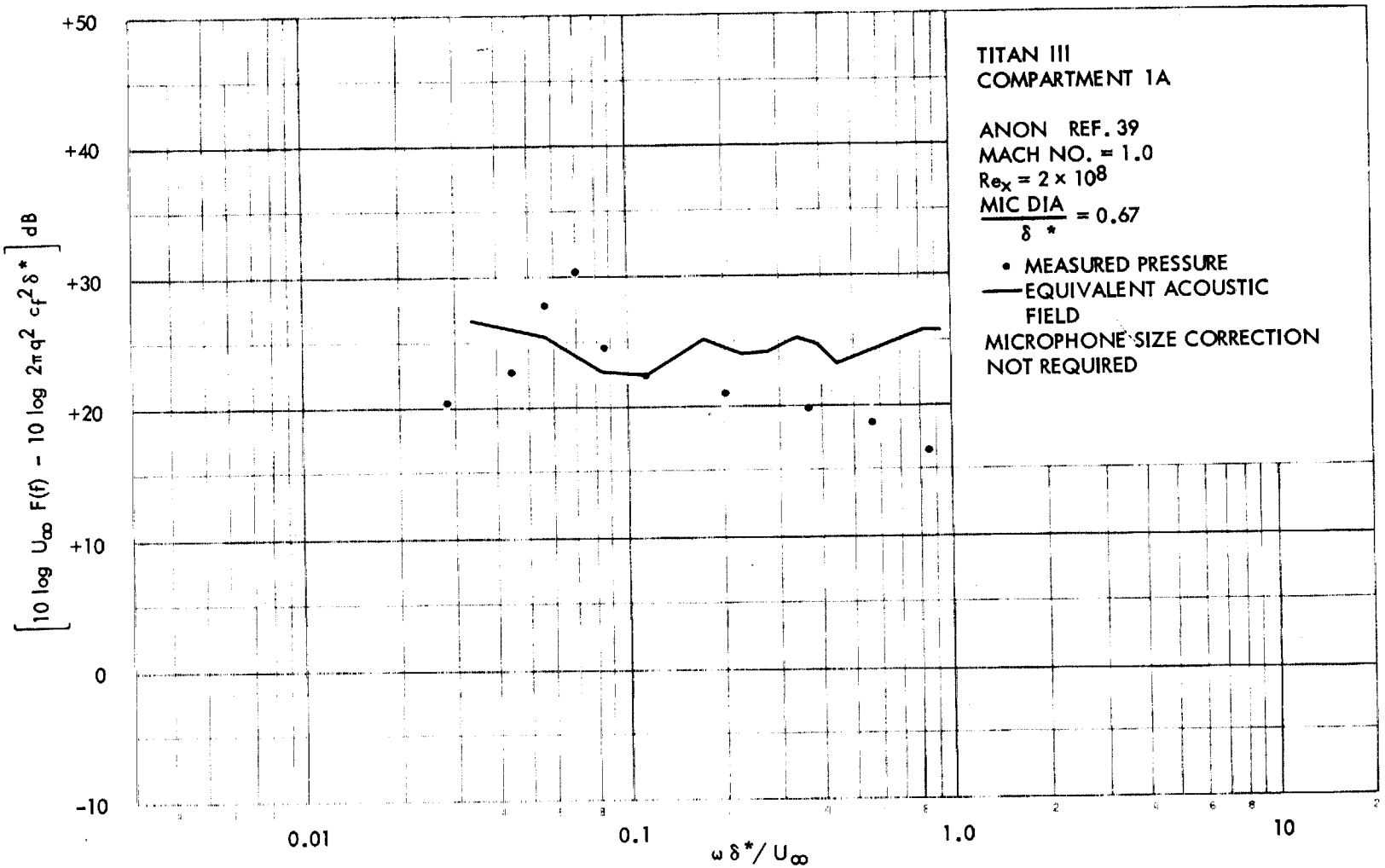

FIGURE 37. FLIGHT MEASUREMENTS OF BOUNDARY LAYER PRESSURE FLUCTUATIONS AND AN EQUIVALENT ACOUSTIC FIELD BASED ON MEASURED STRUCTURAL RESPONSE (see test)

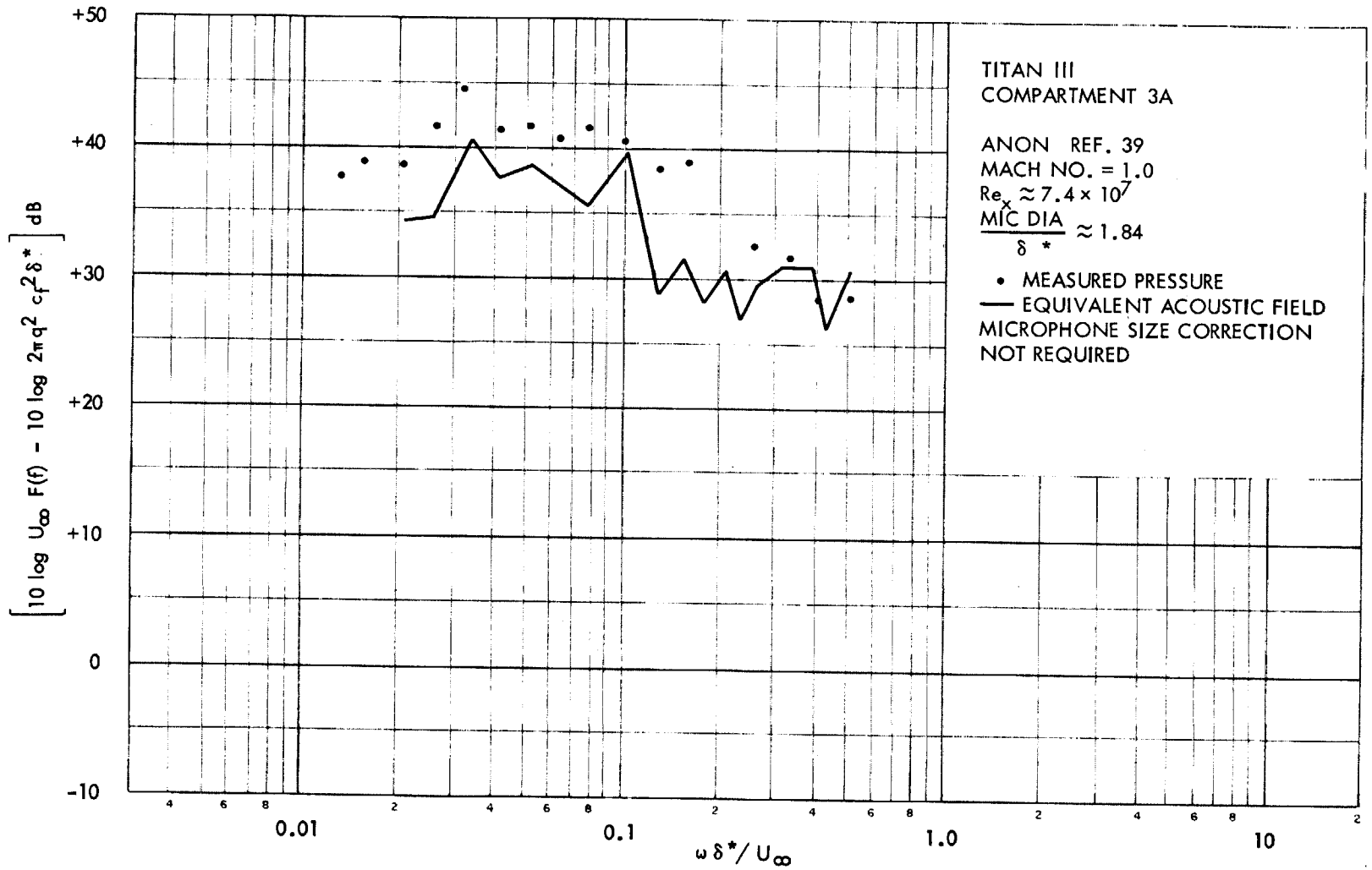

FIGURE 38. FLIGHT MEASUREMENTS OF BOUNDARY LAYER PRESSURE FLUCTUATIONS AND AN EQUIVALENT ACOUSTIC FIELD BASED ON MEASURED STRUCTURAL RESPONSE (see text)

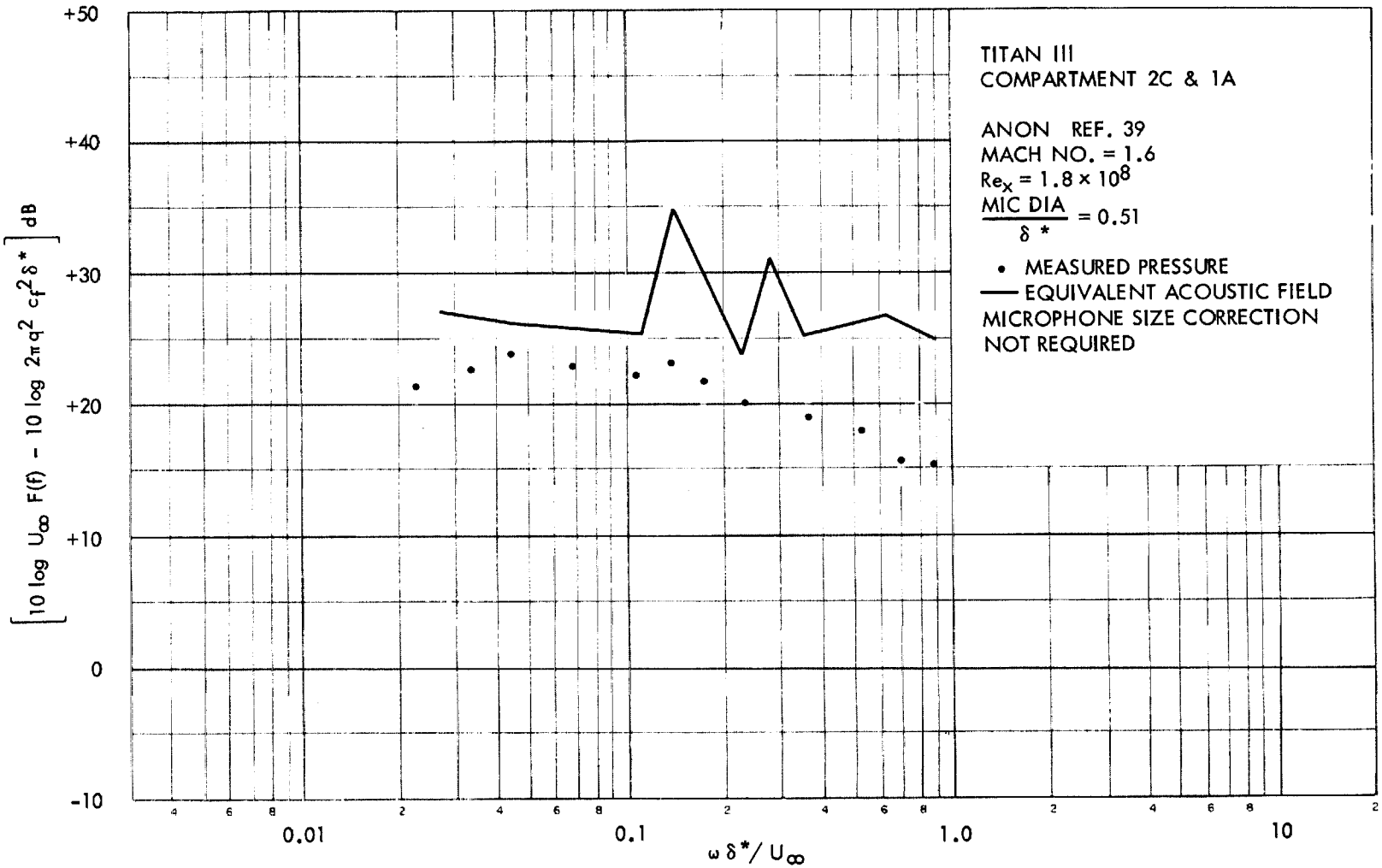

FIGURE 39. FLIGHT MEASUREMENTS OF BOUNDARY LAYER PRESSURE FLUCTUATIONS AND AN EQUIVALENT ACOUSTIC FIELD BASED ON MEASURED STRUCTURAL RESPONSE
(see text)

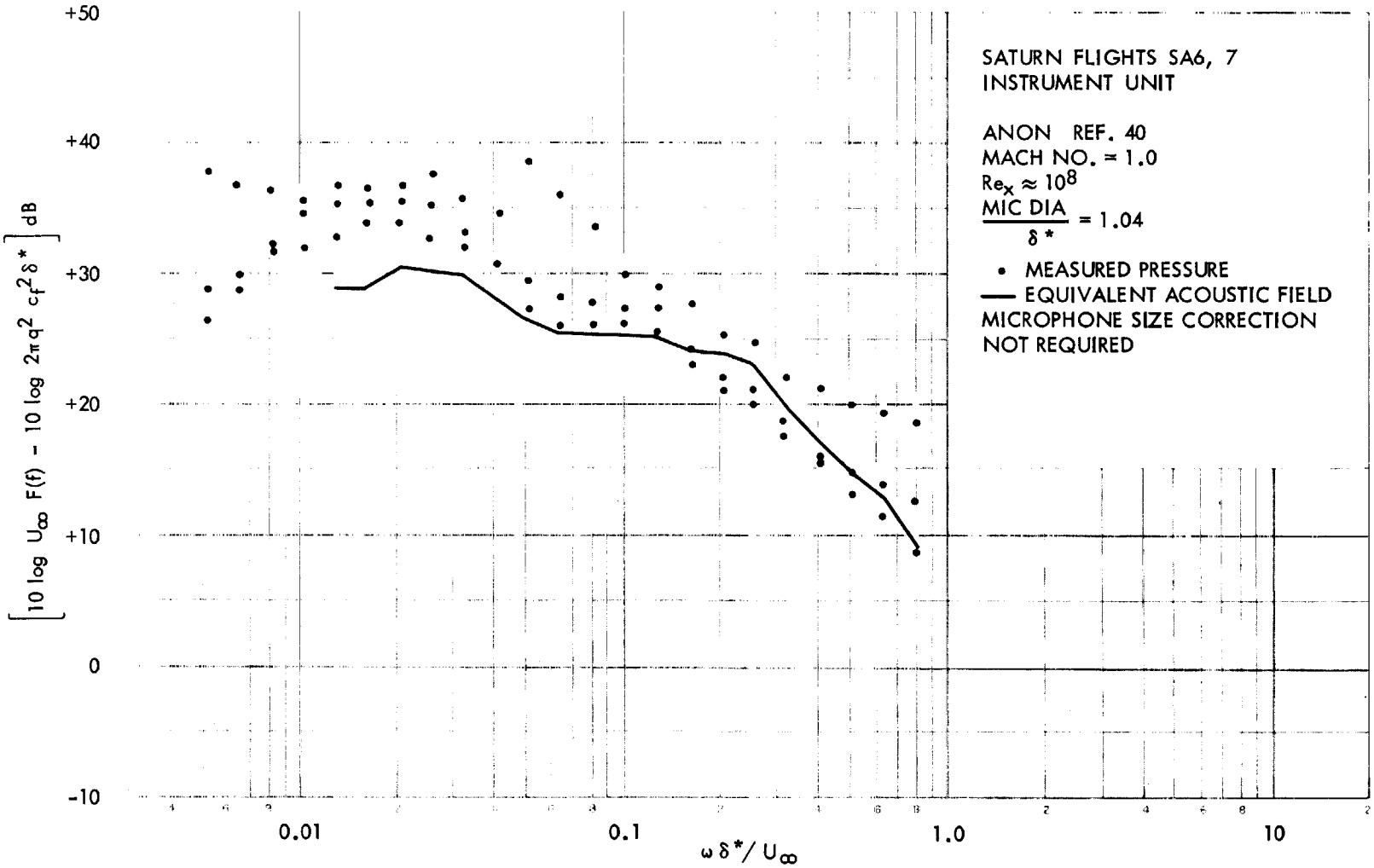

FIGURE 40. FLIGHT MEASUREMENTS OF BOUNDARY LAYER PRESSURE FLUCTUATIONS AND AN EQUIVALENT ACOUSTIC FIELD BASED ON MEASURED STRUCTURAL RESPONSE (see text)

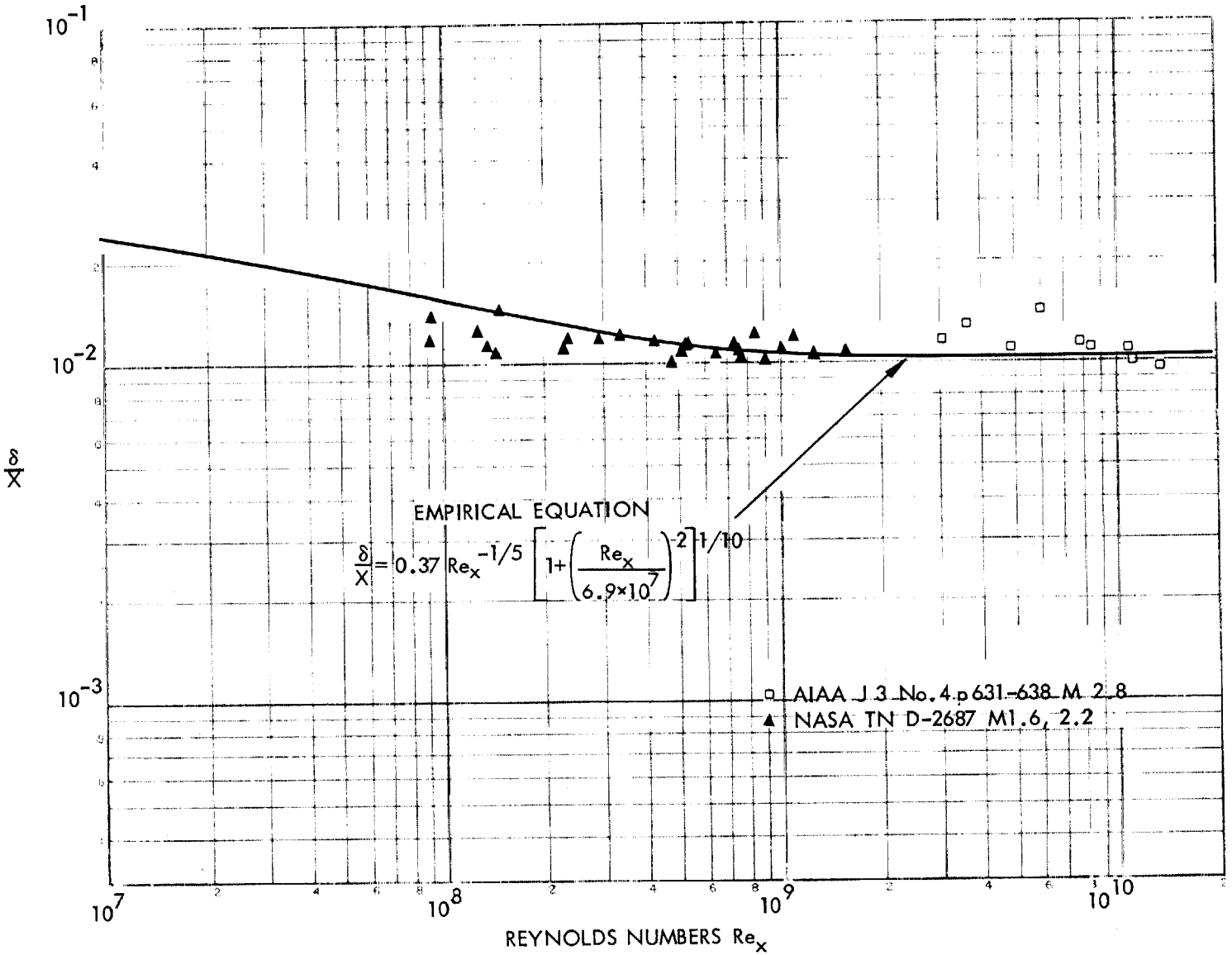

FIGURE A1. EXTENTION OF EMPIRICAL EQUATIONS FOR BOUNDARY LAYER PARAMETERS TO HIGH REYNOLDS NUMBERS AND MACH NUMBERS NORMALIZED BOUNDARY LAYER THICKNESS δ/X

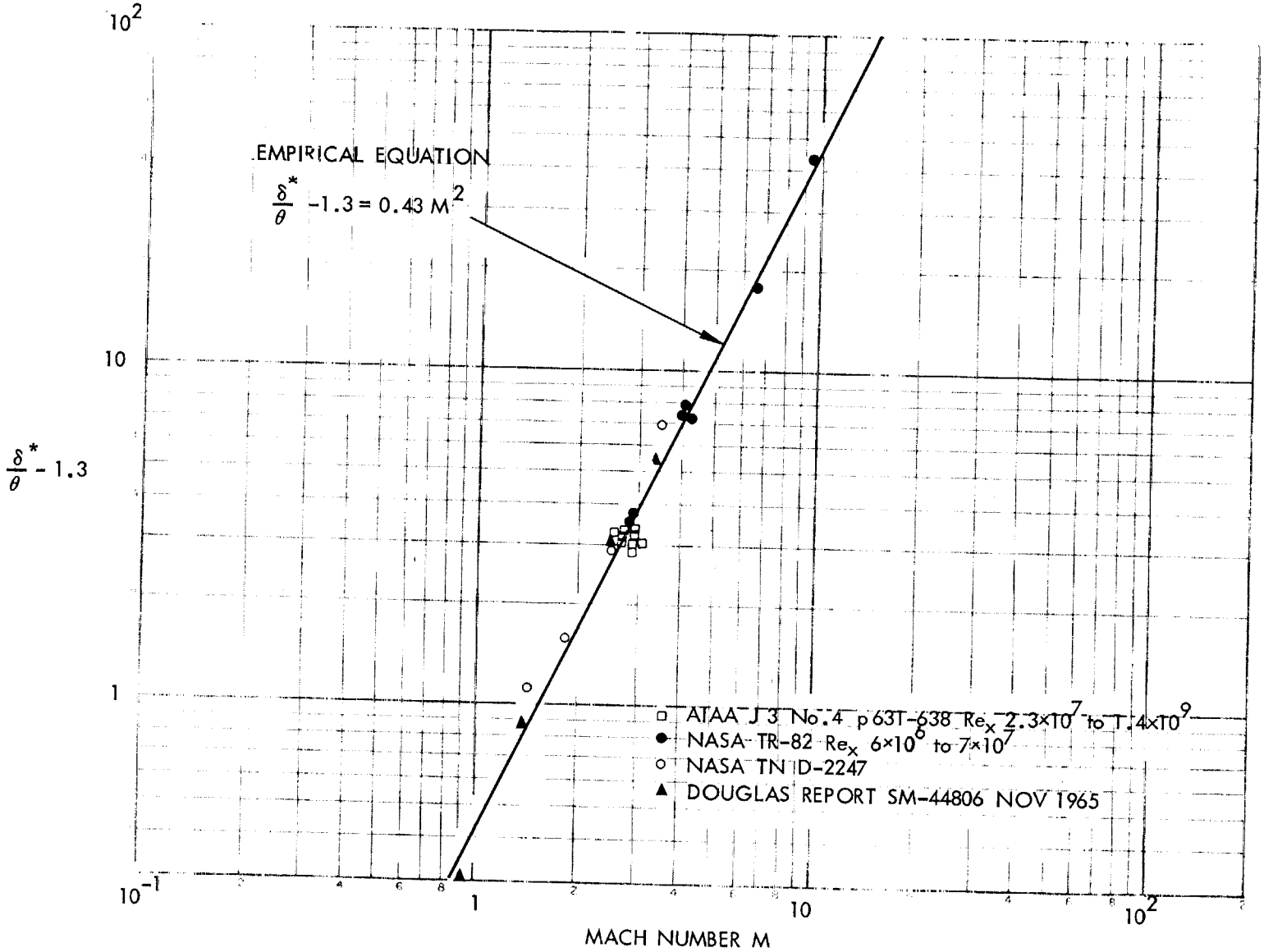

FIGURE A2. EXTENSION OF EMPIRICAL EQUATIONS FOR BOUNDARY LAYER PARAMETERS TO HIGH REYNOLDS NUMBERS AND MACH NUMBERS
BOUNDARY LAYER SHAPE PARAMETER δ^*/θ

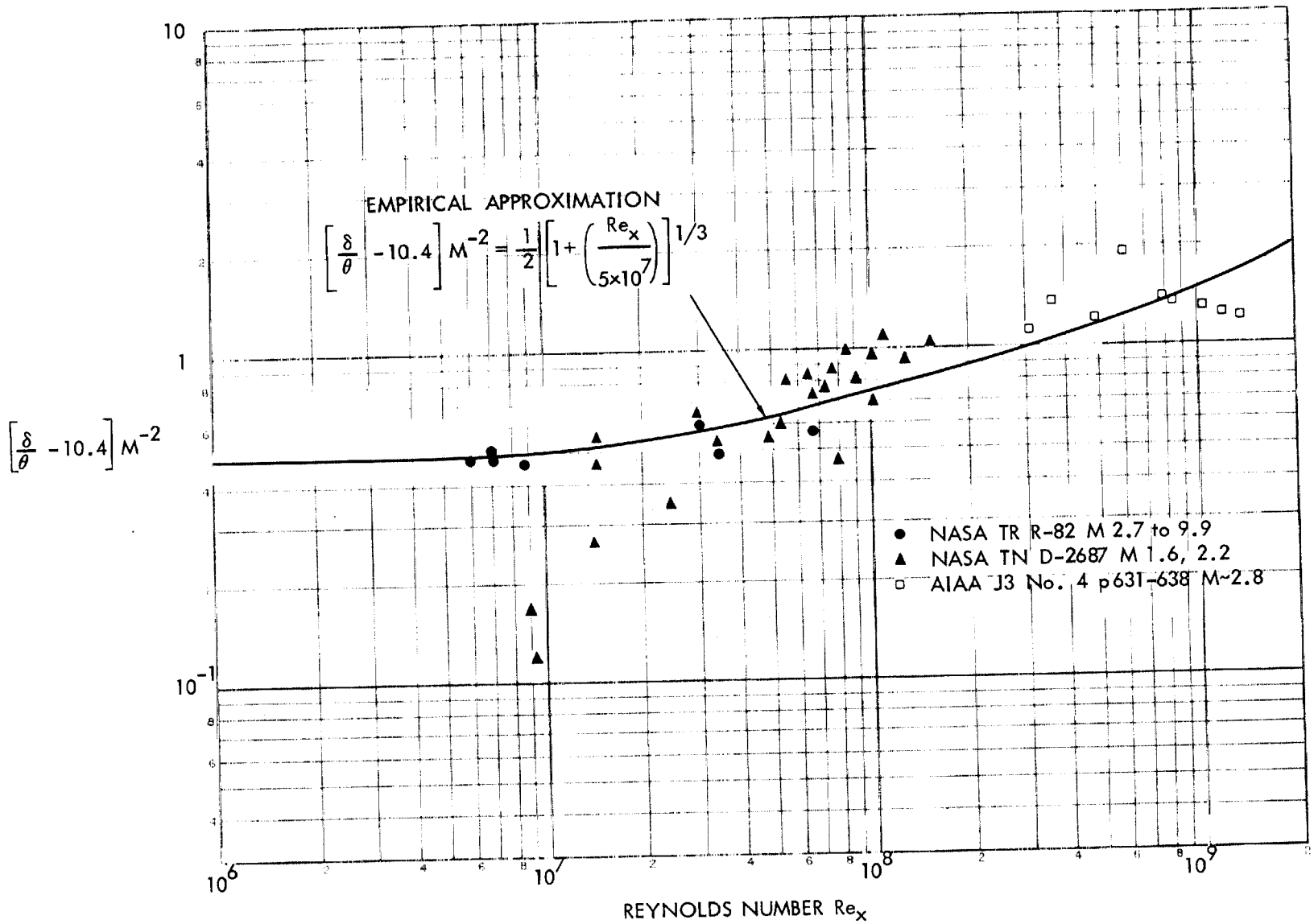

FIGURE A3. EXTENSION OF EMPIRICAL EQUATIONS FOR BOUNDARY LAYER PARAMETERS TO HIGH REYNOLDS NUMBERS AND MACH NUMBERS RATIO OF BOUNDARY LAYER THICKNESS TO MOMENTUM THICKNESS δ/θ

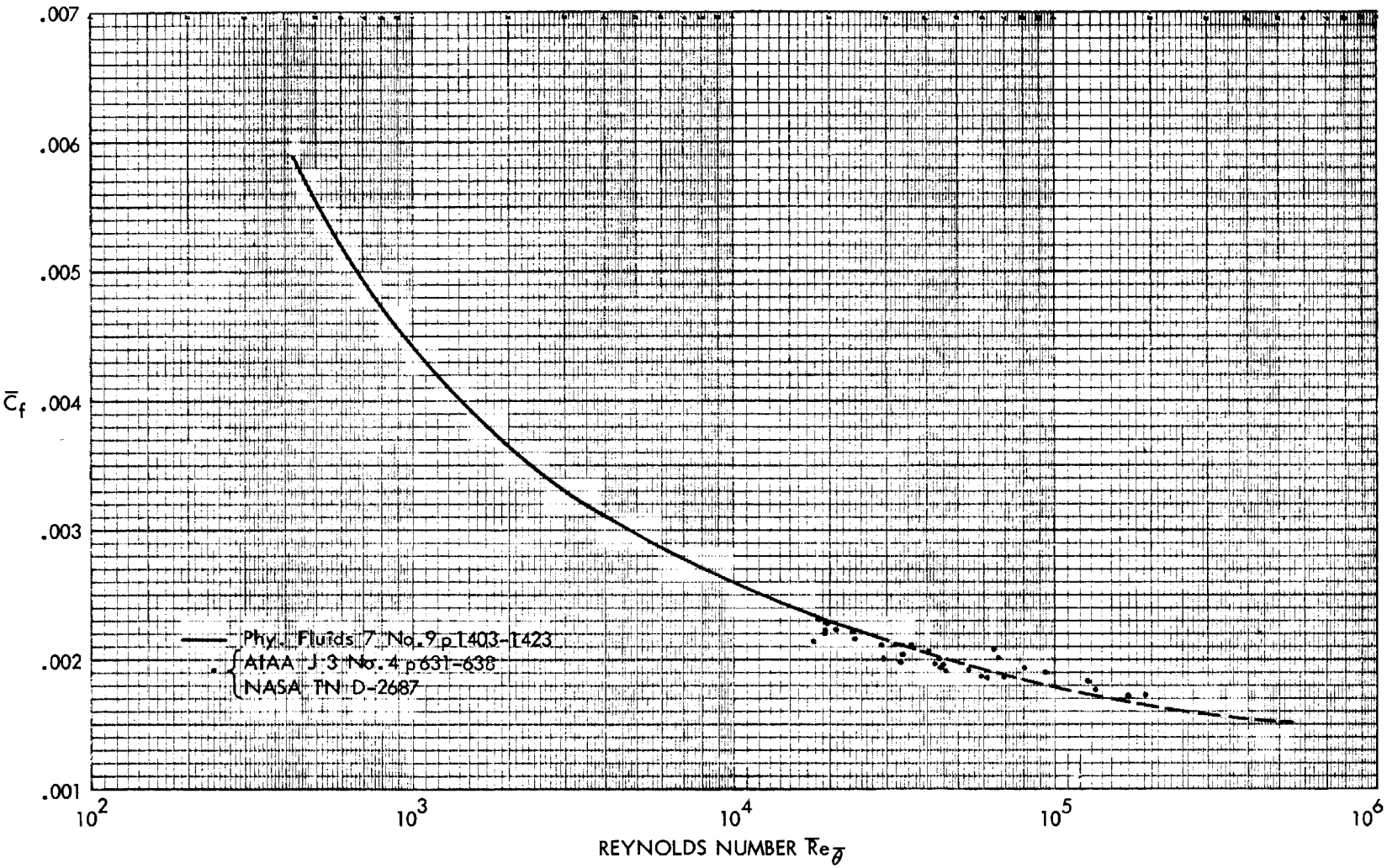

FIGURE A4 EXTENSION OF EMPIRICAL EQUATIONS FOR BOUNDARY LAYER PARAMETERS TO HIGH REYNOLDS NUMBERS AND MACH NUMBERS
Skin friction coefficient $\bar{c}_f$ as a function of Reynolds number in transformed coordinates

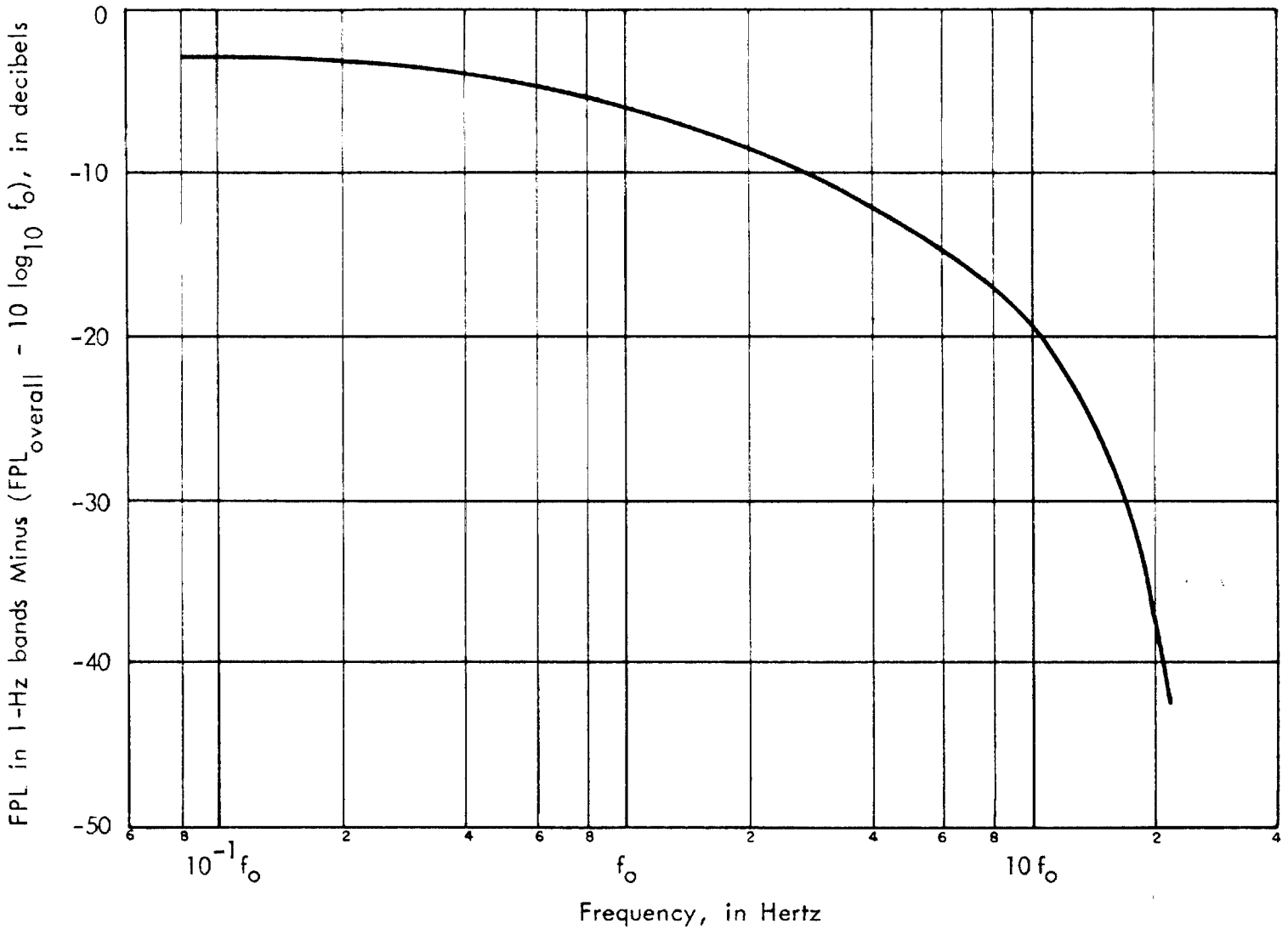

FIGURE B1 CHART FOR ESTIMATING BOUNDARY LAYER PRESSURE SPECTRA

Fluctuating Pressure Level (FPL) in 1-Hz bands

NASA-Langley, 1966 CR-626